Master's thesis

NTNU
Norwegian University of Science and Technology
Faculty of Natural Sciences
Department of Chemical Engineering

Jørgen Troøyen

Nonlinear model predictive control of a semi-batch reactor for miniemulsion polymerization of vinyl chloride monomer

Master's thesis in Chemical Engineering and Biotechnology
Supervisor: Johannes Jäschke
Co-supervisor: Peter Singstad, Cybernetica AS
June 2023

NTNU
Norwegian University of
Science and Technology

Jørgen Troøyen

Nonlinear model predictive control of a semi-batch reactor for miniemulsion polymerization of vinyl chloride monomer

CYBERNETICA

Master's thesis in Chemical Engineering and Biotechnology
Supervisor: Johannes Jäschke
Co-supervisor: Peter Singstad, Cybernetica AS
June 2023

Norwegian University of Science and Technology
Faculty of Natural Sciences
Department of Chemical Engineering

NTNU
Norwegian University of
Science and Technology

Preface

This thesis was written during the spring of 2023 as the final part of the master's degree program Chemical Engineering and Biotechnology at the Norwegian University of Science and Technology (NTNU). The work performed in this master thesis was an extension of a specialization project (TKP4580 - Chemical engineering, specialization project) performed during the fall of 2022. The work and results from the specialization project are utilized in this thesis and the most relevant results are included in condensed form for completeness. Both the specialization project and this master thesis were conducted in collaboration with Cybernetica AS, which proposed the projects. INOVYN Norge provided necessary process data from their plant in Porsgrunn.

I would like to express my gratitude to Cybernetica for giving me the opportunity of a summer internship which extended into the specialization project and this master thesis. During the last year I have spent a lot of time at Cybernetica's offices, and I would like to thank all the employees at Cybernetica for making me feel welcome.

A big thanks to Peter Singstad for proposing such an interesting project and for the helpful insight during the summer internship, specialization project and this master thesis. Thanks to my supervisor at NTNU, Johannes Jäschke, for agreeing to be my supervisor and providing helpful input. I would especially like to thank Anne Halås Koren and Fredrik Gjertsen for all the invaluable help and tips they have provided during both the specialization project and this master thesis. I would also like to thank Karly Sjølie at INOVYN for valuable insights to understand the process.

June 2023, Trondheim
Jørgen Troøyen

Abstract

The aim of this thesis was to implement and test nonlinear model predictive control (NMPC) on a semi-batch reactor for a miniemulsion polymerization process. The motivation behind the work in this thesis was to apply NMPC to the reactor system to improve operation. A typical polymerization process has nonlinear dynamics and lacks online measurements of polymer quality. This makes a model-based control scheme, such as NMPC, an attractive approach since quality parameters could be modelled by using available measurements. Implementation of the NMPC application was performed by establishing an environment for the control system in Cybernetica's software. The process model developed in the preliminary project was used as a plant replacement in addition to being used in the controller. The controller was tuned and evaluated by simulations and case studies.

Extensions and refinements of the process model developed in the preliminary project were performed to make it more applicable for NMPC. The extensions were implemented in the existing C-code and validated against measurements provided by INOVYN. Modifications of the existing control structure were performed during the control structure design in this thesis. The modifications included moving away from the currently deployed cascade- and split range structure. Instead, the NMPC provided setpoints to the manipulated variables which are considered slave controllers in the current control structure. The modifications were performed due to the lack of available measurements in the plant. Controlled- and manipulated variables for the NMPC were chosen based on specifications from INOVYN and process knowledge.

The implemented control structure was tested for various operating conditions and control strategies. Three approaches for reactor temperature control were tested and the simulations showed promising results in terms of safe operation and quality control. Different cases for the initiator dosing were tested and the simulations showed satisfactory results for the majority of the cases. The controller in conjunction with the estimator handled a decrease in the cooling capabilities for the cooling jacket well. Simulations with few control blocks showed similar results compared to simulations with more control blocks. A long prediction horizon was not achievable due to the system being open-loop unstable.

The implementation of NMPC on the process was considered successful in this thesis. The simulation results indicated that the control system was able to handle various operating conditions and control strategies while still maintaining safe operation and meet the desired product quality.

Sammendrag

Målet med denne avhandlingen var å implementere og teste ulineær modellbasert prediktiv regulering (NMPC) på en semi-batch reaktor for en miniemulsjonspolymerisasjonsprosess. Motivasjonen bak arbeidet i denne avhandlingen var å anvende NMPC på reaktorsystemet for å forbedre driften. En typisk polymerisasjonsprosess har ulineær dynamikk og mangler online målinger av polymerkvalitet. Dette gjør en modellbasert kontrolltilnærming, slik som NMPC, til en attraktiv tilnærming siden kvalitetsparametere kan modelleres ved hjelp av tilgjengelige målinger. Implementeringen av NMPC applikasjonen ble utført ved å etablere et miljø for kontrollsystemet i Cybernetica programvare. Prosessmodellen utviklet i forprosjektet ble brukt som en erstatning for anlegget i tillegg til å bli brukt i regulatoren. Regulatoren ble justert og evaluert ved hjelp av simuleringer og case-studier.

Utvidelser og forbedringer av prosessmodellen utviklet i forprosjektet ble utført for å gjøre den mer anvendelig for NMPC. Utvidelsene ble implementert i den eksisterende C-koden og validert mot målinger fra INOVYN. Modifikasjoner av den eksisterende kontrollstrukturen ble utført i designet av kontrollstrukturen i denne avhandlingen. Modifikasjonene inkluderte å gå bort fra den nåværende kaskade- og split range strukturen. I stedet ga NMPC settpunkter til de manipulerte variablene som blir betraktet som slavekontrollere i den nåværende kontrollstrukturen. Modifikasjonene ble utført på grunn av mangelen på tilgjengelige målinger i anlegget. Regulerte- og manipulerte variabler for NMPC'en ble valgt basert på spesifikasjoner fra INOVYN og prosesskunnskap.

Den implementerte kontrollstrukturen ble testet for ulike driftsforhold og reguleringsstrategier. Tre tilnærminger for kontroll av reaktortemperaturen ble testet, og simuleringene viste lovende resultater med tanke på sikker drift og kvalitetskontroll. Ulike scenarioer for dosering av initiator ble testet, og simuleringene viste tilfredsstillende resultater for flertallet av scenarioene. Regulatoren håndterte sammen med estimatoren en reduksjon i kjølekapasiteten til kjølekappen bra. Simuleringer med få kontrollblokker viste lignende resultater sammenlignet med simuleringer med flere kontrollblokker. En lang prediksjonshorisont var ikke oppnåelig på grunn av at systemet er åpen-sløyfe ustabilt.

Implementeringen av NMPC på prosessen ble ansett som vellykket i denne avhandlingen. Simuleringsresultatene indikerte at kontrollsystemet klarte å håndtere ulike driftsforhold og kontrollstrategier samtidig som det opprettholdt sikker drift og oppnådde ønsket produktkvalitet.

Table of contents

List of Figures

List of Tables

List of symbols

Some comments regarding notation are listed to establish consistency:

- Superscript lower case letters are used for phases when describing mass, volume, concentration, moles, etc: Free phase (f), gas phase (g), polymer phase (p), water/aqueous phase (w).
- Subscript upper case letters are used for species when describing mass, volume, concentration, moles: Initiator (I), monomer (M), polymer (P), radical (R), surfactant/cosurfactant (S), water (W).
- Superscript lower case letters are also used when describing physical properties: Gaseous state (g), liquid state (l), solid state (s)

Latin symbols

Symbol	Description	Unit
$A_{J,amb}$	Cooling jacket - ambient area	m^2
A_k	Jacobian	
$A_{R,amb}$	Reactor - ambient area	m^2
A_{reflux}	Reflux condenser area	m^2
$A_{J,R}$	Reactor - cooling jacket area	m^2
AX	Chain transfer agent	
a_S	Interfacial area of particles	m^2
B_k	Jacobian	
C	Relative rate coefficient, radical termination in polymer phase	1/s
$c_i(\cdot)$	Constraint functions	
CF	Correction factor for kinetic parameters	
$C_{p,cw}^{reflux}$	Heat capacity, cooling water to condenser	J/kg/K
$C_{p,i}^{feed}$	Heat capacity, inlet specie i	J/kg/K
$C_{p,J}$	Heat capacity, water inside jacket	J/kg/K
$C_{p,reflux}$	Heat capacity, water inside condenser	J/kg/K
D_i	Dead polymer chain of length i	
$d(\cdot)$	Noise function for process parameters	
d_p	Particle diameter	m
$E(\cdot)$	Terminal cost	
f	Initiator efficiency	
$f(\cdot)$	Process model	
F_k	Jacobian	
$\hat{f}_i^0$	Fugacity of specie i at standard state	Pa
$\hat{f}_i^j$	Fugacity of specie i in phase j	Pa
$g(\cdot)$	Path constraints	
H_k	Jacobian	
$h(\cdot)$	Measurement function	
I	Initiator	
$J(\cdot)$	Objective function	
K_c	Intermediate calculation parameter	m^3/mol/s

K_H	VCM-in-water solubility constant	kgVCM/kgH_2O
K_k	Kalman filter gain matrix	
K_s	Correction factor for solubility of VCM in PVC	
k	Parameter in Smith & Ewart equation	
k'	Rate coefficient for radical desorption	1/s
k_{abs}	Absorption rate constant	m^3/mol/s
k_{ct}^{AX}	Rate constant, chain transfer to CTA	m^3/mol/s
k_{ct}^{M}	Rate constant, chain transfer to monomer	m^3/mol/s
k_{ct}^{P}	Rate constant, chain transfer to polymer	m^3/mol/s
k_{des}	Desorption rate constant	1/s
k_i	Rate constant, chain initiation	1/s
k_i^A	Rate constant, chain initiation by CTA	1/s
k_d	Rate constant, initiator decomposition	1/s
k_p	Rate constant, propagation reaction	m^3/mol/s
k_t	Rate constant, termination	m^3/mol/s
k_{tc}	Rate constant, termination by combination	m^3/mol/s
k_{td}	Rate constant, termination by disproportionation	m^3/mol/s
k_t^p	Rate constant, termination in polymer phase	m^3/mol/s
k_t^w	Rate constnat, termination in water phase	m^3/mol/s
L_k	Jacobian	
M	Monomer; Vinyl chloride	
M_i	Molar mass of specie i	kg/mol
$\hat{m}_{cw}^{reflux}$	Mass flow, cooling water to condenser	kg/s
$\hat{m}_{gas}$	Gas flow through reflux	kg/s
m_i	Total mass of specie i	kg
$\hat{m}_i^{feed}$	Inlet mass flow of specie i, reactor	kg/s
m_i^j	Mass of specie i in phase j	kg
m_J	Mass of water inside cooling jacket	kg
$\hat{m}_J$	Inlet mass flow, water to jacket	kg/s
M_k	Jacobian	
m_M^{tot}	Total mass of monomer fed	kg
m_P	Total mass of polymer	kg
m_{reflux}	Mass of water inside condenser	kg
N_A	Avogadros number	1/mol
$N_{p(n)}$	Number of particles with n radicals	
N_T	Total amount of moles of particles	mol
$\bar{n}$	Average number of radicals per particles	
n_i	Total amount of moles of specie i	mol
$\hat{n}_i$	Inlet molar flow of specie i	mol/s
$n_{i,0}$	Initial moles of specie i	mol
n_i^j	Amount of moles of specie i in phase j	mol
n_u	Number of inputs	
n_x	Number of states	
P	Polymer; Polyvinyl chloride	
P_i	Growing polymer chain of length i	
P_k^+	A posteriori covariance	
P_k^+	A priori covariance	
P_{tot}	Total amount of moles of radicals	mol
p_k	Subset of all model parameters, online estimation	

p_M	Partial pressure of monomer	Pa
p_M^{sat}	Saturation pressure of monomer	Pa
p_R	Reactor pressure	Pa
p_W	Partial pressure of water	Pa
p_W^{sat}	Saturation pressure of water	Pa
Q_{demand}	Total cooling demand	kW
$Q_{J,R}^{cap}$	Cooling capacity, jacket	kW
Q_{reflux}^{cap}	Cooling capacity, reflux	kW
Q_{tot}^{cap}	Total cooling capacity	kW
Q_k	Weighting matrix	
q_k	Finite control parameters	
R	Gas constant	J/mol/K
$R\cdot$	Radical	
R_d	Reaction rate, decomposition of initiator	mol/m^3/s
R_I	Reaction rate, chain initiation	mol/m^3/s
R_k	Measurement noise covariance	
R_p	Reaction rate, propagation/polymerization	mol/s
R_t	Reaction rate, termination	mol/m^3/s
$r(\cdot)$	Terminal constraint	
r_1	Linear weight on slack variables	
r_2	Quadratic weight on slack variables	
S	Surfactant	
$S_{1,k}$	Weighting matrix	
$S_{2,k}$	Weighting matrix	
T_{amb}	Ambient temperature	K
$T_{cw,r}^{in}$	Temperature, cooling water to condenser	K
$T_{cw,r}^{out}$	Temperature, cooling water from condenser	K
T_i^{feed}	Temperature, inlet specie i, to reactor	K
T_J	Cooling jacket temperature	K
T_J^{in}	Temperature, water to jacket	K
T_J^{min}	Minimum temperature of cooling jacket	K
$T_{J,min}^{in}$	Minimum inlet temperature to cooling jacket	K
$T_{J,SP}^{in}$	Setpoint, inlet temperature to jacket	K
T_J^{out}	Temperature, water from jacket	K
T_R	Reactor temperature	K
T_{reflux}	Reflux condenser temperature	K
T^g	Gas temperature	K
$\bar{T}_{X_M}$	Conversion average temperature	K
t_{batch}	Batch time	s
$U_{J,amb}$	Cooling jacket-ambient heat transfer coefficient	W/m^2/K
$U_{R,amb}$	Reactor-ambient heat transfer coefficient	W/m^2/K
U_{reflux}	Condenser heat transfer coefficient	W/m^2/K
$U_{J,R}$	Reactor-cooling jacket heat transfer coefficient	W/m^2/K
u	Input vector	
u_k	Input vector at time k	
x^{high}	Upper constraint on inputs	
x^{low}	Lower constraint on inputs	
$V_{fluid,s}$	Volume of liquid and solids with neither monomer or water in gas phase	m^3

V_k	Process noise covariance	
V_R	Reactor volume	m^3
$\hat{V}_{cw}^{reflux}$	Volume flow of water to reflux	m^3/h
$\hat{V}_{cw,SP}^{reflux}$	Setpoint, volume flow of water to reflux	m^3/h
V^j	Volume of phase j	m^3
v_k	Process noise vector	
v^p	Volume of a polymer particle	m^3
W	Water	
w_k	Measurement noise vector	
x	State vector	
x_k	State vector at time k	
x'_k	Augmented state vector at time k	
$\hat{x}_k^+$	A posteriori state estimate	
$\hat{x}_k^-$	A priori state estimate	
x^{high}	Upper constraint on states	
x^{low}	Lower constraint on states	
$[X]^j$	Concentration of specie X in phase j	mol/m^3
X_M	Monomer conversion	
X_M^{final}	Final monomer conversion	
y_M	Molar fraction of monomer in gas phase	
y_W	Molar fraction of water in gas phase	
z_k	Output variable vector at time k	
z_k^{ref}	Reference trajectory	

Greek symbols

Symbol	Description	Unit
α_M	Monomer activity	
ΔH_{rx}	Heat of reaction	kJ/mol
ΔH_{VCM}^{vap}	Heat of vaporization, VCM	J/kg
ΔQ_{tot}	Difference between cooling capacity and demand	kW
Δu_k	Input moves	
Δu^{high}	Upper constraint, input move	
Δu^{low}	Lower constraint, input move	
$\mathcal{E}$	Index set of equality constraints	
ϵ	Ratio of total termination that is due to termination by disproportionation	
ε	Slack variable	
η	Subset of all process parameters, offline estimation	
θ	Model parameters vector	
θ_{max}	Upper bounds on model parameters	
θ_{min}	Lower bounds on model parameters	
$\mathcal{I}$	Index set of inequality constraints	
μ	Rate of increase in volume of particle	m^3/s
ϱ	Volumetric rate of formation of radicals	
ρ_i^j	Density of specie i in phase j	kg/m^3

σ	Average rate of radical absorption to particles	1/s
τ_{FIC}	Time constant	s
τ_{TIC}	Time constant	s
φ	Volume fraction of polymer in polymer phase	
Φ	Parameter that varies between 0 and 2	
ϕ	Vector of decision variable	
χ	Flory-Huggins interaction parameter	

List of abbreviations

CMC	Critical Micelle Conscentration
Controlled Variable	CV
CTA	Chain Transfer Agent
DCS	Distributed Control System
EKF	Extended Kalman Filter
GUI	Graphic User Interface
KF	Kalman Filter
LP	Linear Program
Manipulated Variable	MV
MHE	Moving Horizon Estimator
MPC	Model Predictive Control
NLP	Nonlinear Program
NMPC	Nonlinear Model Predictive Control
OPC	Open Platform Communication
P-PVC	Paste-Polyvinyl Chloride
PSV	Pressure safety valves
PVC	Polyvinyl Chloride
S-PVC	Suspension-Polyvinyl Chloride
SQP	Sequential Quadratic Programming
VCM	Vinyl Chloride Monomer
QP	Quadratic program

1 Introduction

This chapter provides an introduction to this thesis. The background for this thesis is presented first, and it includes issues related to polymerization reactor control and why model-based strategies can improve operation. Then some related literature are presented. Finally, the scope of the work in this thesis is presented and it includes a short summary of the preliminary project which was the predecessor of the thesis.

1.1 Background

A majority of the aspects related to our daily life involve the use of synthetic polymers. In 2016 the worldwide production of synthetic polymers was 335 million tonnes, which illustrates the enormous demand[1]. The term polymer is an umbrella term used to describe chemicals that are built up by chains of molecules, but the material most people associate with the term polymer is plastics[1]. A large variety of plastics with different properties are produced in large amounts, one of which is poly vinyl chloride (PVC). PVC is one of the most applied types of plastics due to its wide range of properties and relatively low cost[2]. It is produced by the polymerization of vinyl chloride monomer (VCM)[2]. Some of the production of PVC takes place in Norway, at INOVYN's plant located at Herøya industrial park. Several PVC types are produced here, and the polymerization process utilized is the determining factor for which PVC type is produced.

One of the polymerization processes taking place at INOVYN's plant is miniemulsion polymerization of VCM, which produces paste-PVC (P-PVC). Miniemulsion polymerization, and polymerization processes in general, are highly nonlinear due to complex reaction mechanisms and intertwined phenomena[3]. Polymerization reactions are also typically exothermic which makes tight temperature control critical to ensure safe operation of the reactor. Polymerization reactor control is a difficult exercise as a result of the nonlinear dynamics and the lack of online measurements of the polymer quality[4]. This makes model-based control schemes an attractive approach as the polymer quality parameters can be predicted based on the available measurements, such as the reactor temperature[4]. Significant improvements can be obtained both in terms of economics, but also in terms of reactor operation by the application of model predictive control (MPC)[4]. Due to the nonlinear dynamics, NMPC could be a promising control approach to improve operation of the reactor. The polymer industry becomes increasingly competitive and the product requirements get tougher. In addition, more stringent regulations regarding environmental issues are put on the polymer producers[5]. Consequently, the challenge is to produce consistently high-quality polymers in a safe, environmentally friendly and as efficient manner as possible.

This thesis investigated the implementation of NMPC on a semi-batch reactor for miniemulsion polymerization of VCM. Due to the nonlinear nature of polymerization processes, NMPC could prove beneficial for the control of the reactor. The batch time, which is an important factor for the profitability of the process, can be reduced by utilizing the potential of the reactor in a more efficient manner. More efficient use of the cooling capacity and the initiator dosing might prove to increase the polymerization rate and consequently reduce the batch time. Additionally, more efficient use of the available resources will reduce waste which is beneficial from both an economic and environmental perspective. The NMPC has the potential to solve the mentioned challenges.

1.2 Literature

Several studies have investigated the control of polymerization reactors. These studies ranges from review articles which look into the recent contributions and technology, to studies of various control strategies. The control strategies utilized are both based on MPC and simple PID control structures.

Hidalgo et al.[6] applied MPC to a simulated, nonlinear, open-loop unstable process. The process considered was the polymerization of styrene in a continuously stirred tank reactor, and the manipulated variables were the flow rate of water to the cooling jacket and the flow rate of styrene to the reactor. Both a perfect and imperfect model was used to illustrate the predictive capabilities. The results showed that satisfactory control of the reactor was achieved despite significant model error.

Kiparissides et al.[7] developed a model of a PVC batch suspension reactor. Several aspects of the process were modelled, such as the polymerization rate, phase equilibria, monomer distribution, reactor temperature and reactor pressure. The phase equilibria calculations in this article form the basis of the phase equilibria calculations for the process developed in the preliminary project, which makes this article highly relevant. An experimental reactor was deployed to verify the model. For the experimental reactor a control system consisting of a cascade structure was utilized to maintain the reactor temperature within $\pm 0.1\,^{\circ}\mathrm{C}$ of its setpoint value. The reactor temperature was the master controller, while there were two slave controllers. Cold and hot water to the cooling jacket surrounding the reactor were controlled by the two slave controllers. The model predictions were in good agreement with the experimental results for the reactor temperature, reactor pressure and the conversion among others. The predictive capabilities of the model were also demonstrated through simulations of experimental data reported in literature.

Dimitratos et al.[8] reviewed the major issues related to control of emulsion polymerization reactors and includes discussions about the latest contributions in process understanding, mathematical modelling and process control approaches. The article discusses some highly relevant issues for this thesis, such as challenges regarding reactor temperature control and the use of a reflux condenser if foaming is not a problem. Additionally, the importance of polymerization rate control in context of cooling capacity and cooling demand is discussed. Both these aspects of polymerization reactor control are highly relevant for the work conducted in this thesis. Several of the same considerations discussed by Dimitratos et al. were taken into account during this work.

1.3 Scope of work

Prior to this thesis a preliminary project was conducted during the fall of 2022[9]. The preliminary project was in turn a continuation of a summer internship at Cybernetica. In the preliminary work a dynamic model of a semi-batch reactor for miniemulsion polymerization of VCM was developed. Additionally, the theoretical foundation of chapter 2 was thoroughly researched. The work included offline parameter estimation, online state- and parameter estimation and simulations of the model using Cybernetica's software. Measurements were provided by INOVYN such that the model could be validated against an industrial case. Ballistic simulations showed acceptable results, but deviations from the measurements were observed. Especially deviations in the reactor temperature motivated the implementation of online- state and parameter estimation. The online state- and parameter estimation was implemented by tuning a Kalman filter, with the correction factor

for the kinetic model, the heat transfer coefficient for the reflux condenser and the heat transfer coefficient between the cooling jacket and the reactor chosen as the estimated parameters. The reactor temperature, the outlet temperature of the cooling jacket and the outlet temperature of the reflux condenser were chosen as the active measurements. Simulations with the Kalman filter showed great improvements in terms of deviations from the measurements. A total of four batches were simulated to validate the model. The obtained results proved promising regarding the use of the process model in a NMPC application. The main results from the preliminary project are included in appendix B in condensed form.

A wide variety of tasks have been conducted in this thesis. Extensions and finalization of the developed model from the preliminary work were conducted in the initial phase of the thesis. The extensions made the model more tailored for the use in the NMPC application. An environment for the control system was established using Cybernetica's software, which supported the implementation of the NMPC application. In order to test the controller on the process, the process model was used as a plant replacement in addition to being used in the NMPC controller. With a fully operating environment for the control system, the resulting controller implementation was tested by simulations and case studies.

1.4 Thesis structure

The remaining chapters in thesis are structured in the following manner:

Chapter 2 presents the foundation of polymerization processes. General theory about polymers and polymerization reactions are briefly presented. Then more thesis-specific topics such as free-radical polymerization and emulsion- and miniemulsion polymerization are presented. The two latter topics form the foundation of the developed model which is used in the NMPC. The theory presented in this chapter highlights the same aspects of the theory presented in the preliminary project.

Chapter 3 starts by presenting the theoretical aspects of constrained optimization, which is the foundation of MPC. Then nonlinear MPC is presented in addition to aspects of the implementation of MPC. State- and parameter estimation are presented last and covers the theory of the Kalman filter.

Chapter 4 describes the software used in the preliminary project and in this thesis. The chapter aims to provide an overview of the various programs used to implement the process model, the estimator and the NMPC application. The concept of plant replacement is also discussed.

Chapter 5 presents the process that is modelled. A process description that includes the preparation of a batch and the reactor system layout is presented first. Then a description of how the reactor is currently controlled is presented. Limitations which have implications for the control structure design in this thesis are briefly discussed.

Chapter 6 provides the extensions to the model that was implemented to make the model more tailored for the use in the NMPC application. The extensions build on the process model developed in the preliminary project which is presented in appendix A.

Chapter 7 presents the considerations that were taken into account when developing the resulting control structure in this thesis. This includes considerations about

various control strategies, candidates for controlled variables and controller tuning.

Chapter 8 presents and discusses the obtained results. The results include finalization of the model, implementation of the NMPC and six case studies. For the case studies, selected simulations are presented and discussed.

Chapter 9 gives conclusions based on the considerations done and the obtained results. At last, recommendations about further work are made.

2 Polymerization processes

This chapter presents the theory behind polymerization processes. Some general theory of polymers and polymerization reactions are first covered, before the mechanisms of free-radical polymerization and emulsion- and miniemulsion are presented in further detail.

Extensive research of literature on the theory of polymerization was conducted during the preliminary project[9]. Both the reactor model developed in the preliminary project and the NMPC implementation performed in this master thesis have their foundation on the theory presented in this chapter. Additionally, an understanding of the presented theory is beneficial when considering the NMPC implementation in this thesis. This implies that the theory presented in this chapter highlights the same aspects as the theory presented in the preliminary project since it is based on the same literature research.

2.1 Polymers

Polymers are macromolecules built up by the linking together of a large number of much smaller molecules, typically called monomers[10]. The large macromolecules are often referred to as polymer chains. Polymer chains can arrange themselves in almost an infinite number of ways, which give rise to a wide range of properties[11]. Some of these properties, such as rubber-like properties, are unique to polymers because of the chain structure. Properties of the polymer are also dependent on which type of monomer the polymer chain is built up of[10]. A polymer chain can consist of only one type of monomer or several types of monomers. Polymers comprised of only one type of monomer are called homopolymers, while polymers comprised of several types of monomers are called copolymers[12]. Copolymers can be further divided into groups depending on how the monomer types arrange themselves in the chain. These subgroups are periodic-, random-, block- and graft-polymers, and are shown in figure 2.1 along with a homopolymer[13].

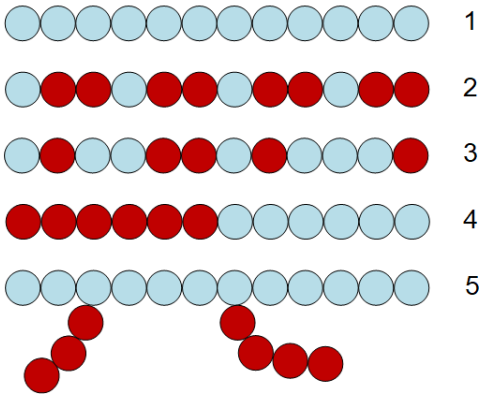

Figure 2.1: Homopolymer (1), Periodic polymer (2), Random polymer (3), Block polymer (4) and Graft polymer (5). The figure is adapted from Store norske leksikon[13].

An example of a copolymer is ABS-plastic which is comprised of three monomers, namely acrylonitrile, butadiene and styrene[13]. PVC is a typical homopolymer, where the polymer chain is built up of vinyl chloride monomers. The PVC polymer chain is shown in equation 2.1[2].

$$[- C_2H_3Cl -]_n \tag{2.1}$$

Here n is the number of repeating monomer units, i.e. the number of vinyl chloride molecules linked together. In addition to being a homopolymer, PVC is also a linear polymer which is the simplest arrangement of the polymer chain. A more complex arranged polymer chain is a branched polymer chain. Branched polymers have branches reaching out from the main chain which have a large impact on properties such as stiffness and strength[11]. A schematic illustration of branched polymers are shown in figure 2.2.

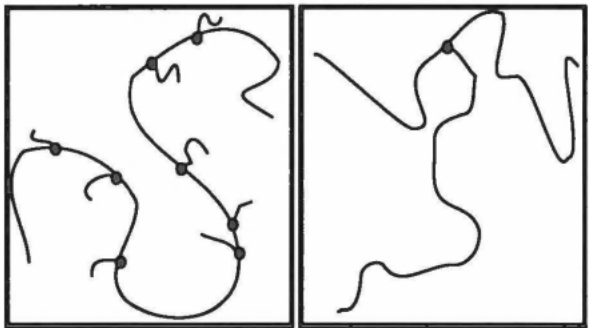

Figure 2.2: A polymer chain with short branching (left) and a polymer chain with long branching (right). The figure is taken from Painter[11].

2.2 Polymerization reactions

The reactions that combine the monomers into polymer chains are termed polymerization reactions. Polymerization reactions can be divided into two distinct mechanisms, namely step- and chain polymerization. A step polymerization is performed with monomers which have two or more reactive groups that may condense intermolecularly to eliminate a by-product[14]. Monomer disappears fast as one proceeds to dimers, trimers, tetramers, and so on. In a step polymerization any two molecules in the reaction mixture can react with each other[10].

A chain polymerization proceeds with addition the of monomer units to an unsaturated chain in rapid succession until the growing chain is deactivated. The monomer units are added to the polymer chain at the active site[10]. For each addition the active site transfers to the end of the chain. A simplified chain polymerization is shown in equation 2.2. It is worth noting that only monomer and the growing chains can react with each other, as opposed to the situation in a step polymerization[14].

$$\mathrm{M} \xrightarrow{activation} \mathrm{M}_1 \cdot \xrightarrow{+M} \mathrm{M}_2 \cdot \xrightarrow{+M} \mathrm{M}_3 \cdot \xrightarrow{+M} ... \xrightarrow{+M} \mathrm{M}_\mathrm{x} \tag{2.2}$$

Here $\mathrm{M}_\mathrm{i} \cdot$ is a growing polymer chain of length i and M_x is a deactivated polymer chain of length x. The synthesis of a single polymer chain is finished in seconds, whereas the overall reaction in the bulk can take hours to reach a satisfactory conversion[15].

2.3 Free-radical polymerization

A free-radical polymerization is a type of chain polymerization where the active site is radicals, which are highly reactive[15]. The polymerization of VCM to PVC follows a free-radical polymerization and consists of three main mechanisms, namely initiation, propagation and termination.

2.3.1 Initiation

The initiation process is the first reaction step in a free-radical polymerization and involves two parts; initiator decomposition and chain initiation. The decomposition of the initiator creates primary radicals which further can react with monomer to initiate a polymer chain. Primary radicals can be produced in different ways with the most simple mechanism being that of thermal decomposition[10]. Thermal decomposition involves the homolytic dissociation of a covalent bond which splits the initiator molecule into two radicals[15]. This mechanism is shown in equation 2.3.

$$\mathrm{I} \xrightarrow{k_d} 2\,\mathrm{R}\cdot \tag{2.3}$$

Here I is the initiator, R· is the primary radical and k_d is the decomposition rate constant. The associated rate expression for the thermal decomposition of initiator can be written as

$$R_d = k_d[I], \tag{2.4}$$

where R_d is the reaction rate for the decomposition of initiator and $[I]$ is the initiator concentration[15]. As briefly mentioned the primary radicals formed in equation 2.3 can react with monomer in the chain initiation step, as shown in equation 2.5[15].

$$\mathrm{R}\cdot + \mathrm{M} \xrightarrow{k_i} \mathrm{P}_1 \tag{2.5}$$

Here M is a monomer molecule, P_1 is a growing polymer chain of length one and k_i is the rate constant for chain initiation. The growing polymer chain is a radical which means that the active site has relocated to the polymer chain[15].

It is emphasized that not all primary radicals formed in equation 2.3 initiate a polymer chain. This is due to various phenomena that make the radicals inactive. Examples of such phenomena are the cage effect where the radicals are trapped in a solvent cage that surrounds them, and recombination where the radicals recombine shortly after initiator decomposition[15]. The ability of the primary radicals to initiate a polymer chain is quantified by the initiator efficiency f. The initiator efficiency is defined as the fraction of primary radicals formed in reaction 2.3 that initiates a polymer chain. The value of f is less than unity and typically lies in the range of 0.4-0.9[16]. In most polymerization processes the chain initiation is much faster than the decomposition, implying that the initiator decomposition is the rate determining step[10]. As a result, the choice of initiator is important due to its influence on the initiation and consequently the system dynamics[15]. Utilizing the fact that the initiator decomposition is the rate determining step and introducing the initiator efficiency yields the reaction rate for chain initiation shown in equation 2.6[10].

$$R_I = 2k_d f[I] \tag{2.6}$$

Radical initiation reactions can be divided into two general types based on how the primary radicals are formed. The first type, thermal decomposition, has already been discussed. The second type involves electron transfer. An effective way of generating free radicals by electron transfer reactions is redox initiation[17]. This method has found wide applications and has industrial importance in low-temperature emulsion polymerization, for instance[17]. A prime reason for its wide application is the reasonable rate of radical production over a very wide range of temperatures[10]. Thermal initiators usually give a too

small or too large decomposition rate at the polymerization temperatures used in industry[17]. Consequently, thermal initiators offers less flexibility in terms of polymerization temperature than redox initiators. A typical redox initiator system is shown in equation 2.7[15].

$$\mathrm{ROOH} + \mathrm{Mt^k} \longrightarrow \mathrm{Mt^{k+1}} + \mathrm{RO\cdot} + \mathrm{OH^-} \tag{2.7}$$

Here ROOH is a peroxide, $\mathrm{Mt^k}$ is a metal in oxidation state k, $\mathrm{RO\cdot}$ is an alkoxy radical and $\mathrm{OH^-}$ is hydroxide. If monomer is present the alkoxy radical will react with it and initiate the polymerization reaction[15]. In equation 2.7 the metal is part of a complex formed with other species in the reaction mixture. This complex acts as a catalyst for the radical formation[17]. Redox systems have been used to initiate the polymerization of several vinyl monomers, including VCM.

Equation 2.7 is a simplified description of a redox system. In reality there are several other side reactions that occur simultaneously, which leads to an intertwined and complicated reaction system[17]. Some of the initiator systems used are not well understood and their reaction mechanisms are yet debated. As a result, initiator systems based on a redox mechanism are much harder to model than thermal decomposition systems.

2.3.2 Propagation

The propagation step consists of the growth of the initiated polymer chain in equation 2.5 with the successive additions of a large number of monomer units to the chain end. Each addition transfers the active site to the end of the polymer[10]. The generalized form of the propagation reaction is shown in equation 2.8.

$$\mathrm{P_i} + \mathrm{M} \xrightarrow{k_p} \mathrm{P_{i+1}} \tag{2.8}$$

Here $\mathrm{P_i}$ is a polymer chain radical of length i and k_p is the propagation rate constant. The propagation reaction is usually highly exothermic[10]. Consequently, it is the main culprit for thermal runaways in polymerization reactors due to it being the main source of heat. The associated reaction rate for the propagation reaction can be expressed as

$$R_p = k_p[M]P_{tot} \ , \tag{2.9}$$

where $[M]$ is the monomer concentration and P_{tot} is the amount of chain radicals[10]. Usually the propagation rate constant, k_p, is much larger for very short chains than for longer chains. It drops quickly when the number of repeated units grows, and attains a constant value before the chain contains ten repeated monomer units[18]. When developing theory and models for propagation reactions, k_p is assumed to be independent of chain length. This is considered a reasonable assumption as the number of repeated monomer units, i.e. chain length, typically are in the hundreds[18].

2.3.3 Termination

At some point the propagating polymer chains stop growing and terminates. The termination reaction is a bimolecular reaction between two live polymer chains and can occur through two mechanisms, namely termination by combination or termination by disproportionation[10]. Termination by combination creates a dead polymer with a chain length equal to the sum of the two reacted chains and is shown in equation 2.10[10].

$$\mathrm{P_i} + \mathrm{P_j} \xrightarrow{k_{tc}} \mathrm{D_{i+j}} \tag{2.10}$$

Termination by disproportionation creates two dead chains with lengths equal to their respective live counterparts before the termination reaction and is shown in equation 2.11[10].

$$\mathrm{P_i} + \mathrm{P_j} \xrightarrow{k_{td}} \mathrm{D_i} + \mathrm{D_j} \tag{2.11}$$

In the two equations $\mathrm{D_i}$ represents dead polymer chains, while k_{tc} is the rate constant for termination by combination and k_{td} is the rate constant for termination by disproportionation. The total termination rate is shown in equation 2.12 and it is the weighted sum of the two modes of termination[10].

$$R_t = 2k_t[P_{tot}]^2 \tag{2.12}$$

Here k_t is the total termination rate and is defined as

$$k_t = (1-\epsilon)k_{tc} + \epsilon\, k_{td}\ , \tag{2.13}$$

where $(1-\epsilon)$ and ϵ are the fractions of the total termination which proceeds by combination and disproportionation, respectively[10]. Which mode that contributes more to the total termination rate is to a large extent dependent on the structure of the monomer unit[15].

The termination reaction is diffusion dependent, which introduces some interesting, but often problematic phenomena. As the reaction proceeds, the viscosity of the reaction mixture usually increases. Consequently, diffusion limitations hinder the movement of the polymer chains which in turn slow down the termination reaction. This has unwanted effects which are further discussed in section 2.4.4.

2.4 Emulsion- and miniemulsion polymerization

Emulsion- and miniemulsion polymerization are both covered as the two process share most of their features. Additionally, an understanding of emulsion polymerization is beneficial in order to understand miniemulsion polymerization. Both of the two processes follows the free-radical chain mechanism presented in section 2.3 and the reaction mixtures are comprised of virtually the same species, with only few exceptions. The main distinction between emulsion- and miniemulsion polymerization is how the polymer particles are created, or in other words how the nucleation stage proceeds. After the nucleation stage the mechanisms which govern the polymerization process are the same[19].

The basis for both an emulsion- and miniemulsion polymerization is the emulsification of a water insoluble monomer in water. Shear is applied to the mixture to create monomer droplets which are stabilized by a surfactant[19]. Monomer droplets formed in a miniemulsion are significantly smaller than the ones formed in an emulsion due to the intensity of the shear applied[20]. The surfactant acts as a surface-active agent with both hydrophilic and hydrophobic properties. It has different tasks in the two processes. In emulsion polymerization the surfactant is used to stabilize the large monomer droplets and polymer particles, as well as to create micelles[18]. Micelles are small colloidal clusters made up of 50-100 surfactant molecules and are swelled by monomer[18]. In miniemulsion polymerization the surfactant is supplemented by a cosurfactant to help with stabilizing the monomer droplets. The surfactant prevents coalescence of the small monomer droplets,

while the cosurfactant reduces Ostwald ripening which is monomer diffusion from small to large monomer droplets[21]. In order to function properly the cosurfactant needs to be highly soluble in the monomer and highly insoluble in water[21].

The polymerization reaction is in both processes initiated by the introduction of a water soluble initiator to the mixture[18]. The reaction loci for the polymerization reaction in an emulsion polymerization is the monomer-swollen micelles, while for a miniemulsion polymerization it is the monomer droplets. The difference in the reaction loci is a result of the nucleation process which is further discussed in section 2.4.1. Except for this difference in the reaction loci, the mechanisms governing the process are very much the same and the polymerization reaction proceeds in three intervals[21]. The three intervals are illustrated in figure 2.3.

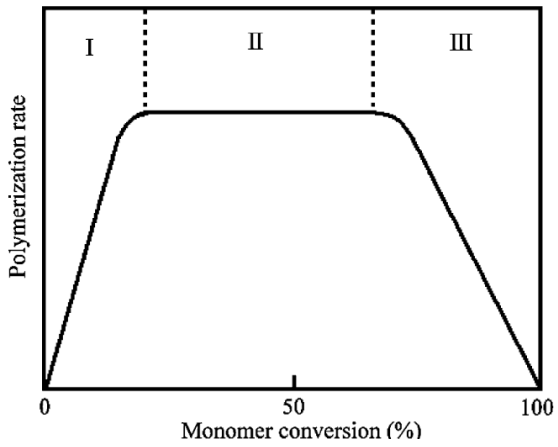

Figure 2.3: Polymerization rate as a function of conversion. The three distinct intervals in which the polymerization reaction proceeds in are also indicated. The figure is taken from Chern[21].

In interval I polymer particles are created by the micelles or monomer droplet being nucleated, all depending on which nucleation mechanism takes place. Interval II starts when the particle number becomes approximately constant and it is characterized by the polymer chains propagating with a free monomer phase present. Interval III is characterized by propagation without a free monomer phase present, which means that it starts at the cessation of the free monomer phase.

2.4.1 Interval I - particle nucleation

Interval I is characterized by the nucleation of particles. Figure 2.3 shows that the polymerization rate increases in interval I. The increased polymerization rate is mainly caused by an increase in the number of particles as more and more particles are nucleated[18]. Interval I is usually the shortest interval, ending when the number of particles becomes approximately constant. The length of interval I is typically to about 2-15% conversion[10].

There are three principal mechanisms in which the nucleation occurs, namely homogeneous nucleation, micellar nucleation and droplet nucleation[18]. All three mechanisms can occur simultaneously, but usually only one mechanism is considered due to the preponderance of it[20]. The starting point for each of the three nucleation mechanisms is the same: the water-soluble initiator creates radicals which initiates a polymer chain in the water phase. The polymer chain first propagates in the water phase, creating an oligomer. An

oligomer is a polymer chain of just a few repeating units[18]. The polymerization rate in the water phase is relatively slow due to the scarce concentration of monomer in the water phase[21]. As the oligomer continues to propagate it becomes less water-soluble until it reaches a critical chain length where one of the three nucleation mechanisms will dominate depending on system conditions.

In the case of homogeneous nucleation the oligomer either terminates or becomes water-insoluble. When the oligomer becomes water-insoluble it precipitates from the water phase to create a primary particle, and it is another reason for the initiator efficiency introduced in section 2.3.1 being less than unity[18]. Homogeneous nucleation is the only mechanism of all three mentioned that can occur in all emulsion polymerization processes, even without any surfactant present[18].

The two remaining nucleation mechanisms are covered in more detail as these are the ones that distinguish emulsion- and miniemulsion polymerization.

Micellar nucleation

Micellar nucleation is the predominant nucleation mechanism in emulsion polymerization and was first proposed by Harkins[22]. If surfactant is present above its critical micelle concentration (CMC) the majority of surfactant is present in the form of micelles and only some surfactant is used to stabilize the large monomer droplets. The micelles have a large number density compared to the monomer droplet in addition to being a lot smaller[21]. This results in the micelles having a much greater total surface area than the monomer droplets. Consequently, the probability of oligomers entering monomer-swollen micelles is much greater than entering monomer droplets[21]. The entering of a oligomer into a micelle is called nucleation and results in a polymer particle where the propagation reaction proceeds.

Droplet nucleation

Due to their large size and low number density, droplet nucleation is usually neglected in regular emulsion polymerization[20]. However, droplet nucleation do occur and Ugelstad et al.[23] showed how small monomer droplets can be made stable enough to become the predominant nucleation mechanism. As already mentioned, the small droplets are formed by a high shear rate and a cosurfactant is needed to help stabilize the droplets.

If the monomer droplet size can be reduced the total surface area of the monomer droplets increases significantly, and this leads to two events. The first is that the increased total surface area increases the probability of oligomers entering the monomer droplets, and the second is that the increase in surface area requires additional surfactant to stabilize the monomer droplets[20]. The surfactant is provided by the break-up of micelles. Decreasing the monomer droplet size make the droplets more competitive with respect to oligomer capture, as well as destroying micelles who also compete for oligomers. The two events described contribute to making droplet nucleation the predominant nucleation mechanism[20]. When an oligomer enters a monomer droplet, a polymer particle is formed where the propagation reaction proceeds. As opposed to polymer particles formed from micelles, polymer particles formed from monomer droplets are self-sufficient on monomer. The polymer particles from micelles are dependent on monomer diffusion from the large monomer droplets that act as reservoirs, while the polymer particles from monomer droplets already have the necessary monomer inside the particles[18, 20].

The distinguishing feature of droplet nucleation as opposed to micellar and homogeneous nucleation is nature of the particles right at the start. Particles which are formed by droplet nucleation start out as nearly 100% monomer, while particles nucleated by homogeneous or micellar mechanisms have much lower monomer concentration[20]. The large monomer concentration is illustrated in figure 2.4a where the green circles represents the monomer droplet. The figure also shows how most of the surfactant is used to stabilize the monomer droplets and with only trace amounts located away from the monomer droplets.

2.4.2 Interval II - particle growth in the presence of free monomer

As already mentioned, interval II begins when the number of particles becomes constant. The polymerization loci are considered to be the particles created in interval I. For both emulsion- and miniemulsion polymerization interval II is characterized by particle growth in the presence of a free monomer phase. In an emulsion polymerization the free monomer phase is located in the large monomer droplets which then act as reservoirs for the nucleated micelles[18]. The free monomer phase is located inside the nucleated monomer droplets in a miniemulsion polymerization, as shown in figure 2.4b[20]. In addition to the free monomer phase, a gas phase, a water phase and a polymer phase are also present, resulting in a total of four phases present during interval II.

Due to the presence of the free monomer phase the monomer concentration inside the polymer particles is approximately constant during interval II[20]. The cessation of the free monomer phase marks the end of interval II. Consequently, the number of phases decreases from four to three. The transition from interval II to interval III occurs at about 70-80% for the polymerization of VCM[10].

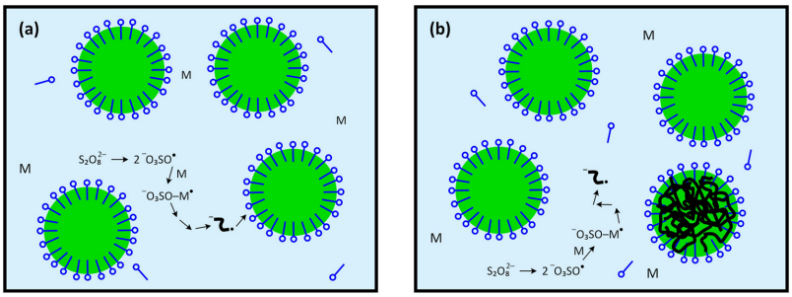

Figure 2.4: **a)** The reaction mixture at the onset of polymerization when the oligomer (black line) is about to enter the monomer droplet(green). **b)** The reaction mixture during the polymerization with a propagating chain inside a nucleated monomer droplet(polymer particle). The surfactant (blue dots with a tail) is located mostly at the monomer droplets. The figure is taken from Lovell & Schork[18].

2.4.3 Interval III - particle growth in the absence of free monomer

As the free monomer phase disappears most of the monomer left in the system resides in the polymer phase, and the polymer particles remain the loci of the polymerization reaction[18]. Due to the absence of excess monomer, the monomer concentration in the polymer phase decreases during interval III. Consequently, the monomer concentration in the water phase and gas phase also decreases. The decreasing amount of monomer in the gas phase leads to a pressure drop, and it is another indication that the polymerization reaction enters interval III[18]. As the pressure decreases the gas temperature also decreases. The concentration decreases in all three phases until all monomer is consumed

or limiting factors stop the reaction[18]. As the monomer concentration in the polymer phase decreases, the internal viscosity inside the polymer particles increases. The increased viscosity results in a greatly reduced termination rate which is the basis for the autoacceleration phenomenon[21].

2.4.4 Trommsdorff effect

Polymerization processes, such as miniemulsion polymerization, which follow the free-radical chain polymerization are characterized by the presence of an autoacceleration at an intermediate or high degree of conversion[24]. The effect is often referred to as the Trommsdorff effect.

As mentioned in section 2.4.3 the viscosity inside the polymer particles increases when the monomer concentration decreases, resulting in a significant drop in the termination rate. The drop in the termination rate can be of several orders of magnitude and is due to the termination rate being diffusion controlled[18, 24]. Due to the increased viscosity, diffusion of polymer radical chains are hindered which in turn affect the termination rate. The decreased termination rate corresponds to a dramatic increase in the radical concentration inside the polymer particles[20]. Consequently, the large radical concentration results in an autoacceleration of the effect through an increase of the propagation reaction which further increases the viscosity[20].

The Trommsdorff effect is highly undesired in industrial applications because it causes a dramatic temperature increase due to the exothermic nature of the polymerization reaction[24]. The dramatic temperature increase might lead to hot spots, instabilities and erratic behavior in the polymerization reactor[24]. Industrial plants often operate at conditions far from optimal in order to reduce the risk of unstable operation caused by the Trommsdorff effect[24]. Implementing NMPC might help to push the operating conditions to the limit if the Trommsdorff effect can be accounted for in the model. This would in turn result in better reactor performance, and simultaneously not jeopardize safety considerations.

2.4.5 Number of particles

The number of particles in an emulsion- and miniemulsion polymerization process is hard to model. This is because all three nucleation mechanisms presented in section 2.4.1 happen simultaneously. This makes the particle nucleation stage complex and it is yet not well understood even though it has been subject of many investigations over the years[25].

Smith & Ewart were the first to quantify the nucleation mechanism when micellar nucleation is predominant with the expression shown in equation 2.14[26].

$$N_{T,n} = k \left(\frac{\varrho}{\mu} \right)^{0.4} (a_S S)^{0.6} \tag{2.14}$$

Here $N_{T,n}$ is the total number of particles, k is a parameter which can vary between 0.37 and 0.53, ϱ is the volumetric rate of formation of free radicals, μ is the rate of increase in volume of a particle, a_S is the interfacial surface area occupied by a surfactant molecule and S is the total concentration of surfactant[10]. The basis for Smith & Ewarts derivation of equation 2.14 was a styrene system which the theory describes well[26]. Even though equation 2.14 describes the styrene system well, the equation is only rarely in accord with experiments and large deviations have been observed when describing other monomer

systems[15, 25]. Despite this, the work of Smith & Ewart is considered the foundation of later development in emulsion polymerization.

There are two reasons that alternative approaches should be utilized in order to obtain the total number of particles for the miniemulsion polymerization of VCM. As already mentioned, equation 2.14 fails for most monomer systems, including polymerization of VCM[27]. Secondly, the theory was derived for a system where micelle nucleation was the most dominant nucleation mechanism. A viable approach is to model the total number of particles as a constant calculated from measurements of a previous batch. The system is then modelled as a seeded system, which is a system where polymer particles of known size are added to the reaction mixture. The nucleation stage is hard to reproduce consistently and with this approach the nucleation stage is skipped and the reaction then starts out in interval II with a constant number of particles[20]. This outlined approach is presented in appendix A.2.6.

2.4.6 Radical distribution and compartmentalization

Radical compartmentalization

Perhaps the most striking feature of both emulsion- and miniemulsion polymerization is the segregation of free radicals among the polymer particles[21]. In bulk polymerization the radicals reside in the same space, which implies that a radical can easily terminate with every other radical present in the entire system. In emulsion- and miniemulsion however, the radicals are only able to terminate with other radicals inside the same polymer particle[19].

This compartmentalization effect in emulsion- and miniemulsion polymerization offers some fascinating properties which are not possible in any other polymerization process[21]. Since radicals are only able to terminate with other radicals in the same polymer particle the probability of termination is reduced significantly[21]. This reduction results in longer lifetimes of the growing polymer chains, which corresponds to a higher molecular weight[18]. In addition, the compartmentalization can also result in a higher polymerization rate[28]. Both of these features can be obtained by altering just the number of particles: the radical concentration increases with the number of particles, while the entry frequency of radicals decreases[16]. A higher radical concentration increases the polymerization rate due to the sensitivity towards $\bar{n}$ in equation 2.19. As already mentioned, a lower entry frequency allows for longer lifetimes of the growing polymer chains which in turn result in higher molecular weights.

Average number of radicals per particle

In addition to the total number of particles, the average number of radicals per particle is one of the parameters which is the hardest to predict in emulsion- and miniemulsion polymerization[21]. The importance of the average number of radicals per particle can not be overemphasized due to its central role in the understanding of the kinetics for both emulsion- and miniemulsion polymerization. The average number of radicals per particle, $\bar{n}$, is defined as

$$\bar{n} = \frac{\sum_{n=0}^{\infty} n N_{p(n)}}{\sum_{n=0}^{\infty} N_{p(n)}} \,, \tag{2.15}$$

where $N_{p(n)}$ is the number of particles with n radicals[16]. The value of $\bar{n}$ is determined by

radical absorption from the water phase into particles, radical desorption from particles and bimolecular radical termination within particles[15]. In order to calculate $\bar{n}$, Smith & Ewart formulated a population balance describing $N_{p(n)}$ in the form of an infinite set of ordinary differential equations. The general population balance equation for $n = [0, 1, 2, ..., \infty]$ is shown in equation 2.16[26].

$$\begin{aligned}\frac{dN_{p(n)}}{dt} = \sigma \left[N_{p(n-1)} - N_p(n)\right] + k' \left[(n+1)N_{p(n+1)} - nN_{p(n)}\right] \\ + C \left[(n+1)(n+2)N_{p(n+2)} - n(n-1)N_{p(n)}\right]\end{aligned} \tag{2.16}$$

Here σ is the rate coefficient of radical absorption, k' is the rate coefficient for radical desorption and C is the rate coefficient for radical termination in polymer phase[29]. Various approaches for solving the set of equations have been reported by several authors, with Smith & Ewart presenting helpful solutions for three limiting cases at pseudo-steady state[21]. These cases are presented below and illustrated in figure 2.5.

- **Case 1,** $\bar{n} < 0.5$: This case is characterized by fast desorption[18]. Consequently, particles contain at most one radical with an average of far less than unity. In general, systems which proceeds under case 1 conditions usually have small particles[18]. Several emulsion polymerization processes proceed under such conditions, including emulsion polymerization of VCM. For emulsion polymerization of VCM the value of $\bar{n}$ ranges from 0.0005 to 0.1[30].
- **Case 2,** $\bar{n} = 0.5$: This case is the result of instantaneous termination when a second radical enters a particle already containing a radical, along with a complete absence of radical desorption[18]. Since termination is instantaneous the average particle will contain either zero or one radical, with an average of 0.5. Case 1 and case 2 are known as zero-one systems where the probability of a particle containing more than one radical is much less than it containing zero or one[18]. Miniemulsion polymerization processes typically proceed under case 2 conditions with values of $\bar{n}$ close to 0.5[31].
- **Case 3,** $\bar{n} > 0.5$: The conditions for case 3 is fast absorption of radicals into particles in addition to the termination rate no longer being instantaneous when a second radical enters a particle[18]. An underlying presumption for this case made by Smith & Ewart were that a particle was large enough to accommodate more than one propagating chain radical[18]. Suspension polymerization systems generally have large particles and thus proceed under case 3 conditions[15].

Obtaining $\bar{n}$ from equation 2.15 requires solving the set of ordinary differential equations in equation 2.16. Other less extensive approaches for obtaining $\bar{n}$ have been researched, with Li & Brooks[29] being one example of such an approach. The approach is further presented in appendix A.2.4.

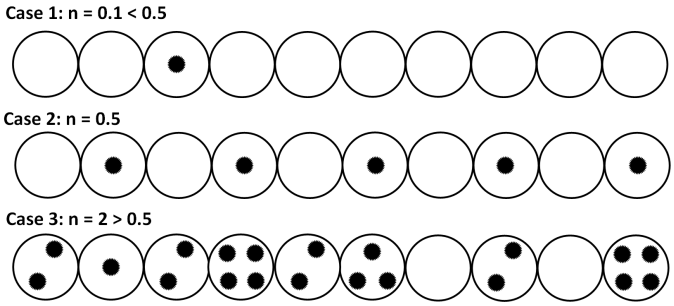

Figure 2.5: Illustration of the three limiting cases. Each circle represents a polymer particle and the black dots represent radicals.

2.4.7 Polymerization rate

The rate of polymerization is usually defined as the rate of consumption of monomer[28]. In the case of a miniemulsion polymerization process which follows a free-radical chain mechanism, the polymerization rate is set equal to the propagation rate in equation 2.9. The assumption that the polymerization reaction happens mainly inside the polymer particles (polymer phase) leads to the expression for the polymerization rate shown in equation 2.17[16].

$$R_p = k_p[M]^p P_{tot}^p \tag{2.17}$$

Here $[M]^p$ is the monomer concentration in the polymer phase and P_{tot}^p is the amount of chain radicals in the polymer phase. The rate expression in equation 2.17 depends on the amount of chain radicals in the polymer phase which is hard to measure and varies randomly from particle to particle due to the stochastic absorption and desorption of radicals[10, 16]. Instead, a more convenient approach of considering an average polymer particle is utilized which leads to the expression for P_{tot}^p shown in equation 2.18.

$$P_{tot}^p = \bar{n} N_T \tag{2.18}$$

Here $\bar{n}$ is the average number of radicals per particle and N_T is the molar amount of particles in the system[16]. The resulting expression for the reaction polymerization can then be written as

$$R_p = k_p[M]^p \bar{n} N_T \tag{2.19}$$

From equation 2.19 it is evident that modelling $\bar{n}$ and N_T sufficiently accurate are of great importance. This is again because of the exothermic nature of the polymerization reaction. Even tiny deviant values for either $\bar{n}$ or N_T have a large impact on the heat of reaction. From a control perspective, deviations between the modelled polymerization rate and the real polymerization rate can make the controller provide wrong input moves to the reactor. An example can be that the controller provides too little cooling which can cause a thermal runaway.

3 Constrained optimization, model predictive control and estimation

This chapter aims to provide the background theory on constrained optimization, model predictive control and estimation. Constrained optimization is presented first as it is the foundation of model predictive control, which is presented next. State- and parameter estimation will prove important for the implementation of model predictive control and the concepts behind the celebrated Kalman filter are covered towards the end of this chapter.

3.1 Constrained optimization

Constrained optimization is about minimizing functions subject to constraints on the variables. This means that the variables have to lie in some range in order to give an acceptable solution.

3.1.1 The general optimization problem

A typical constrained optimization problem is comprised of three main components, namely an objective function, decision variables and constraints. The objective function is a scalar function which is to be minimized or maximized and a typical objective function could include energy usage, profit or raw material usage. The minimization/maximization is achieved by altering the decision variables while still obeying the constraints[32]. Constraints are mainly divided into two main types; equality constraints and inequality constraints. A mathematical description of a constrained optimization problem is shown in equation 3.1[32].

$$\min_{\phi \in \mathbb{R}^n} J(\phi) \tag{3.1a}$$

subject to

$$c_i(\phi) = 0, \quad i \in \mathcal{E} \tag{3.1b}$$

$$c_i(\phi) \geq 0, \quad i \in \mathcal{I} \tag{3.1c}$$

Here $J(\phi)$ is the objective function and it takes in the n-dimensional vector ϕ, which contains the decision variables. The constraints are represented by $c_i(\phi)$, $\mathcal{E}$ is the index set of the equality constraints and $\mathcal{I}$ is the index set of the inequality constraints[32]. The problem stated in equation 3.1 is a minimization problem, but if the objective function is profit we clearly want to solve a maximization problem. Converting from a minimization problem to a maximization problem can be done by utilizing the simple identity $\max J(\phi) = \min -J(\phi)$[32].

The general problem in equation 3.1 can be divided into more specific problems based on the nature of the objective function and the constraints. If both the objective function and all the constraints $c_i(\phi)$ are linear, equation 3.1 is a linear program (LP). When the objective function is a quadratic function and all constraints $c_i(\phi)$ are linear, equation 3.1 is a quadratic program (QP). When either the objective function or at least one of the constraints $c_i(\phi)$ are nonlinear, equation 3.1 is a nonlinear program (NLP). For examples and more details on the classification of constrained optimization problems, the reader is advised to Foss & Heirung[32] where the material in this section is adapted from.

The mentioned types of optimization problems require different techniques to be solved. Solution methods range from explicit solutions to complex iterative procedures. NLP's require such iterative procedures, and one of the most effective methods for solving NLP's is a sequential quadratic programming (SQP) approach. This method involves iteratively solving a QP subproblem[33].

When solving LP's and QP's with an iterative procedure, the initial point ϕ_0 has to lie in the feasible region, i.e. where the constraints are satisfied. In the case of a NLP the initial point does not have to lie in the feasible region[32]. The termination criteria may include one or several criteria, namely a maximum number of iterations, some progress metrics or a characterization of the optimal point[32]. For further details on solution methods for constrained optimization problems, the reader is advised to Nocedal & Wright[33].

3.1.2 Dynamic optimization

Utilizing optimization in real life processes require the handling of dynamic systems. Dynamic systems change with time, implying that variables in the system are time dependent. Such systems are often modelled using differential equations and there exist different approaches to optimize these systems. The two main approaches are quasi-dynamic optimization and dynamic optimization. Quasi-dynamic optimization involves optimizing a dynamic system by repetitive optimization on a static model. This approach works well on slowly varying systems where the dynamic changes can be compensated for by the frequent reoptimization of the static model. For systems where the dynamics plays a major role, like in a polymerization process, dynamic optimization is necessary. Dynamic optimization involves optimizing on a dynamic model and all the decision variables will be time dependent. For further information on dynamic optimization, the reader is advised to Foss & Heirung[32] where the material in this section is adapted from.

A common way of representing dynamic systems is the state space form shown in equation 3.2[32].

$$\begin{aligned} \dot{x} &= f(x,u) \\ x &\in \mathbb{R}^{n_x} \\ u &\in \mathbb{R}^{n_u} \end{aligned} \tag{3.2}$$

Here $f(\cdot)$ is the function of model equations, x is a vector of n_x system states and u is a vector of n_u system inputs. Equation 3.2 is continuous in time, but the optimization problems require discrete time models. A discrete time system is sampled at discrete points in time, usually equidistant. Such a system can be described as

$$\begin{aligned} x_{k+1} &= f(x_k, u_k) \\ x_k &\in \mathbb{R}^{n_x} \\ u_k &\in \mathbb{R}^{n_u} \ , \end{aligned} \tag{3.3}$$

where k is the time sample number[32]. The control inputs u_k are assumed to be piece-wise constant, while the states x_k are only defined for discrete time points.

Since the model described by equation 3.3 propagates through time, the objective function will also include time. A general objective function for a dynamic optimization problem can then be defined as

$$J(x_1, ..., x_{k+1}, u_0, ..., u_k) = \sum_{k=0}^{N-1} J_k(x_{k+1}, u_k) \ , \tag{3.4}$$

where the objective function J_k is defined on a time horizon from 0 to N which is called the prediction horizon[32]. The decision variables are x_{k+1} and u_k and it is worth noting that the initial state x_0 is considered to be known.

Dynamic optimization with nonlinear models

Consider the model equations described by equation 3.3. The model equations are typically nonlinear, i.e. $f(\cdot)$ is a nonlinear function. By using the nonlinear model in equation 3.3 and the objective function in equation 3.4, the dynamic optimization problem can be expressed as equation 3.5. It is assumed that the objective function is quadratic, which is a widespread formulation[32].

$$\begin{aligned} \min_{\phi} \sum_{k=0}^{N-1} J_k(x_{k+1}, u_k) = \min_{\phi} \sum_{k=0}^{N-1} \Big(& \frac{1}{2} x_{k+1}^\top Q_{k+1} x_{k+1} \\ & + \frac{1}{2} u_k^\top S_{1,k} u_k + \frac{1}{2} \Delta u_k^\top S_{2,k} \Delta u_k \Big) \end{aligned} \tag{3.5a}$$

subject to

$$x_{k+1} = f(x_k, u_k) \ , \qquad k = 0, ..., N-1 \tag{3.5b}$$
$$x_0, u_{-1} = \text{known} \tag{3.5c}$$
$$x^{low} \leq x_k \leq x^{high} \ , \qquad k = 1, ..., N \tag{3.5d}$$
$$u^{low} \leq u_k \leq u^{high} \ , \qquad k = 0, ..., N-1 \tag{3.5e}$$
$$\Delta u^{low} \leq \Delta u_k \leq \Delta u^{high} \ , \qquad k = 0, ..., N-1 \tag{3.5f}$$

where

$$Q_k \succeq 0 \ , \qquad k = 1, ..., N \tag{3.5g}$$
$$S_{1,k} \succeq 0 \ , \qquad k = 0, ..., N-1 \tag{3.5h}$$
$$S_{2,k} \succeq 0 \ , \qquad k = 0, ..., N-1 \tag{3.5i}$$
$$\Delta u_k = u_k - u_{k-1} \tag{3.5j}$$
$$\phi^\top = (x_1^\top, ..., x_N^\top, u_0^\top, ..., u_{N-1}^\top) \tag{3.5k}$$

The first term in equation 3.5a is the penalization on the states, the second term is penalization on inputs and the last term is penalization on input moves. This formulation allows for different penalization on different states and inputs by adjusting the values in the matrices Q_k and $S_{1,k}$. Altering the values in $S_{2,k}$ adjusts the aggressiveness of the

controller and in turn how much wear and tear the inputs experience due to moving. Equation 3.5b includes the nonlinear state equations as equality constraints such that the system follows the state equations. Upper and lower constraints are placed on the states in equation 3.5d and could for example be an upper and lower temperature limit. The same is done for the inputs in equation 3.5e and this could for example be constraints on a valve. Equation 3.5f is the constraints on how much an input can change in one sample. The matrices Q_k, $S_{1,k}$ and $S_{2,k}$ are assumed to be symmetric and positive semi-definite[32].

The nonlinear state equations introduce nonlinear equality constraints in equation 3.5b. From the classification of optimization problems in section 3.1.1, an optimization problem with nonlinear constraints is a NLP. NLP's are nonconvex optimization problems, which complicates the solving of the optimization problem[33]. The solution requires more runtime and a solution, if it exists, may not be found. In addition there are few ways to determine the quality of the solution.

3.1.3 Single shooting

As mentioned in section 3.1.2 the optimization solvers require a discrete formulation of the optimization problem. This means that the continuous, infinite dimensional problem is approximated by a finite dimensional NLP. One branch of constructing the finite NLP is the direct methods, which can be further divided into direct single shooting, direct multiple shooting and direct collocation[34]. These three methods differ in how they transcribe the infinite problem into a finite NLP. Direct single shooting has the most simple structure and is presented in further detail due to its relevance for this thesis. For more details on direct multiple shooting and direct collocation, the reader is advised to Diehl & Gros[34] where the material in this section is adapted from.

To illustrate the concept of single shooting, a continuous dynamic optimization problem is defined[34].

$$\min_{x,u} \int_0^T J(x(t), u(t))\, dt + E(x(T)) \tag{3.6a}$$

subject to

$$\dot{x} = f(x(t), u(t)) \tag{3.6b}$$

$$g(x(t), u(t)) \leq 0 \tag{3.6c}$$

$$r(x(T)) \leq 0 \tag{3.6d}$$

$$x(0) = x_{t_0} \tag{3.6e}$$

Here $J(\cdot)$ is the objective function, $E(\cdot)$ is the terminal cost, $f(\cdot)$ are the model equations, $g(\cdot)$ are the path constraints on states and inputs, while $r(\cdot)$ are the terminal constraints. An optimization solver can not handle this formulation of the problem, so the problem is transcribed to a finite problem that the optimization solver can handle[34].

First the control function $u(t)$ is discretized into a piecewise constant profile. The finite control parameters are denoted q_k, yielding the control profile

$$u(t, q) = q_k \ , \ t \in [t_k, t_{k+1}] \tag{3.7}$$

where $q = [q_0, ..., q_{N-1}]$. For single shooting the states $x(t)$ on $t \in [0, T]$ are regarded as dependent variables that are obtained from forward integration of the model equations starting at x_0 and using the control profile in equation 3.7[34]. The resulting state trajectory is labeled $x(x_0, t, q)$. The finite NLP can be written as

$$\min_q \sum_{k=0}^{N-1} J(x(x_0, t, q), u(t, q)) + E(x(x_0, T, q)) \tag{3.8a}$$

subject to

$$g(x(x_0, t_k, q), u(t_k, q) \leq 0 \tag{3.8b}$$

$$r(x(x_0, T, q) \leq 0 \ , \tag{3.8c}$$

where the path constraints $g(\cdot)$ are evaluated at time check points t_k, also called coincidence points[34]. In equation 3.8 the decision variables are the discretization variables q_k and the states $x(t)$ are obtained using an integrator. The concept of direct single shooting is summarized in algorithm 1.

Algorithm 1: Single shooting

1. Discretize $u(t)$
   (a) $u(t) \rightarrow q = [q_1, ..., q_N]$
2. Integrate the system to obtain states as a function of q
   (a) $x = x(x_0, t, q)$
3. Feed the new problem to an optimizer with q as decision variable. The solution is the vector $q*$ which minimizes the objective function in eq. 3.8

The main advantage of the single shooting method is the relatively small number of decision variables and its simple structure. However, the direct single shooting method often suffers from propagation of nonlinearity if the integration time is set too large[34]. A solution to this is to choose a smaller integration time or to choose another method like direct multiple shooting which handles the nonlinearity issues better.

3.2 Model predictive control

Model predictive control (MPC) is a form of control in which at each sample, the control action is obtained by solving a finite horizon open loop optimal control problem with the current state of the plant used as an initial point[32]. The optimization problem yields an optimal control sequence, but only the first control element is implemented to the plant before the the procedure repeats at the the next sample. The system to be controlled is usually described by differential equations[35].

Figure 3.1 shows the concept behind MPC. At each sample the MPC solves a similar optimization to that in equation 3.5 with only the initial point changed from the previous sample. The use of the current state of the system as the initial point for the optimization problem is what couples open loop optimization with feedback[36]. How to obtain this initial point is a central question. One option is to utilize the predicted model behavior to find the next point and this is called state feedback MPC. However, this prediction does not account for errors in the discrete time model or disturbances that occur between the samples[32]. A better option is to compute a state estimate which relies on the latest available measurements[32]. This is called output feedback MPC. The state estimate updates

the process model to maintain satisfactory predictions of the future process behavior. The state estimation is often performed using a Kalman Filter (KF) which is presented in section 3.3.

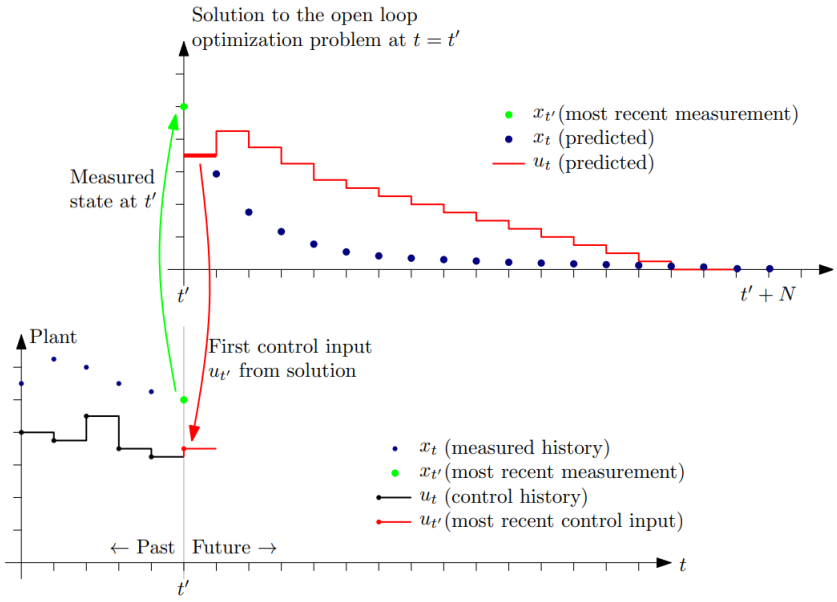

Figure 3.1: Conceptual sketch of how MPC works. The top graph shows the prediction of both the state and the input. The bottom graph shows the past trajectory of the state and input. The green dot is the measurement at the current sample time and is used as an initial point for the optimization problem which finds an optimal input trajectory. Only the first control move in this trajectory is implemented to the process. The figure is taken from Foss & Heirung[32].

The MPC predicts the behavior of the plant for a finite set of time intervals. This finite set of time intervals is called the prediction horizon and is represented by the blue dots in figure 3.1. Control inputs are computed for the entire control horizon and is represented by the red "stairs" in the top graph in figure 3.1. The control horizon is the interval where the inputs are allowed to change and after the control horizon the inputs are constant until the end of the prediction horizon[32]. Both the length of the prediction and control horizon can be regarded as tuning parameters for the MPC, and the control horizon should be equal to or less than the prediction horizon. As time progresses the point t' in figure 3.1 will move forwards in time, meaning that the prediction horizon also will move forward in time. Hence MPC uses a so-called moving horizon approach[36].

The optimization problem for MPC resembles that of equation 3.5, but instead of controlling states, output variables of the model are controlled in the MPC problem. The output variables are related to the system states by a measurement function as shown in equation 3.9[32].

$$z_k = h(x_k, u_k) \tag{3.9}$$

A general optimization problem used in NMPC is shown in equation 3.10[32]. As mentioned above, it is often desired to control the output variables z, so the optimization problem is formulated using the output variables. It is worth noting that the variable z_k represents the difference between the actual variable and its respective setpoint, $(z_k - z_k^{ref})$[36].

$$\min_{u} \sum_{k=0}^{N-1} \left(\frac{1}{2} z_{k+1}^{\top} Q_{k+1} z_{k+1} + \frac{1}{2} u_k^{\top} S_{1,k} u_k + \frac{1}{2} \Delta u_k^{\top} S_{2,k} \Delta u_k \right) + z_N^{\top} Q_N z_N \tag{3.10a}$$

subject to

$$x_{k+1} = f(x_k, u_k) \,, \qquad k = 0, ..., N-1 \tag{3.10b}$$
$$z_k = h(x_k, u_k) \,, \qquad k = 0, ..., N-1 \tag{3.10c}$$
$$x_0, z_0, u_{-1} = \text{known} \tag{3.10d}$$
$$z^{low} \leq z_k \leq z^{high} \,, \qquad k = 1, ..., N \tag{3.10e}$$
$$u^{low} \leq u_k \leq u^{high} \,, \qquad k = 0, ..., N-1 \tag{3.10f}$$
$$\Delta u^{low} \leq \Delta u_k \leq \Delta u^{high} \,, \qquad k = 0, ..., N-1 \tag{3.10g}$$

The matrices Q, S_1 and S_2, in addition to Δu are defined as in section 3.1.2. The last term in equation 3.10a is used to ensure stability of the MPC controller[32]. Weights in Q_N are usually set quite large to penalize any deviations towards the end of the prediction horizon more. In practice stability is not an issue if the controller is tuned properly with respect to the model and the length of the prediction horizon. Stability can also be ensured by increasing the length prediction horizon[36].

In the above formulation of the NMPC problem, infeasible solutions may occur. An example of this may be a disturbance which pushes the states outside its constraints for all possible input moves. This leads to an infeasible solution and a control move is not available, which is an unacceptable situation. A solution to prevent the controller finding infeasible solutions leading to no control moves is introducing soft constraints in the form of slack variables[36].

3.2.1 Feasibility and constraint handling

There is one general distinction between input constraints, and state or output constraints; the input constraints often represent physical limits, while the state or output constraints are normally just desirable[35]. Constraints on model states and outputs may be relaxed, becoming soft constraints. Soft constraints differ from hard constraints in that they can be violated. They are introduced by adding penalty functions and slack variables to the optimization problem[32]. This results in there being no mathematical infeasible solutions with respect to states or outputs, and violation of the constraints are only penalized. With the addition of soft constraints, the optimization problem used for NMPC can be rewritten as in equation 3.11[32].

$$\min_{u} \sum_{k=0}^{N-1} \left(\frac{1}{2} z_{k+1}^{\top} Q_{k+1} z_{k+1} + \frac{1}{2} u_k^{\top} S_{1,k} u_k + \frac{1}{2} \Delta u_k^{\top} S_{2,k} \Delta u_k \right. \\ \left. + r_1^{\top} \varepsilon + \frac{1}{2} \varepsilon^{\top} diag(r_2) \varepsilon \right) + z_N^{\top} Q_N z_N \tag{3.11a}$$

subject to

$$x_{k+1} = f(x_k, u_k) \,, \qquad k = 0, ..., N-1 \tag{3.11b}$$
$$z_k = h(x_k, u_k) \,, \qquad k = 0, ..., N-1 \tag{3.11c}$$
$$x_0, u_{-1} = \text{known} \tag{3.11d}$$
$$z^{low} - \varepsilon \leq z_k \leq z^{high} + \varepsilon \,, \qquad k = 1, ..., N \tag{3.11e}$$
$$u^{low} \leq u_k \leq u^{high} \,, \qquad k = 0, ..., N-1 \tag{3.11f}$$
$$\Delta u^{low} \leq \Delta u_k \leq \Delta u^{high} \,, \qquad k = 0, ..., N-1 \tag{3.11g}$$
$$\varepsilon, r_1, r_2 \geq 0 \tag{3.11h}$$

Here ε represents the slack variables, while r_1 and r_2 represents the weights on the slack variables. The two terms in equation 3.11a containing ε represents the linear cost and quadratic cost of violating the soft constraints in equation 3.11e, respectively. It is desirable to drive these two terms to zero, and the slack variables should be nonzero only if the corresponding constraints are violated[32].

3.2.2 Input blocking

A common industrial practice when employing MPC is to utilize input blocking. The purpose of input blocking is to reduce the number of independent variables in the dynamic optimization problem used in the NMPC. For linear MPC the effect of input blocking is marginal, but for NMPC the effect may be significant[32]. Reducing the number of independent variables (decision variables) will lower the computational cost when solving the optimization problem. To substantiate the effect of input blocking, consider a system with 5 input variables and a chosen control horizon of 20 time samples, where a single-shooting approach is deployed without input blocking. This results in there being 100 decision variables. If, on the other hand, input blocking is utilized with (for example) five control blocks, the number of decision variables are reduced to only 25. The concept of input blocking is illustrated in figure 3.2.

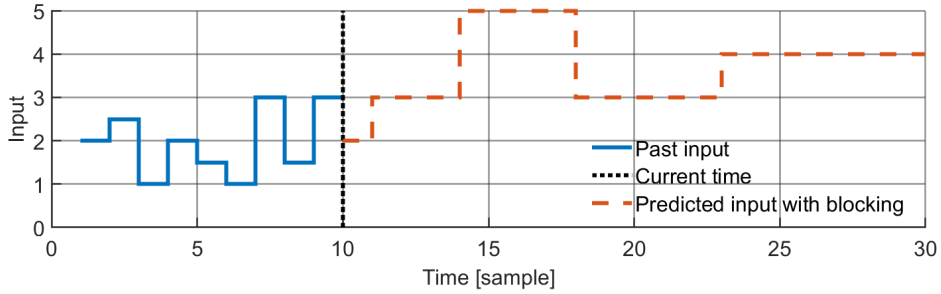

Figure 3.2: Illustration of the concept of input blocking. The past control moves varying at each time sample, while the future control are blocked together in blocks of length 1, 3, 4, 5 and 8 time samples.

The control blocks usually are of increasing size, meaning that the 5 blocks described above could have had lengths equal to that in figure 3.2, namely 1, 3, 4, 5 and 8 samples. Early on in the control horizon, control moves can be quite accurately computed, but further out the control moves does not have to be as accurate. The reason for this is that only the first control move in the prediction is introduced to the plant. The predicted controller moves towards the end of the control horizon will most likely never be implemented. This is because the control moves are recalculated at each time instant and disturbances that the model does not account for might occur in the future[32].

3.2.3 Control hierarchy

The control of a chemical process can generally be divided into a hierarchical structure. Figure 3.3 shows a simplified sketch of two such structures.

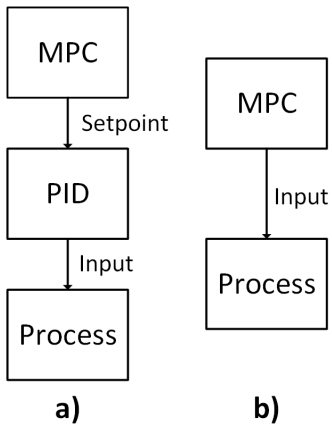

Figure 3.3: Simplified outline of the two control approaches: **a)** The MPC provides setpoints to PID controllers which control the valves/process. **b)** The MPC controls the valves/process directly.

The approach in figure 3.3a is the most common. In this approach the MPC controller is located in the supervisory layer and its manipulated variables (MV's) are typically setpoint values for the underlying PID controllers in the regulatory layer[37]. The PID controllers are organized as a distributed control system (DCS) and they will regulate the process to follow the setpoints provided from the MPC controller[38]. Usually, the PID controllers are tuned according to the SIMC rules which are simple, yet robust and

accurate tuning rules[39]. An important part of this approach is the structure of the DCS, and fortunately a DCS strategy is usually in place when implementing MPC[38]. The existing DCS strategy can then be evaluated and changed, if necessary.

A major advantage of the approach illustrated in figure 3.3a is that when the MPC is switched off or fails, the process still has a fully functioning control system in the form of the DCS. On the other side, a challenge with the approach is to keep the controlled variables (CV's) in a region such that their associated valves do not saturate[38]. If a valve associated with a PID controller saturates a significant portion of the time, it may be preferable to utilize the approach illustrated in figure 3.3b[38].

The approach in figure 3.3b lets the MPC controller directly control the valve openings. This is the main advantage of this approach as it allows for the physical limits of the valve to be strictly enforced by including input constraints in the control formulation[38]. This approach is less widespread and does not include the possibility of using the DCS as a fallback strategy if the MPC fails[38].

3.3 State- and parameter estimation

As discussed briefly in section 3.2 state feedback where the model predictions are used to choose the initial point for the MPC is no realistic option. This approach does not account for model errors or disturbances to the process. For this reason, output feedback, where state estimation is performed based on process measurements is needed.

The purpose of the estimator is to establish a link between the real measured system and the model used in the controller. As mentioned on several previous occasions, a process model will never reflect the real process perfectly. Consequently, the need for an estimator is always present in implementations of a controller in the real world. The grade of updating by the estimator will vary, with an accurate process model requiring less dramatic updates than a poor process model.

The estimation can be performed using various estimation algorithms, with two main estimator classes being the most used. These two classes are moving horizon estimators (MHE) and Kalman filter (KF) estimators. MHE is optimization based and the estimation is performed by solving a finite horizon optimization problem based on past measurements and states[36]. The celebrated Kalman filter is probably the most widely used and it is also used for the work done in this thesis. A linear time-discrete system is the starting point for the basic KF, but the algorithm can be extended to nonlinear systems by deploying the extended Kalman filter (EKF). Both the theory of the KF and the EKF is presented in this section.

3.3.1 Kalman filter

Suppose that the dynamic system is represented by a linear time-discrete model[40].

$$x_k = A_{k-1}x_{k-1} + B_{k-1}u_{k-1} + v_{k-1} \tag{3.12}$$

$$y_k = H_k x_k + w_k \tag{3.13}$$

Here v_k is the process noise and w_k is the measurement noise and they are assumed to be uncorrelated[40]. The process noise v_k has the known covariance matrix V_k, while the measurement noise w_k has the known covariance matrix R_k. The matrix H_k is a selection

matrix and decides which states, or combination of states, that goes into the measurement vector y_k[40].

The KF gives an estimate of the states at time t_k which is then fed to the optimizer as an initial state for the optimization problem. In the calculation process, two state estimates at time t_k are performed. The only difference is the information used to perform the calculation, and it is emphasized that they are estimates of the same quantity x_k. Some notation are introduced to distinguish the different state estimates.

$$\hat{x}_k^- = \text{a priori state estimate} \tag{3.14}$$
$$\hat{x}_k^+ = \text{a posteriori state estimate} \tag{3.15}$$

The a priori state estimate at time t_k is performed with measurements up to y_{k-1}, while the a posteriori state estimate at time t_k is performed with measurements up to y_k[40]. As one additional measurement value is utilized for the a posteriori state estimate, this estimate is expected to be more accurate.

The term P_k is used to denote the covariance of the state estimate error at time t_k and it follows the same notation as the state estimates.

$$P_k^- = E\left[\left(x_k - \hat{x}_k^-\right)\left(x_k - \hat{x}_k^-\right)^\top\right], \text{ a priori covariance} \tag{3.16}$$
$$P_k^+ = E\left[\left(x_k - \hat{x}_k^+\right)\left(x_k - \hat{x}_k^+\right)^\top\right], \text{ a posteriori covariance} \tag{3.17}$$

With the terms for P_k an expression for the a priori state estimate can be formulated, and this formulation is shown in equation 3.18[40].

$$\hat{x}_k^- = A_{k-1}\hat{x}_{k-1}^+ + B_{k-1}u_{k-1} \tag{3.18}$$

Equation 3.18 is called the time-update equation for $\hat{x}$. The propagation of the covariance with time is calculated by

$$P_k^- = A_{k-1}P_{k-1}^+A_{k-1}^\top + V_{k-1} \tag{3.19}$$

and is called the time-update equation for P[40]. Equation 3.18 and 3.19 give the relations for how state estimations and covariances propagate in time, i.e. $\hat{x}_k^+ \to \hat{x}_{k+1}^-$ and $P_k^+ \to P_{k+1}^-$. Relations describing the transitions from a priori estimates to a posteriori estimates, $\hat{x}_k^- \to \hat{x}_k^+$ and $P_k^- \to P_k^+$, are also needed. Equation 3.20 - 3.22 represents the a posteriori estimates[40].

$$\hat{x}_k^+ = \hat{x}_k^- + K_k\left(y_k - H_k\hat{x}_k^-\right) \tag{3.20}$$
$$K_k = P_k^-H_k^\top\left(H_kP_k^-H_k^\top + R_k\right)^{-1} \tag{3.21}$$
$$P_k^+ = \left(I - K_kH_k\right)P_k^- \tag{3.22}$$

Equation 3.20 is the measurement correction of the state estimate, equation 3.21 is the expression for the KF gain matrix and 3.22 is the a posteriori state estimate error covariance. In equation 3.22 the matrix I is the identity matrix.

3.3.2 Extended Kalman filter

In section 3.3.1 the KF for linear systems was introduced. Unfortunately, linear systems do not exist in the real world. All systems are, to some extent, nonlinear[40]. However, many systems are linear enough such that linear estimation approaches yield satisfactory results. A widespread approach is to linearize the nonlinear system and apply linear estimation methods, such as the KF, on the linearized system[40]. This approach is put to use in the EKF.

The system is described by a nonlinear time-discrete model, shown in equation 3.23 and 3.24[40].

$$x_k = f(x_{k-1}, u_{k-1}, v_{k-1}) \tag{3.23}$$
$$y_k = h(x_k, w_k) \tag{3.24}$$

Here $f(\cdot)$ is the nonlinear model and $h(\cdot)$ is the measurement model. The a priori estimates are given by equation 3.25 - 3.27[40].

$$\hat{x}_k^- = f(\hat{x}_{k-1}^+, u_{k-1}, 0) \tag{3.25}$$
$$y_k = h(\hat{x}_k^-, 0) \tag{3.26}$$
$$P_k^- = F_{k-1} P_{k-1}^+ F_{k-1}^\top + L_{k-1} V_{k-1} L_{k-1}^\top \tag{3.27}$$

Here the update equation for the states in equation 3.25 is based on the original nonlinear system, whereas the update for the estimation error covariance matrix in equation 3.27 is based on a linearization of equation 3.23 and 3.24[40]. The update for the estimation error covariance requires the calculation of two Jacobian matrices, which are defined in equation 3.28 and 3.29[40, 41].

$$F_k = \frac{\partial f}{\partial x}\Big|_{x_k^+} \tag{3.28}$$

$$L_k = \frac{\partial f}{\partial v}\Big|_{v_k^+} \tag{3.29}$$

The a posteriori estimates are given in equation 3.30 - 3.32[40].

$$\hat{x}_k^+ = \hat{x}_k^- + K_k \left(y_k - h(\hat{x}_k^-, w_k)\right) \tag{3.30}$$
$$K_k = P_k^- H_k^\top \left(H_k P_k^- H_k^\top + M_k R_k M_k^\top\right)^{-1} \tag{3.31}$$
$$P_k^+ = \left(I - K_k H_k\right) P_k^- \left(I - K_k H_k\right)^\top + \left(K_k M_k\right) R_k \left(K_k M_k\right)^\top \ , \tag{3.32}$$

where the matrices H_k and M_k are defined as in equation 3.33 and 3.34, respectively[40].

$$H_k = \frac{\partial h}{dx}\Big|_{x_k^-} \tag{3.33}$$

$$M_k = \frac{\partial h}{\partial w}\Big|_{w_k^-} \tag{3.34}$$

There exist more accurate approaches with regards to online estimation that are not considered in this thesis. Such methods include iterated EKF and higher order EKF, and the reader is advised to Simon[40] for more elaborate discussions about these methods. These filters provide ways to reduce the linearization error inherent to the EKF. As a result, these approaches typically provide better estimation performance than the EKF. However, this comes with the price of higher complexity and computational cost. This can be a major concern for online applications where it is important for the runtime to be shorter than the time between samples.

3.3.3 Parameter estimation

Online parameter estimation

The theory presented above can be used not only to estimate the states of the system, but also to estimate the unknown parameters of the system. Parameter estimation is probably the most important task of the estimator since we more often than not are interested in estimating unknown parameters rather than the states[40].

Consider the nonlinear model

$$\begin{aligned} x_{k+1} &= f(x_k, u_k, v_k, p) \\ p &\in \theta \end{aligned} \tag{3.35}$$

where p is a subset of all process parameters, θ. In order to estimate the parameter vector p, the state vector is augmented with the parameter vector, resulting in

$$x'_k = \begin{pmatrix} x_k \\ p_k \end{pmatrix} , \tag{3.36}$$

where x_k is the original state vector and x'_k is the augmented state vector. The parameters are modelled as constant, but the model includes a small artificial noise on the parameters. The introduction of noise to the parameters is shown in equation 3.37[40].

$$p_{k+1} = d(p_k, v_{p,k}) \tag{3.37}$$

Here $d(\cdot)$ is the function that adds the noise $v_{p,k}$ to the parameters. The introduction of noise on the parameters allows for the EKF to change its estimate of p_k[40].

The augmented model can be written as equation 3.38[40].

$$x'_{k+1} = \begin{pmatrix} f(x_k, u_k, v_k) \\ d(p_k, v_{p,k}) \end{pmatrix} = f(x'_k, u_k, v_k, v_{p,k}) \tag{3.38}$$

The augmented state vector x'_k can then be estimated by using the same approach as described in section 3.3.2.

For a model derived from first principles the known accuracy of the model parameters vary. Some parameters are known to a high degree of accuracy, while others are practically unknown. Offline parameter estimation, where the parameters are tuned such that model outputs resembles process measurements, is an important tool in the model development. However, offline estimation does not consider time-varying behaviour of some parameters. Adding an estimator to the implementation will capture the time-varying

behavior. Parameters that can benefit from being estimated online are for example heat transfer coefficients and model correction factors. Consider the system of interest in this thesis, namely a semi-batch reactor with a surrounding cooling jacket. During the course of a batch, operating conditions inside the reactor will change, which in turn changes the physical properties of the reaction mixture inside the reactor. Such a physical property may be the viscosity of the mixture. A change in viscosity may have a large impact on the heat transfer coefficient between the reactor and the cooling jacket. By estimating the heat transfer coefficient online, its variation during a batch can be accounted for.

Offline parameter estimation

Offline parameter estimation is used to make the model predictions better reflect the measurements. This is done by adjusting certain model parameters such that the difference between the model predictions and the measurements is minimized. To be able to handle nonlinear systems, a sequential quadratic programming (SQP) algorithm is needed[33]. Such an algorithm is implemented in Cybernetica ModelFit which is presented in section 4.2.

The formulation of the optimization problem that is solved in order to obtain the optimal process parameter values is shown in equation 3.39[33].

$$\min_{\eta} \sum_{k=1}^{N} \left(y_k - y_{m,k}\right)^2, \qquad \eta \in \theta \tag{3.39a}$$

$$\text{s.t. } x_{k+1} = f(x_k, u_k, \theta) \tag{3.39b}$$

$$y_k = h(x_k, u_k, \theta) \tag{3.39c}$$

$$\eta_{min} \leq \eta \leq \eta_{max} \tag{3.39d}$$

Here y_k is a vector containing model outputs, $y_{m,k}$ is a vector containing measurements and x_k is a vector containing the model states. η is the vector of decision variables for the optimization problem, and the decision variables must lie within the bounds η_{min} and η_{max}. It is worth noting that η is a subset of all the process parameters θ. $f(x_k, u_k, \theta)$ and $h(x_k, u_k, \theta)$ are the state- and measurement models, respectively. The SQP algorithm will minimize the objective function in equation 3.39a while still fulfilling the constraints in equations 3.39b, 3.39c and 3.39d.

4 Software

The purpose of this chapter is to provide an overview of the software that has been used during the completion of the work performed in this thesis. Section 4.1 describes the model template used. Cybernetica ModelFit is introduced in section 4.2. Both the model template and ModelFit were utilized in the preliminary project. Section 4.3 gives an introduction to Cybernetica CENIT which is the software used for NMPC. Finally, RealSim which acts as a plant replacement in this thesis, is presented in section 4.4.

The software and the implemented code utilized during the preliminary project and this master thesis is in its entirety confidential. This implies that the exact details regarding the implementation of the model, estimator and controller is not presented here. Instead, this section aims to present the necessary foundation to give an understanding of the how the different programs were used to produce the results presented in this thesis.

4.1 Model code

The model equations were implemented in C-code by using Cybernetica's model template for polymerization processes. The code for the template is confidential and is not presented in its entirety in this report. To be able to perform simulations of the system, states, inputs, outputs, constraints, parameters, constants and internal calculation variables are all defined by the model. Several numerical integration routines such as Euler, second order Runge-Kutta and Sundials CVODES are readily available. Both in the preliminary project and in this master thesis the Euler integration routine was chosen due to its simple structure. Even though the Euler integrator can be prone to numerical issues for stiff systems such as a polymerization process, this has not been a problem in neither the preliminary project or the master thesis. A short integration step has been sufficient to avoid numerical issues and consequently more computationally demanding methods were decided to not be necessary. The equations for Euler integration are presented in appendix D.

The model template is structured in a way that encourages a decoupling of the reactor model and the kinetic model. The decoupling makes it easy to perform changes to the code and try different approaches during the development stage. This was especially helpful in the preliminary project, but also in the initial phase of the master thesis. Since the reactor model and the kinetic model are decoupled, the two models can be implemented independently. For example, the same reactor model can be tested with different kinetic models, and vice versa.

In addition to the implementation of the process model in the model template, code for the estimator and the controller were also implemented. The implementation of the estimator and the controller was performed using an existing code structure with predefined functions. Logic statements for both the estimator and the controller were implemented in order to turn them on and off at the correct time during the batch. The predefined code structure enabled quick changes to both the estimator and controller. This implies that various logic statements could easily be tested and simulated.

4.2 Cybernetica ModelFit

ModelFit is Cybernetica's simulation tool and the ModelFit environment is compatible with the model code. ModelFit offers an easy, flexible and intuitive way of plotting the simulation results. In addition to visualizing the simulations, values for model pa-

rameters, constants, initial values and noise can all be adjusted inside the environment. Measurement- and input values from datasets can easily be loaded and used when simulating the model such that the model can be tested on data from the real process. ModelFit also allows for simulation of several datasets with different values for model parameters. This makes it easy to see the effect certain parameters have on the model.

ModelFit can also be used for offline parameter estimation, and a SQP algorithm such as the one presented in section 3.3.3 is utilized. The environment provides an user-friendly way to decide which parameters to estimate and which measurements to optimize the parameters with respect to. Parameter values obtained from the offline estimation can then be implemented to the model if desired. The offline estimation is an important activity to adjust the model such that it reflects the real process as well as possible.

In addition to offline parameter estimation, ModelFit can also be utilized to tune an online estimator before the model is deployed online. Tuning of the estimator is performed by adjusting the noise on selected states, parameters and measurements. When utilizing this feature, ModelFit sees the measurements and inputs from the datasets as if they were online and not preloaded as for offline parameter estimation. The estimator then updates the model according to the theory presented in section 3.3.2. There are two available estimators, namely the MHE and the EKF. As already mentioned, the EKF was used both in the preliminary project and in this master thesis. The estimator will in this thesis not be highlighted as much as the NMPC implementation, but the NMPC is dependent on working in conjunction with an estimator. The estimator was tuned and its performance was illustrated in the preliminary project. The tuned estimator was brought along to the NMPC implementation in this thesis.

4.3 Cybernetica CENIT

Cybernetica CENIT is the program used for the online control in this thesis. A complete solution for the NMPC with appropriate estimator algorithms is provided by CENIT. It consists of several components; CENIT Kernel, CENIT MMI, the process model and a database. Figure 4.1 shows the interconnection between the components within CENIT.

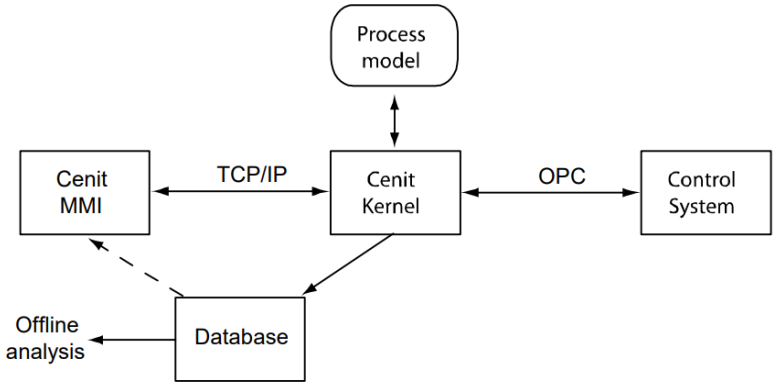

Figure 4.1: System overview that shows the interconnections within Cybernetica CENIT. The figure is included with permission from J.G Dyrset, Cybernetica.

The CENIT Kernel is the main component and it communicates with the process and the calculation algorithms. Communication with the process occurs through an Open Platform Communication (OPC) server that already exists in the control system at the

actual plant. Model updates and controller calculations are performed by the CenitKernel, and are based on predictions from the process model. The database component is optional, but it can prove helpful with respect to offline analysis of the controller performance and operation of the process. The database was used during the work in this thesis.

CENIT MMI is an interactive program with a Windows Graphical User Interface (GUI) and it is used to configure the CENIT Kernel. Configurations that can be performed inside the CENIT MMI environment include estimator tuning, controller tuning, penalization on setpoint deviations and constraint violations, and activation of CV's. As shown in figure 4.1 CENIT MMI communicates with the CENIT Kernel through TCP/IP and can be started on a different computer if desired. This is especially helpful for an application that is implemented in a plant, as one can access the control system remotely. In addition to configuring the CENIT Kernel, CENIT MMI can also be used to monitor model quantities such as CV's, MV's, states and measurements to mention some.

4.4 Cybernetica RealSim and plant replacement

4.4.1 RealSim

In a simulated implementation like in this thesis RealSim acts as a plant replacement. The RealSim GUI offers the possibility to make configurations during the simulations. Parameters and constants can be adjusted, while current values for process inputs, process measurements, calculated variables and process states can be read from the interface. The simulation can be paused, run to a specific sample, and run one sample or one module at a time. The GUI also shows the computation time for each sample. A screenshot of the RealSim GUI is shown in figure 4.2.

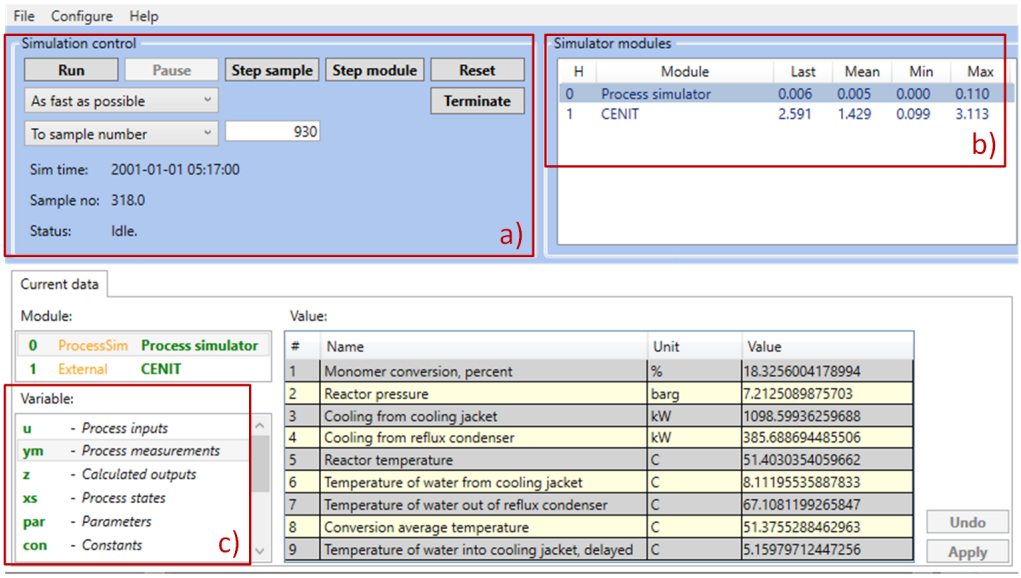

Figure 4.2: Screenshot of the RealSim GUI while the simulation is paused. **a)** Simulation control where the simulation can be paused/run, simulated one sample or one module (simulator-module and NMPC-module), and the desired number of samples can be run. **b)** Mean, minimum and maximum computation time for both the simulator and the NMPC (represented by CENIT). **c)** List of variable types that can be viewed and/or adjusted during the simulation. The screenshot shows the process measurements.

4.4.2 Plant replacement

Testing the controller on the real process was way beyond the scope of this thesis which meant that the concept of plant replacement was used instead. The model developed in the preliminary project, and restated in appendix A was also used as the plant replacement model in addition to being used in the controller. As the term *plant replacement* implies, the real plant is replaced by the developed model. Consequently, the "reality" in this thesis will be the model and not the real plant. Emphasis is put on this fact in order to avoid confusion.

As already mentioned, RealSim was used as the tool for plant replacement. When used as a plant replacement RealSim simulates the behaviour of the process model based on the inputs given to it from the controller. RealSim also provides the necessary measurements to the controller.

The model used for plant replacement can be the same as the model used in the controller, or it can be different. In this thesis the model used in the simulator and the controller was the same. Extensive effort went into tuning the estimator and validating the model against measurements in the preliminary project. A central result from the preliminary project was the estimators ability to closely track the measurements. Since the estimators performance already was established in the preliminary project, it was decided that it was not necessary to introduce model mismatch between the simulator and controller. Consequently, the same model were used in the controller as in the simulator.

5 Process description and control structure

This chapter presents the process and the current control system. Topics covered are the preparation of a batch, description of the different components of the reactor system and a description of how the reactor is currently controlled.

5.1 Process description

This section describes the process which have been considered in the preliminary project and in this thesis. The recipe of the process along with information about some species involved are confidential and are not presented in this report. Instead, generic names are used to describe the process when needed.

The process of interest is a miniemulsion polymerization of VCM into PVC. Relevant mechanisms and phenomena for the process are presented in section 2.3 and 2.4. As this system is part of INOVYN's plant, the names of some species involved in the system are confidential. Consequently, these species are not mentioned in this report, but are rather collected under the generic name *additive*.

The initiator system used in this process is comprised of three main components, each charged into the reactor at separate times. The components create a redox initiator system as described in section 2.3.1. A peroxide is the main part of the initiator system, while the two other components helps with complex formation which act as a catalyst for the production of primary radicals. In a redox initiator system there are several other side reactions in addition to the very simplified reaction in equation 2.7. This makes the redox initiator system extremely entangled. The formation rate of primary radicals are dependent on the concentration of all components participating in the reaction system. Consequently, the initiator system is approximated as the thermal decomposition system described in equation 2.3.

5.1.1 Preparation of a batch

A pre-prepared mixture containing water, surfactant, cosurfactant and the first component of the initiator system is added to the empty reactor. As mentioned above, the specific names of the species are confidential and generic terms are used instead. Additional water is added to the reactor after the pre-prepared mixture is fully loaded into the reactor. The VCM is then added and it diffuses into the already formed droplets. The monomer droplets which function as the reaction loci for the polymerization process described in section 2.4 are at this point formed. A typical nucleated monomer droplet with stabilizers is shown in figure 5.1. The reaction mixture will be comprised of a large number of such particles during the batch.

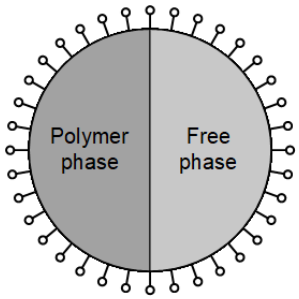

Figure 5.1: A nucleated monomer droplet with the free monomer phase and the polymer phase each occupying some portion of the particle. The spikes on the outside of the particle are the surfactant and cosurfactant which stabilizes the particle.

The initial dose of peroxide is introduced to the reaction mixture when some confidential conditions inside the reactor are met. When the last part of the initiator system is charged into the reactor the polymerization reaction starts.

5.1.2 Reactor system

The reactor is continuously stirred throughout the entire batch. During the course of the batch additives and some water are post-dosed along with the peroxide which is part of the initiator system. This makes the reactor a semi-batch reactor where there are no outlet streams from the reactor during the batch. A sketch of the reactor used for the modelling is shown in figure 5.2.

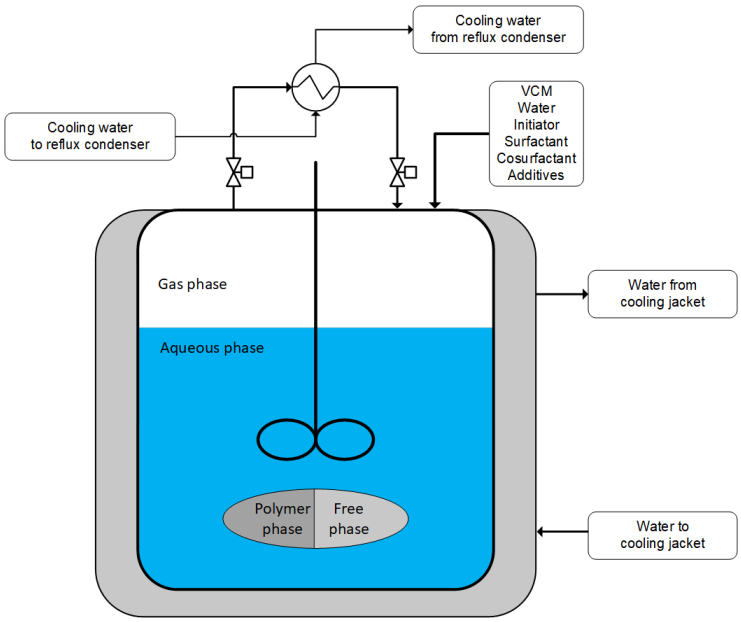

Figure 5.2: Sketch of the reactor, including the four phases present, the cooling jacket with cooling water, the reflux condenser with cooling water and the shut-off valves. In reality there are several inlet streams, but it is shown as one on the sketch for simplicity.

The figure shows that the reactor volume is comprised of either three or four phases depending on the reaction conditions described in section 2.4.1, 2.4.2 and 2.4.3. The illustration of the polymer phase and the free monomer phase is used for illustration

purposes only and does not reflect how the two phases distribute themselves in the reaction mixture. As already shown in figure 5.1 the two phases occupy some portion of the numerous particles present in the reaction mixture.

The polymerization reaction is exothermic as emphasized on several previous occasions. To be able to control the temperature the reactor is surrounded by a cooling jacket. The cooling jacket uses water which flows inside a closed loop to reduce fouling and corrosion inside the cooling jacket. In addition to the cooling jacket a reflux condenser is connected to the top of the reactor, and the reflux condenser further adds to the cooling capacity of the cooling system. At some point in the batch the two valves in figure 5.2 close. This action disconnects the reflux condenser from the reactor and leaves only the cooling jacket in operation. The criteria for when the reflux condenser is closed off is in this thesis set to be when the monomer conversion exceeds 78%.

5.2 Control structure

Both the reflux condenser and the cooling jacket are utilized to control the reactor temperature. The current control structure is based on a cascade structure in addition to split range control. Figure 5.3 shows a simplified sketch of the current control structure.

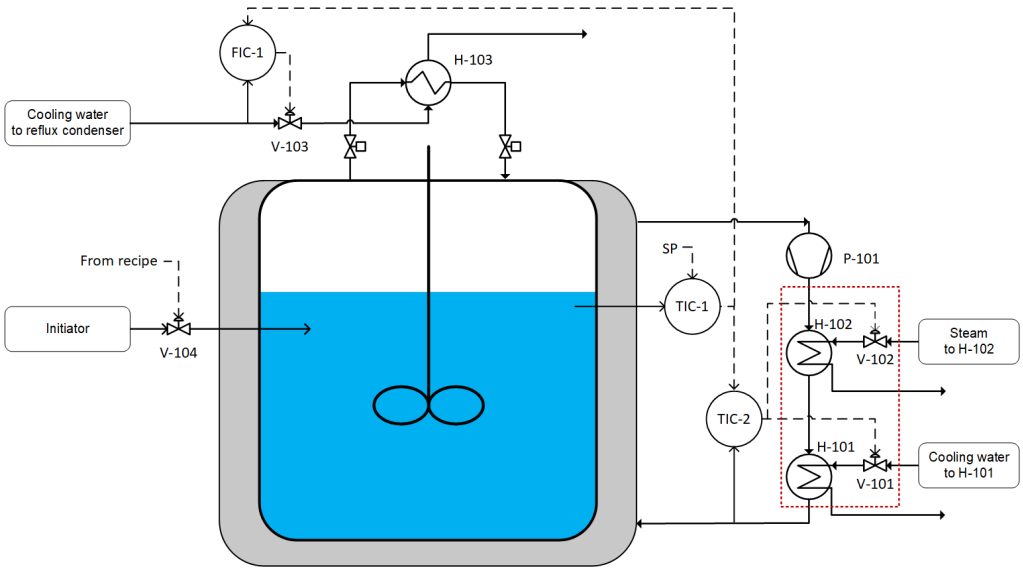

Figure 5.3: Simplified sketch of the current control structure. The main structure is a cascade loop with the reactor temperature as the master and either the volume flow to the reflux condenser or the inlet temperature to the cooling jacket as the slaves, depending on the output signal from TIC-1. A split range structure with V-101 and V-102 is used to control the inlet temperature to the cooling jacket. The initiator dosing is determined from the recipe of the batch. The red box indicates where some modifications were done when implementing the NMPC in this thesis.

The main control structure consists of a cascade with the reactor temperature as the master, and either the volume flow to the reflux condenser or the inlet temperature to the cooling jacket as the slaves. The two slaves are organized in a split range structure. This means that which one of the two slaves is "active" is determined by the output signal from the master controller, and the slave that is not considered to be active operates in a saturated state. The internal control signal graph for this structure is shown in figure 5.4a and it shows that the two slaves operate in different regions of the output signal range.

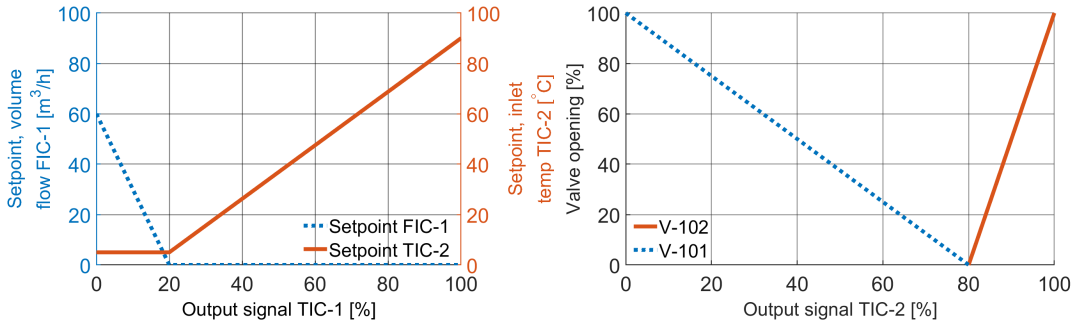

(a) Internal control signal for TIC-1 with scaled y-axis for the two slaves.

(b) Internal control signal for TIC-2.

Figure 5.4: Internal control signals for the current control structure.

To control the inlet temperature to the cooling jacket another split range controller is used. The valve V-101 is used to control the cooling water to H-101, while V-102 is used to control the steam to H-102. Both of the two heat exchangers are used to control the inlet temperature of the water to the cooling jacket, and the internal control signal is shown in figure 5.4b. Steam is only needed when the reactor needs to be heated rather than cooled which means that V-102 is typically closed when the polymerization reaction is proceeding.

The cooling jacket has to be fully saturated, i.e. V-101 fully open, before the reflux condenser starts to cool the reactor. It is worth noting that the volume flow of water through the reflux condenser is limited and V-103 does not open entirely to 100%. This is to prevent a too large cooling effect from the reflux. A too large cooling effect from the reflux condenser will cause a too large gas flow through the reflux condenser. The large gas flow will in turn cause erratic behavior inside the reactor and it had to be taken into account when formulating the control problem in this thesis.

Figure 5.3 also shows the relevant instrumentation that are currently installed at the plant. Both on the steam line to H-102 and the cooling water line to H-101 there are not any measurements of temperature or flow. The lack of measurements has implications for the control structure design inside the red box in figure 5.3 and is further discussed in section 8.2.

6 Modelling of a reactor for miniemulsion polymerization

Some modelling remained to further tailor the model for the use in NMPC. This meant that the introductory phase of the master thesis was used to perform the necessary modelling work. The modelling presented in this chapter is a continuation of the work performed in the preliminary project. The principal goal of the preliminary project was to develop and validate a model of a miniemulsion polymerization process. Process parameters were estimated and the model was compared to measurements from INOVYN's plant. The obtained model with equations and assumptions are presented in appendix A.

In addition to the extensions of the model, adjustments to some model parameters were performed. This was done to adjust the behavior of some model outputs such that the model could be better utilized in NMPC. The details regarding the parameter adjustments are presented in appendix B.

6.1 Conversion average temperature

An important parameter used to describe the quality of the PVC product is the conversion average temperature. The conversion average temperature $\bar{T}_{X_M}$, is defined as

$$\bar{T}_{X_M} = \frac{\int_0^t R_p T_R \, dt}{\int_0^t R_p \, dt} \, , \tag{6.1}$$

where R_p is the polymerization rate and T_R is the reactor temperature. Equation 6.1 can be rewritten to a more practical form by using the relation[42]

$$\int_0^t R_p \, dt = X_M(t) \int_0^t \hat{n}_M \, dt \, , \tag{6.2}$$

where $X_M(t)$ is the monomer conversion and $\hat{n}_M$ is the molar feed rate of monomer. This implies that the integral on the right hand side of equation 6.2 represents the total amount of fed monomer at time t. Since all the monomer is loaded into the reactor before the reaction starts, this integral will in this case be a constant number. Inserting the relation in equation 6.2 into equation 6.1 yields the final expression for the conversion average temperature shown in equation 6.3.

$$\bar{T}_{X_M} = \frac{\int_0^t R_p T_R \, dt}{X_M(t) \int_0^t \hat{n}_M \, dt} \tag{6.3}$$

6.2 Batch time and termination

The batch time is defined as the time it takes to reach a certain monomer conversion, measured from the start of the polymerization reaction. An illustration of the batch time is shown in figure 6.1, where the polymerization reaction starts at about 80 minutes and reaches the final monomer conversion after about 455 minutes. Before 80 minutes the batch is prepared according to section 5.1.1.

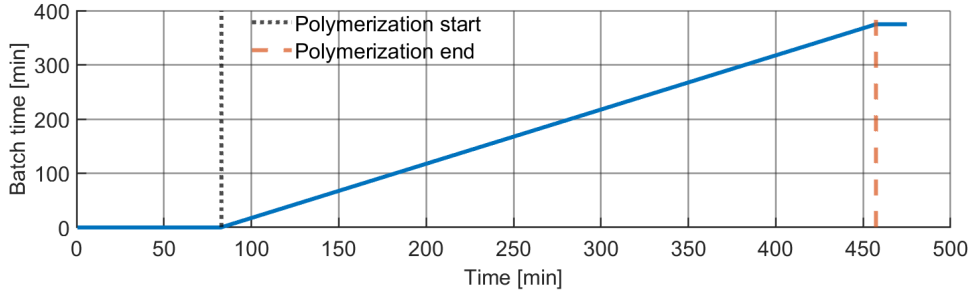

Figure 6.1: Illustration of batch time. Before the polymerization starts the reactor is prepared for the batch. When a conversion of 96% is achieved the polymerization reaction ends and the batch time is frozen along with the rest of the system.

In this work a monomer conversion of 96% was chosen to be the final conversion in which the batch time ends and the entire system is frozen. This results in the definition of the batch time shown in equation 6.4.

$$\frac{dt_{batch}}{dt} = \begin{cases} 1, & \text{for } 0 < X_M \leq 96\% \\ 0, & \text{else} \end{cases} \tag{6.4}$$

Reducing the batch time is an important objective when controlling a batch or semi-batch reactor. A reduction in the batch time results in more batches per time unit and thus an increase in the production volume of the plant.

6.3 Extension of the cooling system

As mentioned in section 5.2 some measurements of temperature and flow were missing with respect to the modelling of the two heat exchangers in relation to the cooling jacket system. Consequently, some extensions were added to the model to be able to control the system. One of which was using the setpoint for the inlet temperature to the cooling jacket as an input. Equation 6.5 shows the expression which captures the dynamics of the inlet temperature to the jacket.

$$\frac{dT_J^{in}}{dt} = \frac{1}{\tau_{\text{TIC}}} \left(T_{J,SP}^{in} - T_J^{in} \right) \tag{6.5}$$

Here T_J^{in} is the inlet temperature to the cooling jacket, $T_{J,SP}^{in}$ is the corresponding setpoint and τ_{TIC} is the time constant describing the delay between the setpoint and the process value of the inlet temperature to the cooling jacket.

The same approach was utilized for the cooling water to the reflux condenser. The setpoint for the volume flow to the reflux was used as an input, and the dynamics of the volume flow to the reflux is captured by equation 6.6.

$$\frac{d\hat{V}_{cw}^{reflux}}{dt} = \frac{1}{\tau_{\text{FIC}}} \left(\hat{V}_{cw,SP}^{reflux} - \hat{V}_{cw}^{reflux} \right) \tag{6.6}$$

Here $\hat{V}_{cw}^{reflux}$ is the volume flow of cooling water to the reflux condenser, $\hat{V}_{cw,SP}^{reflux}$ is the corresponding setpoint and τ_{FIC} is the time constant describing the delay between the setpoint and process value of the volume flow.

The cooling capacity of the reflux condenser is limited by the gas flow through the reflux condenser. Consequently, the model requires a description of this gas flow, and the expression is shown in equation 6.7.

$$\hat{m}_{gas} = \frac{Q_{reflux}}{\Delta H_{VCM}^{vap}} \tag{6.7}$$

Here Q_{reflux} is defined as in equation A.46 and ΔH_{VCM}^{vap} is the heat of vaporization of VCM. The heat of vaporization of VCM is temperature dependent and the expression is listed in appendix C. A basis for equation 6.7 is the assumption that the gas flowing through the reflux condenser only contains VCM.

6.4 Cooling- capacity and demand

The cooling system is comprised of both the cooling jacket and the reflux condenser which both have a certain cooling capacity. The total cooling demand in relation to the total cooling capacity is of great importance from a safety point of view. It is crucial for the cooling demand to not exceed the total cooling capacity, at least for the main portions of the batch.

6.4.1 Total cooling demand

The most significant contribution to the cooling demand is the reaction heat, but some portion of the cooling demand also comes from the post-dosing of species such as water and additives. The total cooling demand can then be written as

$$\begin{aligned} Q_{demand} &= Q_{rx} + Q_{feed} \\ &= (-\Delta H_{rx})R_p + \sum_i \hat{m}_i^{feed} C_{p,i}^{feed} (T_i^{feed} - T_R) \end{aligned} \tag{6.8}$$

where $(-\Delta H_{rx})$ is the heat of reaction from the polymerization reaction. It is worth noting that the contribution from the feed can act as cooling on its own if the temperature of the feed is lower than the reactor temperature. Regardless, the contribution from the feed is minuscule compared to the contribution from the polymerization reaction.

6.4.2 Cooling capacity of the cooling jacket

The available cooling capacity for the cooling jacket is defined by equation 6.9.

$$Q_{J,R}^{cap} = U_{J,R} A_{J,R} (T_J^{min} - T_R) \tag{6.9}$$

Here $U_{J,R}$ is the heat transfer coefficient between the reactor and the cooling jacket, $A_{J,R}$ is the heat transfer area between the reactor and the cooling jacket and T_J^{min} is the minimum achievable temperature of the cooling jacket. The minimum temperature of the cooling jacket is defined as

$$T_J^{min} = \frac{T_{J,min}^{in} + T_J^{out}}{2}\ , \tag{6.10}$$

where $T_{J,min}^{in}$ is the minimum achievable inlet temperature to the cooling jacket, while T_J^{out} is the outlet temperature of the cooling jacket and is modelled as in equation A.49.

6.4.3 Cooling capacity of the reflux condenser

As mentioned in section 5.2 it is important to not exceed a certain cooling effect from the reflux condenser in order to avoid a too large gas flow. Consequently, the cooling capacity of the reflux condenser will be limited by a maximum gas flow through the reflux condenser. If the gas flow through the reflux condenser is assumed to only contain VCM, the cooling capacity of the reflux condenser can be expressed as equation 6.11.

$$Q_{reflux}^{cap} = \hat{m}_{gas}^{max} \Delta H_{VCM}^{vap} \tag{6.11}$$

Here $\hat{m}_{gas}^{max}$ is the maximum allowed mass flow of gas through the reflux condenser.

The cooling capacity of the entire cooling system is the sum of the cooling capacity of the cooling jacket and the reflux condenser,

$$Q_{tot}^{cap} = Q_{J,R}^{cap} + Q_{reflux}^{cap} \tag{6.12}$$

6.5 Parameter profiles

Three parameters were estimated for a total of four batches as part of the preliminary project, namely the correction factor for the kinetic model (CF), the heat transfer coefficient between the reactor and cooling jacket ($U_{J,R}$), and the heat transfer coefficient for the reflux condenser (U_{reflux}). Profiles for these parameters were obtained and these are presented in appendix B. Especially the correction factor for the kinetic model was of great interest due to the systematic trend in all four batches. A polynomial were fitted to the average trend, resulting in a profile for CF as a function of the monomer conversion, $CF(X_M)$. This polynomial was implemented to the model to account for unmodelled aspects of the system and consequently improve the model accuracy. The unmodelled aspects were discussed in the preliminary project[9].

7 Control considerations

This chapter aims to highlight the main considerations that were taken into account when developing the NMPC application section in 8.2. Topics covered are temperature and pressure control, cooling, batch time, quality control, MV's and safety. These topics are presented to illustrate various angles of attack when formulating the control problem.

7.1 Temperature and pressure control

7.1.1 Temperature control

As mentioned on several previous occasions, the polymerization reaction is highly exothermic. This makes the reactor temperature a crucial process parameter to control in terms of safety, but also in terms of the end quality of the polymer. There are several possible approaches when it comes to controlling the reactor temperature, the first of which is to use a setpoint profile, i.e. a setpoint which varies throughout the batch. The setpoint profile will be predetermined such that both safety- and quality requirements are met.

The second approach is to have a constant setpoint for the entire batch. As with the setpoint profile, the constant setpoint will be predetermined such that safety- and quality requirements are met. For both the approach with the setpoint profile and the approach with a constant setpoint, upper and lower constraints can be added to ensure that the reactor temperature operates in a safe region even if it deviates from the setpoint.

A third and final approach is to operate without a setpoint on the reactor temperature and instead use the conversion average temperature for control. The conversion average temperature was introduced in section 6.1 and determines the end quality of the polymer. Excluding the reactor temperature, it is the most important control variable. It is temperature dependent which implies that the reactor temperature can be indirectly controlled by controlling the conversion average temperature. Then the reactor temperature can behave freely (inside its constraints) if the conversion average temperature is controlled within its bounds or to its setpoint at the end of the batch. A variant of this approach is to both have a setpoint profile on the reactor temperature and a setpoint/constraints on the conversion average temperature. Then the reactor temperature is allowed to deviate from its setpoint if the deviation leads to better control of the conversion average temperature. The outlined approach can prove helpful if disturbances that affects the polymerization rate occur. If the reactor temperature tracks its setpoint, but the polymerization rate does not behave as expected, control of the conversion average temperature might not be satisfactory. Allowing the reactor temperature to deviate from its setpoint can account for these disturbances and allow for satisfactory control of the conversion average temperature. For this approach the controller has to be tuned such that the reactor temperature is allowed to deviate from its setpoint.

There are several MV's which affect the reactor temperature, three of which are highly relevant for this thesis. The three MV's are the setpoint for the water flow to the reflux condenser (FIC-1 in fig. 5.3), setpoint for the inlet temperature to the cooling jacket (TIC-2 in fig. 5.3) and the mass flow of initiator (V-104 in fig. 5.3). The setpoint for the water flow to the reflux is used to cool the reactor through the reflux condenser, while the mass flow of initiator is used to heat the reactor by increasing the polymerization rate, and consequently the reaction heat. The setpoint for the inlet temperature to the cooling jacket can act both as cooling and heating depending on whether the inlet temperature is higher or lower than the reactor temperature. When the polymerization reaction is

proceeding the inlet temperature is typically lower than the reactor temperature which implies that it is cooling the reactor.

The observant reader may have noticed that the valves V-101 (cooling water) and V-102 (steam) in figure 5.3 were not mentioned as MV's. Instead the setpoint for the inlet temperature to the cooling jacket was used. This is related to the lack of measurements discussed in section 5.2 which had implications for the implementation of the NMPC in section 8.2.

7.1.2 Pressure control

Controlling the reactor pressure is also an important aspect regarding safe operation of the reactor. The reactor, being a pressure vessel, is equipped with both active and passive safety features, such as high pressure alarms, pressure safety valves (PSV's) and rupture discs. However, it is desirable to not reach the point where these safety features are needed, especially the PSV's and rupture discs. To prevent reaching such high pressures, an upper constraint on the reactor pressure can be introduced to the control formulation. The penalty for not satisfying the upper pressure constraint should be set large enough such that no control move leads to a constraint violation. Pressure and temperature are closely linked, which becomes evident by looking at the modelled relation in appendix A.4. This implies that temperature control and pressure control are also closely linked.

7.2 Cooling

The cooling system is comprised of the reflux condenser and the cooling jacket as shown in figure 5.3. Both the reflux condenser and the cooling jacket have their separate capacities which add up to the total capacity of the cooling system. The main contributor to the cooling demand is the heat produced by the polymerization reaction, while only a small contribution comes from the post-dosing of species such as water and initiator. In order to be able to control the reactor temperature it is crucial for the cooling demand to not exceed the total cooling capacity. This can be included in the control formulation by adding a constraint on the cooling demand to be lower than the cooling capacity. The cooling system is designed such that the combined capacity of the reflux condenser and the cooling jacket are sufficient. When the reflux condenser is shut off at 78% conversion in accordance with equation A.46 the total capacity drops and the demand will be greater than the capacity. However, the point where the reflux shuts off is so far into the batch that the temperature rise is predictable.

It is worth noting that the interpretation of the capacity of the reflux condenser and the cooling jacket is different. The capacity of the cooling jacket is a physical limit in the form of a minimum achievable temperature as described in section 6.4.2. On the other hand, the capacity of the reflux condenser is limited by a maximum allowed gas flow through the reflux condenser as described in section 6.4.3. This maximum gas flow is a limit set by the control engineer and is not a physical limit. Consequently, it is possible for the reflux condenser to provide a bigger cooling effect than its capacity, but this is not possible for the cooling jacket. Despite this, the penalty for violating the capacity of the reflux condenser should be set such that no control move causes a constraint violation. This is to prevent erratic behavior in the reactor.

7.3 Initiator feed

The initiator feed is an important MV due to its direct influence on the polymerization rate. A larger feed rate of initiator leads to a larger number of radicals per particle which in turn causes a larger polymerization rate. The relation between the polymerization rate and $\bar{n}$, as well as the modelling of $\bar{n}$ are both presented in appendix A.2.

Depending on the cost of initiator, a certain trade-off between a reduction in batch time and the amount of initiator used has to be considered. For a cheap initiator, any reduction in the batch time is profitable. For an expensive initiator, the reduction in batch time has to be compared with the additional expenses related to the extra initiator used. Either way, a maximum amount of initiator per batch is preset in the recipe of the batch. This is easily implemented to the control formulation in the form of an upper constraint on the accumulated mass of initiator.

An initial dose of initiator is typically used to kick-start the polymerization reaction. It is charged into the reactor as a short burst. The total mass of initiator contained in the initial dose is also a preset value in the recipe of the batch. The importance of the initial dose is demonstrated in section 8.5.

7.4 Batch time

The reduction of the batch time is an important part of the reactor control objective. Reducing the batch time increases production as it allows for more batches per time unit. More batches per time unit means that the cost of operating the process per batch, such as salaries, raw materials and other operating costs, decreases. In addition the increased production results in larger income from the product. To summarize, minimizing the batch time can lead to a larger overall surplus for the process.

Minimizing the batch time can be done in several ways. The first approach is to include the batch time in the objective function for the controller. Then a setpoint for the batch time could be set unrealistically low. For example, if the setpoint is set to zero the deviation from the setpoint will be penalized at every sample. Then the optimizer in the controller will search for ways to minimize the batch time. Instead of a setpoint an upper limit on the batch time could be set instead, but the two approaches are similar.

There are two main problems with the approach outlined above. The main one is that minimizing the batch time explicitly requires that the controller has a prediction horizon at least as long as the entire batch. Such a long prediction horizon will most likely be very computational demanding and the controller might not fulfill the real-time requirement, i.e. the controller is not able to obtain a solution to the optimization problem in between samples. If the requirement is not fulfilled the controller will fall further and further behind. The second problem with the above-mentioned approach is related to the penalization on deviations from the setpoint/constraint set on the batch time. A too large penalization might result in the controller not starting the batch in order to keep the batch time at its setpoint, which in the approach outlined above is zero.

An alternative approach to the one above is maximizing the polymerization rate. Maximizing the polymerization rate implicitly minimizes the batch time as the rate of conversion becomes larger. This approach can be implemented by setting an unrealistically large setpoint or lower constraint on the polymerization rate. Since the polymerization rate always lies below its setpoint or lower constraint, the controller will search for ways to close the gap to decrease the deviation. The penalization must also in this approach not be set

too large as this might result in the controller making the polymerization rate too large. Since the polymerization reaction is exothermic this is problematic from a safety point of view. Implicitly reducing the batch time in the form of maximizing the polymerization rate is a less computational demanding approach. Consequently, this approach is the most attractive.

7.5 Quality control

To describe the product quality the conversion average temperature was introduced in section 6.1. Only the value at the very end of the batch is important with respect to the end quality of the product, and in theory the parameter can behave freely before the end of the batch. Since only the end value is of interest, control of the conversion average temperature can be implemented by introducing a setpoint for the parameter and only weight the setpoint at the end of the batch. However, this would require a prediction horizon at least as long as the entire batch. This would result in the same issues as mentioned in section 7.4.

An alternative approach is to have the setpoint weighted at the end of the prediction horizon, with the length of the prediction horizon being reasonable with respect to the computational demand. The point in which the setpoint is weighted will shift along with the prediction horizon until the end of the batch where the system states are frozen. Penalizing deviations during the batch ensures that the controller works towards the setpoint the entire batch. When the prediction horizon overlaps with the end of the batch where the system is frozen, the setpoint is weighted at the "correct" point, i.e. the end of the batch. A possible problem with this approach is that the controller might leave control actions that reduce the deviation for a later time. If the controller lets the deviation get too large, it might not be able to control the end value to the setpoint before the system is frozen.

7.6 Manipulated variables

Independent of which MV's that are chosen, the weighting of them are an important part in the development of the NMPC controller. The weighting here refers to the penalty on the control moves, represented by $S_{2,k}$ in equation 3.11a. The individual values for the penalty determines the relative aggressiveness of the individual inputs. An input with a lower value for its weight moves more than an input with a larger weight. As an example, consider a process which has an input which it is desirable to move as little as possible. Setting the weight on this input larger than the weights on the other inputs makes the controller "choose" to move the less weighted inputs first. In this way the wear and tear on the more weighted input is less, which can be desirable for some actuators.

The weight on the inputs can also affect the controller performance. A too low penalization might lead to an aggressive controller where the inputs have unnecessary and rapid oscillations. These oscillations typically do not improve the control performance and only causes extra wear and tear on the actuators. Too large penalization can lead to poor control performance as the controller "chooses" to not move the inputs due to the large penalization. Finding a trade-off in the penalization of the inputs are an important part of the development of the NMPC controller.

8 Results and discussion

This chapter presents the results of this thesis and discusses them. It aims to demonstrate the implemented controller through various case studies related to the controller testing. The topics of each section are listed in the order they are presented in this chapter.

- **Section 8.1** presents the results from the finalization of the preliminary project. It includes validation of the extensions added to the model developed in the preliminary project.
- **Section 8.2** presents the implemented control system. The structure is presented along with the chosen CV's and MV's. It also includes the controller tuning and variable parameterization.
- **Section 8.3** presents the results from Case Study 1, which studied three approaches for reactor temperature control.
- **Section 8.4** presents the results from Case Study 2, which studied how the maximum amount of initiator allowed affected the batch time and control of the reactor.
- **Section 8.5** presents the results from Case Study 3, which studied how the the size of the initial dose of initiator affected the batch time and control of the reactor.
- **Section 8.6** presents the results from Case Study 4, which studied how the controller handled a reduction in the cooling capabilities of the cooling jacket.
- **Section 8.7** presents the results from Case Study 5, which studied how varying the lengths of the prediction- and control horizon affected the control of the reactor.
- **Section 8.8** presents the results from Case Study 6, which studied how varying the input blocking affected the computation time per sample and the control of the reactor.

The main tool used to obtain the presented results in section 8.1 was Cybernetica ModelFit. For section 8.2 - 8.8 the main tools used to obtain the presented results were Cybernetica CENIT along with RealSim functioning as a plant replacement.

8.1 Finalization of the model

Simulations to test the extensions of the model introduced in chapter 6 are presented. This includes the implementation of the polynomial for CF, modelling of conversion average temperature and validating the extended cooling system model against measured data. In addition, some comments regarding parameter changes are presented and discussed briefly.

The results presented in this section are based on the parameter values from the parameter adjustments in appendix B.2. The reasoning is from the preliminary project as the main results and discussion from the preliminary project are still highly relevant for the results presented in this section.

8.1.1 Conversion average temperature

Figure 8.1 shows how the conversion average temperature behaves throughout a batch. It does not change drastically, but it varies some through the batch.

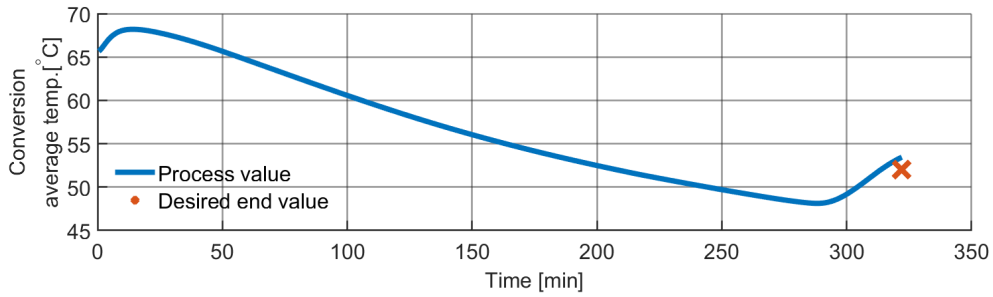

Figure 8.1: Evolution of the conversion average temperature through the batch. The simulation was run with recursive filtering.

At their plant INOVYN aims for a conversion average temperature of approximately 52 °C at the end of the batch. Figure 8.1 shows that the modelled value deviates slightly. Equation 6.3 shows that the conversion average temperature is dependent on both the reactor temperature and the polymerization rate. Since the simulation was run with online state- and parameter estimation, the modelled and measured reactor temperature matches almost perfectly as seen in figure B.4b. This implies that the deviation in figure 8.1 is most likely not caused by the temperature, but rather by a deviation in the modelled polymerization rate compared to INOVYN's calculated polymerization rate. As the polymerization rate is not directly measured, which one of the two polymerization rates that are the best reflection of reality is hard to be certain of. Since the deviation at the end of the batch in figure 8.1 is not significantly large, the model of conversion average temperature in equation 6.3 was considered sufficient for the control purpose in this thesis.

8.1.2 Extensions of the cooling system

During the preliminary project the inlet temperature to the cooling jacket and the volume flow to the reflux condenser were used as inputs to the model. This was considered a good approach when validating the model as it filtered out any unnecessary model errors. When considering the control of the system by using NMPC, the outlined approach was not realistic since a temperature or a flow would normally not be used directly as MV's in the NMPC controller. Consequently, the extensions to the cooling system presented in section 6.3 were implemented. The extensions describe the dynamics going from setpoints to the process values and it facilitates the use of setpoints as MV's in the NMPC. PID controllers were then tasked with controlling the process values to the setpoints provided by the NMPC, and they were modelled by the implemented extensions.

Time constants for the dynamics of the inlet temperature to the cooling jacket and the volume flow to the reflux condenser are listed in table 8.1.

Table 8.1: Time constants for the dynamics of going from the setpoint to the process value.

Parameter	Value	Unit
τ_{FIC}	5	s
τ_{TIC}	90	s

The values listed in table 8.1 were obtained from offline parameter estimation in ModelFit followed by some minor manual adjustments to achieve a better fit in relevant regions.

Using these values, the extensions of the cooling system were validated by comparing the modelled outputs with measurements provided by INOVYN. Figure 8.2 shows both the modelled and measured profiles for the inlet temperature to the cooling jacket and the volume flow to the reflux condenser, along with their respective setpoints.

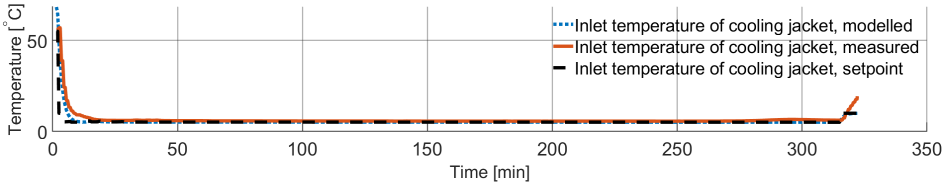

(a) Modelled and measured inlet temperature to the cooling jacket, in addition to the setpoint.

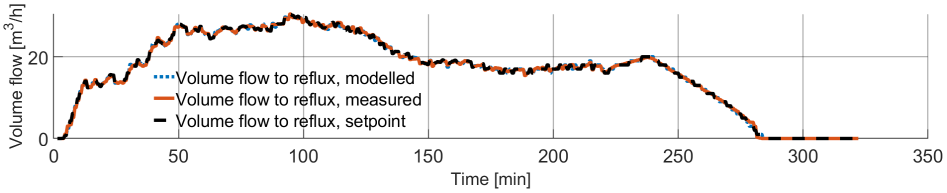

(b) Modelled and measured volume flow to the reflux condenser, in addition to the setpoint.

Figure 8.2: Results from simulation to test the extensions of the cooling system. The simulation was run ballistic.

Figure 8.2a shows that the modelled inlet temperature has small deviations at the start and the end of the batch, but it tracks the measured inlet temperature well for the rest of the batch. The small deviations are not considered to be significant and equation 6.5 describes the dynamics of the inlet temperature to the cooling jacket in a satisfactory manner. Both the modelled and measured inlet temperature show a delay compared to the setpoint, which can be attributed to the large time constant τ_{TIC}. This was expected as it takes some time to heat up or cool all the water circulating in the cooling jacket loop.

Figure 8.2b shows that the modelled, the measured and the setpoint value for the volume flow to the reflux condenser all are located on top each other. Flow control is usually fast, and this is reflected in the small value of the time constant τ_{FIC}. The fast control implies that the dynamics going from a setpoint to the process value is also fast. In the case of flow control, using the process value directly as a MV would probably not have been a bad approach. Despite this fact, equation 6.6 was used to model the volume flow to the reflux condenser based on a provided setpoint.

8.1.3 Parameter profiles

As mentioned in section 6.5, profiles for the three parameters CF, $U_{J,R}$ and U_{reflux} were obtained for a total of four batches. Especially the results for CF was interesting due to the systematic and predictable trend in the four datasets, which is shown in figure 8.3.

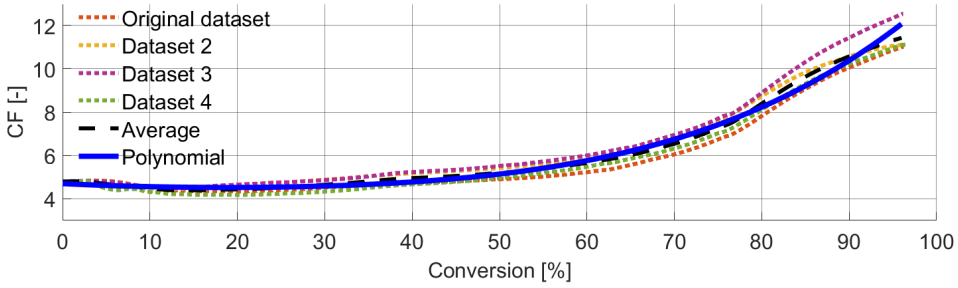

Figure 8.3: CF as a function of conversion for the four datasets, along with the average trend and the fitted polynomial. It is emphasized that the profiles were obtained with the parameter values from the parameter adjustments presented in appendix B.2.

Some individual characteristics can be observed in the four batches. This was expected due to disturbances and other variations from batch to batch. However, the resemblance between the four batches is evident. This implies that a polynomial based on the average trend is a well suited description of the unmodelled aspects of the system. Both the average trend and the polynomial are shown alongside the parameter profiles for the four batches in figure 8.3. The polynomial is a function of conversion in order to account for differences in duration of different batches, and it is shown in equation 8.1.

$$CF(X_M) = 11.72X_M^4 - 7.77X_M^3 + 6.75X_M^2 - 2.01X_M + 4.71 \tag{8.1}$$

It was implemented to the model to account for the unmodelled aspects. The unmodelled aspects were discussed in the preliminary project, but some unmodelled aspects are the Trommsdorff-effect and the simplified initiator mechanism, among others. To illustrate the need for the polynomial, consider the Trommsdorff-effect. The Trommsdorff-effect causes an increase in $\bar{n}$ and a resulting increase in the polymerization rate. Since this is not modelled, CF accounts for this by the increase seen in figure 8.3 towards the end of the batch. It is emphasized that CF accounts for all unmodelled aspects, and not only the Trommsdorff-effect.

Figure 8.4 shows the modelled reactor temperature both with and without the pre-estimated polynomial in equation 8.1, along with the measured reactor temperature. The improvements with the polynomial is the most significant towards the end of the batch. With the polynomial the modelled reactor temperature has a steeper increase than the one without the polynomial implemented.

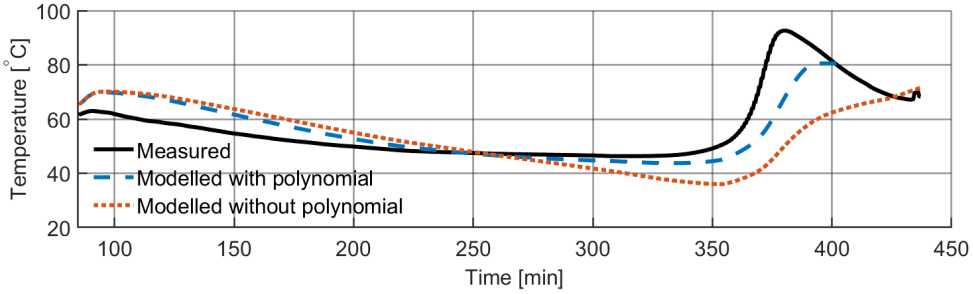

Figure 8.4: Modelled reactor temperature both with and without the pre-estimated polynomial for CF, compared to the measured reactor temperature. The temperature is plotted against time to illustrate the difference in batch time the polynomial contributes to. The simulations were run ballistic. It is emphasized that the profiles were obtained with the parameter values from the parameter adjustments presented in appendix B.2.

The modelled reactor temperature with the polynomial improves the performance of the model as it obtains smaller deviations, especially towards the end of the batch because of the steeper increase. Deviations are smaller, but it does not eliminate them as the implementation of online state- and parameter estimation does (Fig. B.4b). This was however not expected as each batch is different, and the polynomial is based on an average trend. Consequently, the polynomial is not a perfect representation of each batch, even if it improves the accuracy. In addition, when simulating with online state- and parameter estimation both $U_{J,R}$ and U_{reflux} are estimated along with CF. This can account for other aspects than the polynomial, yielding even better performance. The polynomial only affects the kinetic model, but with online state- and parameter estimation practically the entire model is affected. The improvement in the model outputs by implementing the polynomial was however considered to be satisfactory, and it was implemented to account for unmodelled aspects. This made the plant replacement reflect reality better and the predictions in the NMPC controller better.

8.2 Implementation of the NMPC

Numerous considerations were taken into account for the control design, both in terms of the structure, but also in terms of CV's and the objective function for the NMPC controller. The presented implementation was obtained from process knowledge and discussions with INOVYN.

Extensive work were performed during the preliminary project to tune and test the estimator. The tuned estimator was brought along to the NMPC implementation in this thesis. The estimator is not mentioned in detail in this section. However, it is still an integral part of the NMPC implementation and the controller is highly dependent on the estimator established in the preliminary project. The controller and estimator work in conjunction to provide satisfactory control of the process. Some logic for the estimator were implemented in the already existing C-code, but the specifics are confidential. This logic made sure that the controller and estimator worked seamlessly in relation to each other. A brief summary on the estimator with respect to estimated parameters and active measurements is presented in appendix B.1.

8.2.1 Control structure

As mentioned in section 5.2, relevant measurements inside the red box in figure 5.3 were missing. If all necessary measurements were available, the heat exchangers H-101 and H-102, and the valves V-101 and V-102 should have been included in the model. A model which included the valves and heat exchangers could not have been validated due to the lack of available measurements. This could have resulted in the dynamics of the cooling jacket system being poorly represented by the model. Instead, some modifications were made for the control structure design in this thesis. These modifications made it possible to validate the chosen model such that the dynamics of the cooling jacket system were captured satisfactory by the model. The modifications resulted in moving away from the cascade- and split range structure currently deployed.

The setpoints for the inlet temperature to the cooling jacket and the volume flow to the reflux condenser are both determined by the NMPC controller and not through a cascade structure like in figure 5.3. Figure 8.5 shows the final control structure used in this thesis, along with the modifications which are mainly related to the red parts.

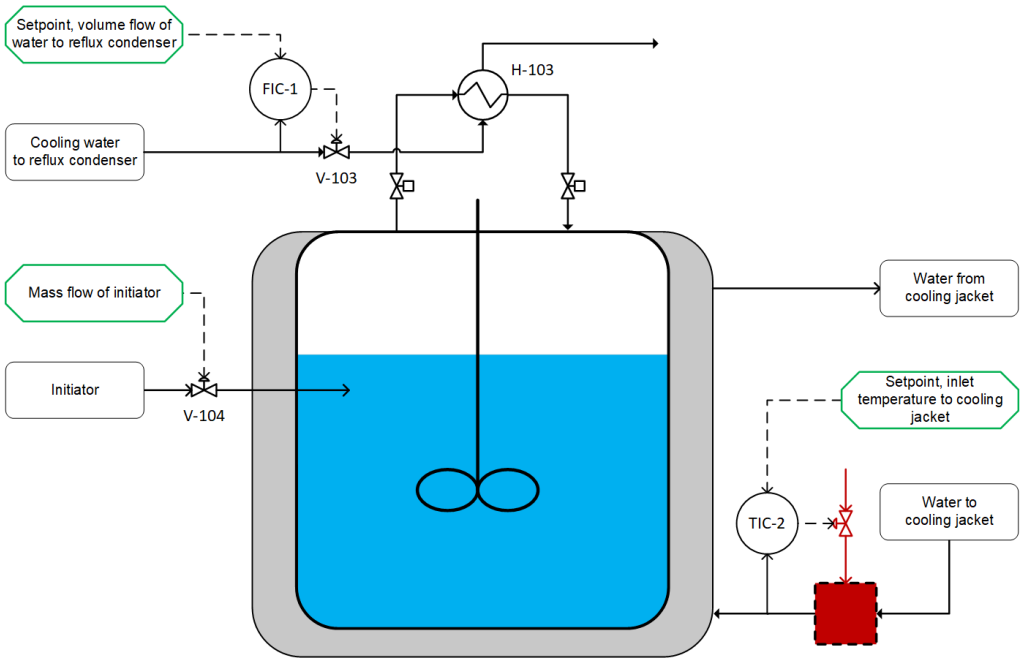

Figure 8.5: Control structure used in this thesis. The green boxes represent the MV's of the NMPC controller. The red parts are the modified structure related to the inlet water of the cooling jacket. It has the same function as the heat exchanger system inside the red section in figure 5.3. In this figure the red box represents heat exchangers that the water to the cooling jacket flows through in order to obtain its setpoint temperature. The valve connected to TIC-2 is a fictional valve connected to the heat exchangers in the red box. It controls the inlet temperature of the water to the cooling jacket to the setpoint provided by the NMPC controller. Since the valve is fictional, it is assumed to provide both heating and cooling. The mass flow of initiator is controlled directly by the NMPC, while the volume flow to the reflux condenser is controlled by FIC-1. FIC-1 gets its setpoint from the NMPC.

The setpoint for the inlet temperature to the cooling jacket was chosen as one of three MV's for the NMPC controller. Setpoint values are provided to TIC-2 which controls the red fictional valve connected to the red box in figure 8.5. The heat exchangers and

valves mentioned above were lumped into the red parts. It was assumed to be able to provide the desired inlet temperature based on the setpoint given to TIC-2 from the NMPC controller, according to equation 6.5. Since the red valve is fictional it was assumed to provide both heating and cooling in order to obtain the desired inlet temperature to the cooling jacket. Figure 8.2a shows that the modelled inlet temperature resembles the measured inlet temperature closely. As a result, it was considered that the modification with the red parts was satisfactory in terms of capturing the dynamics of the cooling jacket loop.

The setpoint for the volume flow to the reflux condenser was also chosen as a MV for the NMPC controller. Setpoint values were provided to FIC-1, which was assumed to be able to provide the corresponding process value according to equation 6.6. The third MV was chosen to be the initiator dosing. Since no relation between the valve opening and the mass flow was available, it was decided to use the mass flow of initiator as a MV for the NMPC controller.

For the current control structure in figure 5.3 the reflux is activated according to the internal control signal in figure 5.4a. This translates to the reflux being activated when the cooling jacket is saturated, i.e. the output signal from TIC-1 is at 20%. Since the cascade- and split range control were removed in the control structure for this thesis, a different criteria was utilized for the activation of the reflux. Instead, the reflux was set to be activated when 90% of the capacity of the cooling jacket was used. This criteria supplemented the conditions in equation A.48 which state that the reflux is active when the conversion is below 78%. When the reflux was activated by the new criteria, it shut off when *Condition 2* in equation A.48 were satisfied, i.e. when the conversion reached 78%.

8.2.2 Controlled- and manipulated variables

The presented constraints and setpoints for the CV's and MV's were obtained from a combination of process knowledge and specifications from INOVYN. A short description about how the values were obtained is presented first, followed by a summary. This is done for both the CV's and MV's. Additionally, variable implementation specifics are also presented where necessary. During the formulation of the control problem presented in this section, the different aspects discussed in chapter 7 were evaluated.

CV - Reactor temperature

- The setpoint was case-dependent and T_R could be controlled with a setpoint profile, a constant setpoint or no setpoint.
- The upper and lower constraints for T_R were set to 110 °C and 0 °C, respectively. Both the upper and lower constraint were based on operating limitations from INOVYN.

CV - Reactor pressure

- The upper and lower constraints for p_R were set to 12 barg and 0 barg, respectively. The upper constraint was defined from when the safety equipment is activated at the plant, while the lower constraint was set to atmospheric pressure.

CV - Conversion average temperature

- The setpoint for $\bar{T}_{X_M}$ was set to 52 °C based on a specification from INOVYN. It is worth noting that the setpoint was only weighted at the end of the prediction

horizon as discussed in section 7.5.

- An upper and lower constraint for $\bar{T}_{X_M}$ were specified as $52\,^{\circ}\text{C} \pm 5\%$.

CV - Polymerization rate

- The lower constraint for R_p was set unrealistically big such that the controller would always work to maximize R_p. This was the approach chosen to minimize the batch time as discussed in section 7.4. The upper constraint was not considered to be relevant, but it was set slightly bigger than the lower limit.

CV - Cooling demand

- The variable $\Delta Q_{tot} = Q_{tot}^{cap} - Q_{demand}$ was defined as the difference between the total cooling capacity and the total cooling demand. A lower constraint on ΔQ_{tot} was set to 0 kW, which translates to the cooling demand being lower than the cooling capacity. The upper constraint was set to the arbitrary value 3000 kW.

CV - Gas flow through the reflux condenser

- The upper and lower constraints on $\hat{m}_{gas}$ were set to 3.1 kg/s and 0 kg/s, respectively. The upper constraint was based on operating limitations from INOVYN, while the lower constraint was trivial.

CV - Maximum amount of initiator

- The upper constraint on m_I^{tot} was set to 45 kg except for the case study in section 8.4 where it was varied, while the lower constraint was set to 0 kg. The upper constraint was based partly on batch specifications from INOVYN, but some were added to this amount. The lower constraint was trivial.

Table 8.2 summarizes the obtained values for the setpoints and constraint values for the CV's.

Table 8.2: Summary of the setpoints and constraint values for the CV's.

CV	Setpoint	Lower constraint	Upper constraint	Unit
T_R	Case-dependent	0	110	°C
p_R	-	0	12	barg
$\bar{T}_{X_M}$	52	49.4	54.6	°C
R_p	-	50	51	mol/s
ΔQ_{tot}	-	0	3000	kW
$\hat{m}_{gas}$	-	0	3.1	kg/s
m_I^{tot}	-	-	Mainly 45, except case study 2	kg

MV - Setpoint for the inlet temperature to the cooling jacket

- The upper and lower constraints on $T_{J,SP}^{in}$ were set to 90 °C and 5 °C, respectively. The upper constraint was based on operating limitations from INOVYN, while the lower constraint was based on the minimum obtainable temperature of the water. This was also provided by INOVYN.
- Control moves per sample, Δu^{high} and Δu^{low}, were set to 40 °C and −40 °C, respectively. The control moves were based on studying data from INOVYN.

MV - Setpoint for the volume flow to the reflux condenser

- No upper constraint were set on $\hat{V}_{cw,SP}^{reflux}$. This was because the constraint on the reflux condenser was determined by the constraint on $\hat{m}_{gas}$. The lower constraint was set to $0\,\mathrm{m}^3/\mathrm{h}$.
- As mentioned in section 5.2, the reflux was implemented to become active when 90% of the capacity of the cooling jacket was utilized. Consequently, the setpoint for the volume flow to the reflux condenser operated at its lower constraint until this condition was fulfilled.

MV - Mass flow of initiator

- The upper and lower constraints on $\hat{m}_I$ were set to $1\,\mathrm{kg/min}$ and $0\,\mathrm{kg/min}$, respectively. The upper constraint was based on process knowledge, while the lower constraint was trivial.
- Control moves per sample, Δu^{high} and Δu^{low}, were set to $0.4\,\mathrm{kg/min}$ and $-10\,\mathrm{kg/min}$, respectively. The control moves were based mainly on process knowledge, but also studying data from INOVYN.
- At the start of each, a preset initial dose was charged into the reactor. The initial dose was delivered in a short time span, implying that the flow rate was larger than the upper constraint. This was accounted for in the implementation by having the upper constraint become active straight after the initial dose was finished.

Table 8.3 summarizes the obtained constraint values for the MV's.

Table 8.3: Summary of the constraint values for the MV's.

MV	Δu^{low}	Δu^{high}	Lower constraint	Upper constraint	Unit
$T_{J,SP}^{in}$	-40	40	5	90	°C
$\hat{V}_{cw,SP}^{reflux}$	-	-	0	-	m^3/h
$\hat{m}_I$	-10	0.4	0	1	kg/min

8.2.3 Controller tuning and variable parameterization

A significant part in the development of the NMPC controller involved controller tuning. Weights on setpoints, penalization of constraint violations and weights on control moves were adjusted to yield a well-performing controller in terms of meeting operating specifications. The final tuning parameters for the CV's and MV's presented in section 8.2.2 are listed in table 8.4. When discussing the final values, focus is not directed at their specific numerical values, but rather their size and interconnection with the weights on the other variables.

Table 8.4: Tuning parameters for the CV's and the MVs.

CV	Weight on setpoint, Q	Linear penalty on constraint violation, r_1	Quadratic penalty on constraint violation, r_2	Weight on control move, s
T_R	30	50	50	-
p_R	-	100	50	-
$\bar{T}_{X_M}$	4.7	4	1	-
R_p	-	0.31	0	-
ΔQ_{tot}	-	5	1	-
$\hat{m}_{gas}$	-	60	140	-
m_I^{tot}	-	100	100	-
MV				
$T_{J,SP}^{in}$	-	-	-	0.1
$\hat{V}_{cw,SP}^{reflux}$	-	-	-	10
$\hat{m}_I$	-	-	-	1

Some tuning parameters were obtained easily from the fact that some constraints could not be violated. This included the constraints on the reactor pressure, the gas flow through the reflux condenser, maximum amount of initiator and the reactor temperature. The large weights on the four sets of constraints reflect the importance of not violating these constraints as it will result in sub-optimal operation at best, and unsafe operation at worst. Small violations of the gas flow through the reflux condenser was tolerated for short periods of time. However, it was desirable to avoid it in order to minimize the probability of erratic behavior if the NMPC application was to be implemented in a real plant.

As described in section 7.2, the cooling demand would at some point during the batch exceed the cooling capacity. This was a predictable event and the penalty for violating the lower constraint on ΔQ_{tot} was not set too large as this could have lead to an unnecessary decrease in the polymerization rate. Consequently, moderate values for the constraint violation penalties were set on ΔQ_{tot}.

Most of the tuning involved the interplay between the polymerization rate and the conversion average temperature. In most cases these two process outputs worked in opposite directions. Increasing the penalization on the polymerization rate lead to a shorter batch time, but the setpoint/constraint values for the conversion average temperature would not necessarily be met at the end of the batch. This implied that the penalization on the polymerization rate could not be set too large as the conversion average temperature is an important quality parameter. On the other side, the penalization should be set as large as possible to minimize the batch time. This interplay was carefully tuned and a trade-off between the two was successfully found with the weight parameters listed in table 8.4.

When a setpoint for the reactor temperature was active the process value should track the setpoint, but not at all costs. The process value should mostly track the setpoint, but it should deviate from the setpoint if this lead to better performance with respect to the conversion average temperature. This is the approach outlined in section 7.1.1 and the obtained weight for the reactor temperature reflects this interchange between tracking and deviating from the setpoint.

Values for the penalties on input moves for the three MV's were obtained after the CV's were tuned. A lower penalty on the input move implied that the input moved more since a control move was not penalized as much as the inputs with a large penalty. In this case this meant that $T^{in}_{J,SP}$ moved more, followed by $\hat{m}_I$ and $\hat{V}^{reflux}_{cw,SP}$. Larger values for the penalties were tested, but this resulted in poorer control due to the inputs being penalized more for every control move. Smaller values resulted in an overly aggressive controller, as discussed in section 7.6.

All CV's except the conversion average temperature had identical parameterization for the coincidence points. The CV's were evaluated every two samples with a prediction horizon of 80 samples. With a sample time of 30 seconds this implied that the prediction horizon had a length of 40 minutes and the coincidence points were at every minute.

A similar approach of equal parameterization was also utilized for the MV's, in the form of input blocking. All three MV's had equal length on their respective blocks and a control horizon of 30 samples (15 minutes). The input values were decided at sample number 0, 8, 16 and 30, yielding four input blocks.

The setpoints and constraint values for their respective variables listed in table 8.2 and 8.3 were used in the control formulation unless something else is explicitly stated. Additionally, the values for the tuning parameters listed in table 8.4 were used in all simulation results presented. The parameterization of both the CV's and MV's were used for all simulations, except for the case studies in section 8.7 and 8.8 where the effect of changing them was investigated.

8.3 Case study 1: Reactor temperature control

This section presents the three approaches for reactor temperature control outlined in section 7.1.1. Simulation results for the three approaches are presented first along with some discussion of the individual results. The three approaches are then compared and discussed in context of each other. The three approaches looked into in this section are:

Case study 1.1: Setpoint profile on the reactor temperature

Case study 1.2: Constant setpoint on the reactor temperature

Case study 1.3: No setpoint on the reactor temperature

In all three simulations the initial dose of initiator was 5 kg and the total amount of initiator allowed was 45 kg. The CV's and MV's were as described in section 8.2.2 and the controller was tuned according to section 8.2.3.

8.3.1 Case study 1.1: Setpoint profile

Figure 8.6 shows the reactor temperature, the reactor pressure, the conversion average temperature and the cooling for the simulation performed with a setpoint profile on the reactor temperature. Figure 8.6a and 8.6b shows that both the reactor temperature and reactor pressure lies well within their bounds in terms of safe operation of the reactor. The conversion average temperature in figure 8.6c obtains a satisfactory value at the end of the batch. Both the cooling demand and cooling capacity are shown in figure 8.6d, and a sufficient cooling capacity can be observed through the batch until the reflux condenser is shut off. The large dip in the cooling capacity at about 310 minutes indicates the shut off. After the shut off the demand is larger than the capacity. Two spikes at approximately 20 minutes and 225 minutes can be observed on the cooling demand in figure 8.6d. These

spikes are a caused by the post-dosing of species such as water.

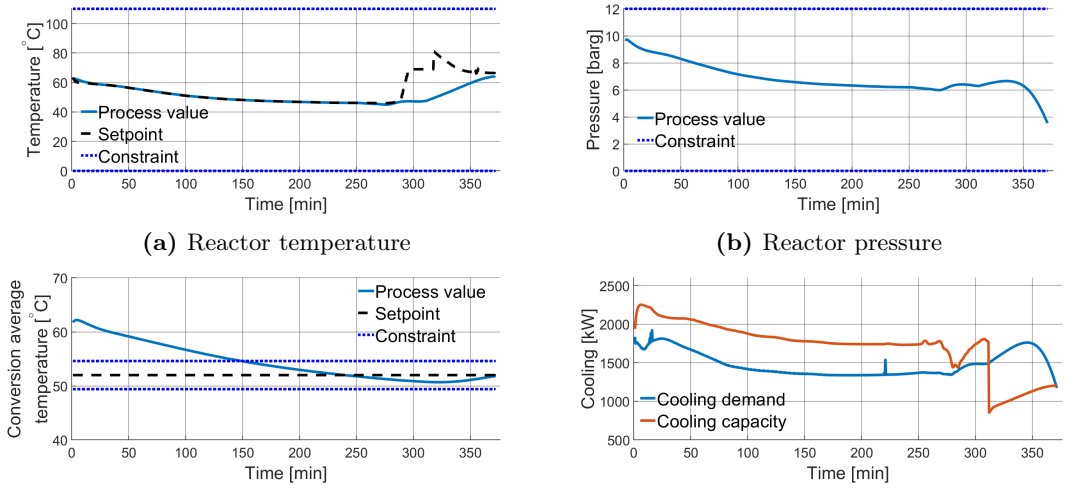

(a) Reactor temperature

(b) Reactor pressure

(c) Conversion average temperature

(d) Cooling

Figure 8.6: Model outputs from simulation with a setpoint profile on the reactor temperature.

The dip in pressure towards the end of the batch is most likely a result of a small amount of monomer left in the reactor. As a result of the small amount of monomer left, the monomer activity drops. Consequently, the pressure drops due to the monomer activity dependence of equation A.40. The small amount of monomer is also most likely the reason for the drop in the polymerization rate and consequently the cooling demand towards the end of the batch.

Figure 8.6d shows a gap between the cooling capacity and the cooling demand. If no quality requirements were necessary, the reactor would ideally be operated with a small as possible difference between the capacity and the demand. Then the polymerization rate would have been maximized while still maintaining safe operation of the reactor. However, due to the quality specification on the conversion average temperature, the controller can not increase the polymerization rate as much as wanted since this would most likely result in poor control of the conversion average temperature. The conversion average temperature in figure 8.6c shows a decreasing trend and it undershoots the setpoint before it comes back up to the setpoint. The decreasing trend is mostly due to the decrease in the reactor temperature throughout most of the batch, while the increase to reach the setpoint due to the increased reactor temperature.

The reactor temperature in figure 8.6a tracks the setpoint well for the majority of the batch. Towards the end the setpoint has an increase which the process value does not follow. There are several reasons to this deviation. One of which is the setpoint on the conversion average temperature. If the process value would have followed the setpoint, the control of the conversion average temperature would have been jeopardized. Another reason might be the fact that the setpoint profile used is from the real plant which achieves a larger increase in the reactor temperature, which can be seen in figure B.4. Despite this, the setpoint profile used was considered a good enough solution with regards to testing the controller. In a real-life application an implemented setpoint profile would have been optimized for the specific process. A method for obtaining a setpoint profile is a batch optimizer which would have operated alongside the NMPC, but at a lower sampling frequency.

Figure 8.7 shows how the three MV's operate through the batch. The setpoint for the inlet temperature to the jacket in figure 8.7a and the setpoint for the volume flow to the reflux in figure 8.7b obtain approximately constant values before they both increase as the reflux is about to shut off. This happens at about 310 minutes into the batch. Figure 8.7c shows the mass flow of initiator. It is emphasized that the initial dose is not shown in this plot as it was decided to focus on the initiator dosing performed by the controller. As a consequence of not including the initial dose in the plot, all the plots of the simulation results presented in this thesis start straight after the initial dose of initiator. This corresponds to the point where the polymerization reaction starts.

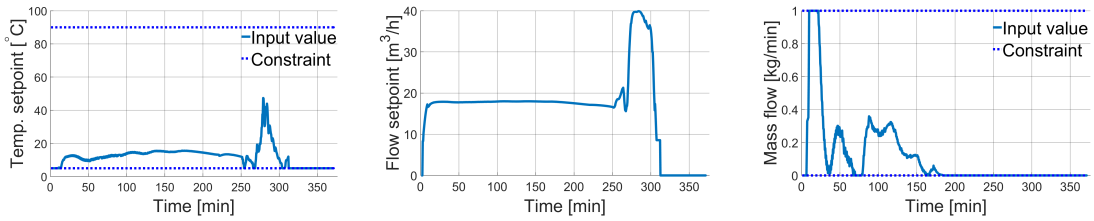

(a) Setpoint, inlet temperature of water to cooling jacket

(b) Setpoint, volume flow of water to reflux condenser

(c) Mass flow of initiator, excluding the initial dose

Figure 8.7: Inputs from simulation with a setpoint profile on the reactor temperature.

Figure 8.7a shows that the setpoint for the inlet temperature to the jacket lies at its lower constraint after the reflux is shut off. The activation of the reflux happens when the cooling from the cooling jacket reaches 90% of its capacity for the first time. Consequently, the jacket does not need to saturate. This is reflected in the setpoint for the inlet temperature to the jacket not being at its lower constraint before the reflux is shut off. The chosen operating strategy distributes the cooling between the jacket and the reflux.

When the setpoint for the inlet temperature to the jacket increases to approximately to 50 °C between 250 and 300 minutes the setpoint for the volume flow to the reflux increases and provides extra cooling before the reflux shuts off. This results in a less steep increase in the reactor temperature in figure 8.6a.

The initiator dosing obtains its upper constraint not so long after the initial dose before it drops down to zero. After dropping down it starts the dosing again for a short while before it drops again. The last period of initiator dosing is the longest. It keeps the polymerization rate at a level where the control of both conversion average temperature and the reactor temperature is satisfactory while still keeping the polymerization rate as large as possible. The dosing stops at about 170 minutes, which is relatively early in the batch. Some accumulation of initiator occurs during the three main sequences of the initiator dosing. Due to various phenomena modelled by the CF-polynomial, the accumulated mass of initiator is sufficient in keeping the polymerization rate up for the rest of the batch.

8.3.2 Case study 1.2: Constant setpoint

Figure 8.8 shows the reactor temperature, the reactor pressure, the conversion average temperature and the cooling for the simulation performed with a constant setpoint on the reactor temperature. For this approach the reactor temperature in figure 8.8a and the reactor pressure in figure 8.8b obtain values well within their respective constraints which ensures safe operation of the reactor. A dip in the reactor pressure can be observed for

this approach as well due to the same mechanism described in section 8.3.1. As a result of the constant reactor temperature, the conversion average temperature in figure 8.8c also has a constant behavior. This also apply to the cooling capacity and cooling demand in figure 8.8d.

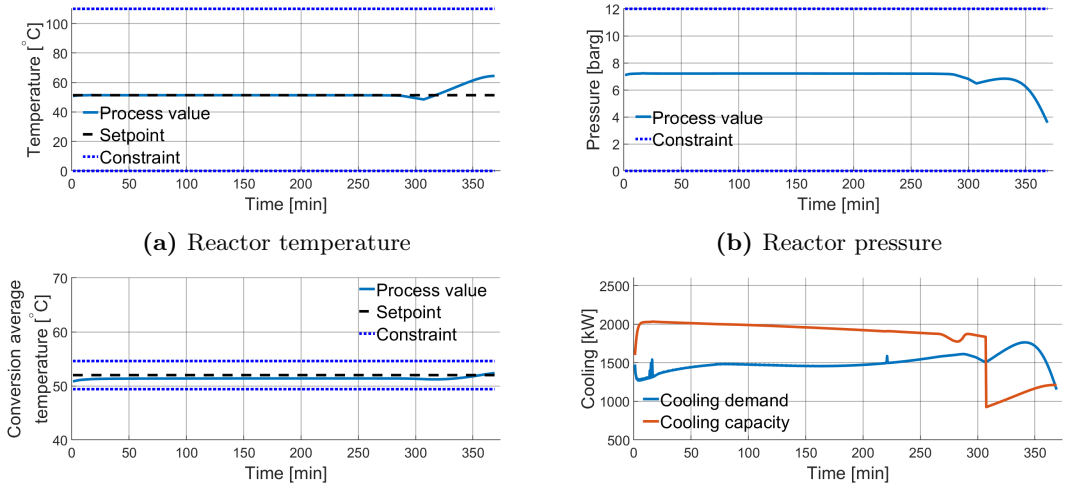

(a) Reactor temperature

(b) Reactor pressure

(c) Conversion average temperature

(d) Cooling

Figure 8.8: Model outputs from simulation with a constant setpoint on the reactor temperature.

The reactor temperature tracks the constant setpoint until about 300 minutes when the reflux condenser shuts off. A slight dip before the increase is observed and this is most likely from the controller predicting an increased reactor temperature in the prediction horizon. It tries to minimize the overall deviation from the setpoint in the entire prediction horizon. Since it predicts a temperature rise, it lowers the temperature while the reflux is still active and the cooling capacity is larger than the cooling demand.

As mentioned above, the conversion average temperature has a constant behavior, which is a result of the constant reactor temperature. The conversion average temperature also has a slight decrease before it increases and obtains a satisfactory end value. It is worth noting that the value of the constant reactor temperature setpoint was chosen such that the obtained end value of the conversion average temperature was satisfactory. The increase in the conversion average temperature was predictable. This implies that the setpoint value for the reactor temperature could easily be obtained by running just a few simulations and varying the reactor temperature setpoint.

Figure 8.8d shows that the cooling capacity has a constant decrease from the start of the batch towards the point where the reflux shuts off. Both the reactor temperature and the setpoint for the inlet temperature to the jacket in figure 8.9a are constant. Additionally, the capacity of the reflux from equation 6.11 is constant due to the reactor temperature (gas temperature) being constant. This implies that the decrease in the cooling capacity probably comes from an increase in the outlet temperature of the cooling jacket. The outlet temperature of the cooling increases as a result of the increase in the cooling demand. Consequently, more heat is added to the water in the cooling jacket. On the other hand, the dip in the cooling capacity at about 280 minutes is mostly due to the increase in the setpoint for the inlet temperature to the jacket.

Figure 8.9 shows how the three MV's operate through the batch. The setpoint for the

inlet temperature to the jacket in figure 8.9a lies close to its lower constraint almost the entire batch, with the exception of the small ramp-up at about 270 minutes. The setpoint for the volume flow to the reflux in figure 8.9b starts out small before it increases, while the mass flow of initiator in figure 8.9c is large in the beginning before it drops.

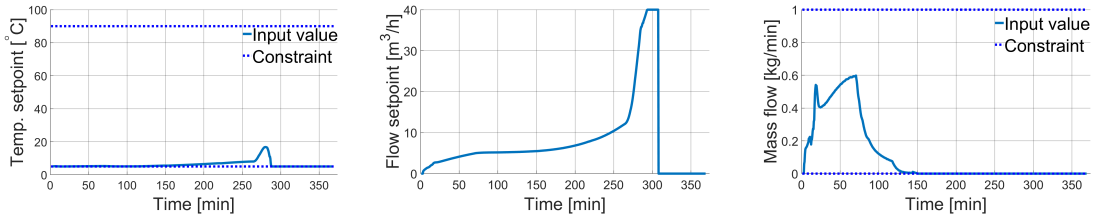

(a) Setpoint, inlet temperature of water to cooling jacket

(b) Setpoint, volume flow of water to reflux condenser

(c) Mass flow of initiator, excluding the initial dose

Figure 8.9: Inputs from simulation with a constant setpoint on the reactor temperature.

A reason for the large mass flow of initiator at the start of the batch can be a result of the low reactor temperature. The polymerization rate is initially small due to the reactor temperature, and the controller tries to increase the polymerization rate by adding initiator to the system. An increase can be observed through the increased demand in figure 8.8d towards 80 minutes into the batch. The maximum amount of initiator is reached early due to the large mass flow of initiator in the start of the batch. Again, phenomena modelled by the CF-polynomial results in the accumulated initiator being sufficient for the rest of the batch after the dosing is finished.

As the demand slowly increases, the setpoint for the volume flow to the reflux in figure 8.9b increases to provide more cooling capabilities to the cooling system. The increased cooling from the reflux is also most likely the main contributor to the dip in the reactor temperature at about 300 minutes.

8.3.3 Case study 1.3: No setpoint

Figure 8.10 shows the reactor temperature, the reactor pressure, the conversion average temperature and the cooling for the simulation performed without setpoint on the reactor temperature. Figure 8.10a shows that the reactor temperature behaves smoothly and does not run away even without a setpoint to track. At the start of the polymerization reaction the reactor temperature was set to be the same as for the case with a setpoint profile. The behavior of the reactor pressure in figure 8.10b ensures safe operation, and the same dip towards the end of the batch as the two other approaches can be observed. Both the cooling capacity and the cooling demand in figure 8.10d decrease at the start of the batch before obtaining a constant value while the reflux is active. The conversion average temperature in figure 8.10c have a small increase right at the start of the batch before it starts decreasing towards the setpoint. It achieves a satisfactory end value.

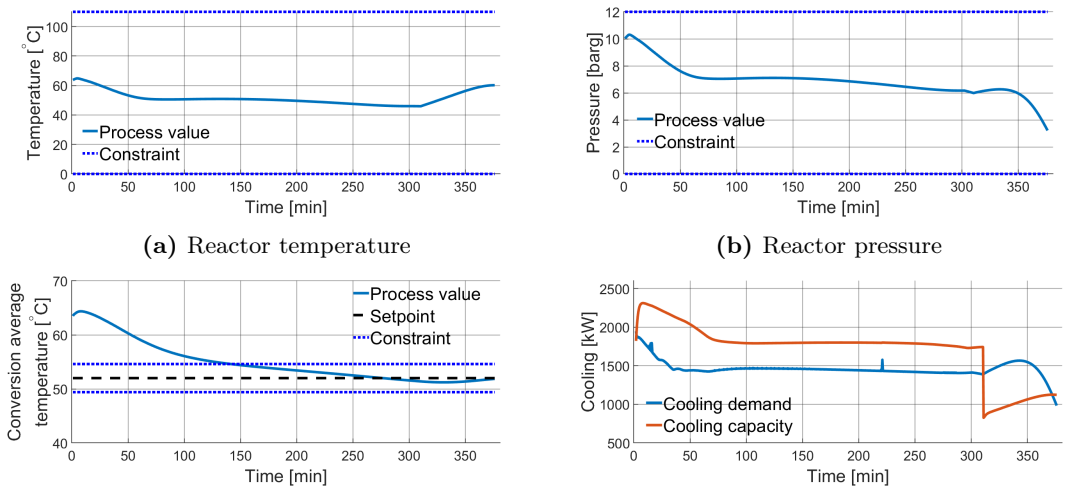

(a) Reactor temperature

(b) Reactor pressure

(c) Conversion average temperature

(d) Cooling

Figure 8.10: Model outputs from simulation without a setpoint on the reactor temperature.

The reactor temperature has an almost isotherm behavior excluding the start and the end of the batch, and it has a similar increase as the two former approaches. Since there is no setpoint on the reactor temperature, it is a result of controlling the conversion average temperature within its bounds and to its setpoint. The conversion average temperature is the principal CV and this case demonstrates that safe operation and quality specifications can be achieved even without a setpoint for the reactor temperature.

Figure 8.11 shows how the three MV's operate through the batch. The setpoint for the inlet temperature to the jacket in figure 8.11a is at its lower constraint at the start of the batch and after the reflux is shut off. An approximately constant value for the setpoint for the volume flow to the reflux in figure 8.11b is quickly obtained. The mass flow of initiator in figure 8.11c has an overall increase before it drops off.

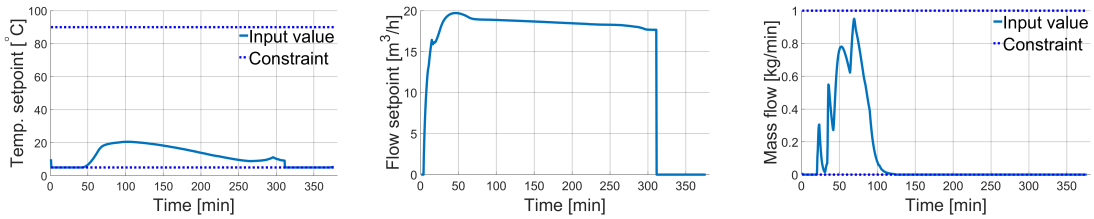

(a) Setpoint, inlet temperature of water to cooling jacket

(b) Setpoint, volume flow of water to reflux condenser

(c) Mass flow of initiator, excluding the initial dose

Figure 8.11: Inputs from simulation without a setpoint on the reactor temperature.

The setpoint for the inlet temperature to the jacket is at its lower constraint at the start of the batch to lower the reactor temperature, and consequently lower the conversion average temperature. It then increases in order to stabilize the reactor temperature at its nearly isotherm value. After this it slowly decreases before saturating again when the reflux shuts off.

Figure 8.11c shows that the mass flow of initiator is zero for a short period after the initial dose. This is to slow the polymerization reaction down and decrease the temperature. After the wait it varies, but has an overall increase before it drops to zero when the

maximum amount of initiator is used. The increase is most likely due to compensate for the lowering of the reactor temperature. This leads to a decrease in the polymerization rate, but the controller wants to maximize it, so it increases the mass flow of initiator.

8.3.4 Comparison of the simulation results

All three approaches achieved safe operation and met the quality specification at the end of the batch. In terms of batch time, the two approaches with a setpoint on the reactor temperature achieved similar results. The approach with a setpoint profile had a batch time of 371 minutes, while the approach with a constant setpoint had a batch time of 369 minutes. With a batch time of 376 minutes, the approach without a setpoint had a poorer performance even though it met the product quality specifications.

For all three approaches the reactor pressure is well within its constraints and safe operation is achieved. It is recognized that the pressure does not show any signs of violating its constraint, but it is included to emphasize the importance of keeping the pressure under control in a pressure vessel. When operating a real plant, disturbances which cause a temperature runaway and thus a pressure increase can occur and this can have fatal consequences if the controller is unable to limit the pressure.

The reactor temperature in figure 8.10a obtained without a setpoint has a close resemblance to the reactor temperature in figure 8.6a when a setpoint profile was utilized. Consequently, the other process outputs also look similar, but they are not identical. This can be seen by comparing the two conversion average temperature profiles in figure 8.6c and 8.10c. For the approach with a setpoint profile it has a constant decline, while for the approach without a setpoint it drops faster at the start before it flattens out. Despite the similarities in the process outputs, the behavior of the MV's differs. For the approach with the setpoint profile both the setpoint for the inlet temperature to the jacket and the setpoint for the volume flow to the reflux have a peak at about 270 minutes. The peak is most likely caused by the increase in the setpoint for the reactor temperature. As a result, this peak does not occur for the approach without a setpoint.

An observed trend for all three approaches is that the total mass of initiator is fully used before half of the batch time has proceeded. Even though the mass flow of initiator operates differently for the three approaches, it drops to zero early in the batch for all three cases. As mentioned, this is a result of various phenomena which cause an increased polymerization rate towards the end of the batch. The various phenomena are modelled by the CF-polynomial and makes the accumulated mass of initiator sufficient in keeping the polymerization rate going.

Compared to the two approaches with a setpoint, the approach without a setpoint has a smaller difference between the cooling capacity and the cooling demand. For the two approaches with a setpoint the difference is approximately 500 kW for the majority of the batch, while for the approach without a setpoint the difference is approximately 350 kW. A possible explanation to this is that the controller has the freedom to lower the reactor temperature due to the absence of a setpoint. This action drags the cooling capacity down, while the controller increases the polymerization rate with initiator. These actions push the capacity and demand closer together.

The approach with a setpoint profile for the reactor temperature was chosen to be the approach put to use for the remaining simulation results presented. Current operation of the reactor utilizes a setpoint profile, so this approach was considered the most relevant.

The setpoint profile in figure 8.6a was used. It is recognized that this setpoint profile is based on the real plant and not the plant replacement. Despite this, it was considered to be sufficient in terms of testing the controller and various operating conditions.

8.4 Case study 2: Maximum allowed initiator

The effect of varying the amount of initiator allowed for a batch was studied, both in terms of batch time, but also in terms of control. Varying the amount of initiator can reveal the effect it has on the batch time, but it also demonstrates how the controller performs with the varying initiator amounts and consequently operating conditions.

In all simulations presented in this section the initial dose of initiator was 5 kg and the total amount of initiator was varied. The CV's and MV's were as described in section 8.2.2 and the controller was tuned according to section 8.2.3.

Figure 8.12 shows the batch time for the different amounts of initiator allowed. An almost linear trend can be observed.

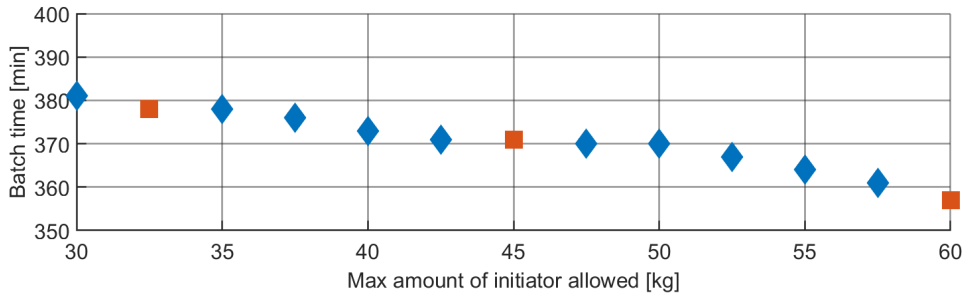

Figure 8.12: Batch time as a function of maximum amount of initiator allowed. The data points displayed with a red square are the data points used to illustrate the polymerization rate in figure 8.13.

The trend of a decreasing batch time with an increasing amount of initiator was expected as the initiator directly affects the polymerization rate. Depending on the cost of initiator, different considerations must be taken into account. For a cheap initiator any decrease in the batch time is profitable, while for an expensive initiator a trade-off between a reduction in batch time and the expenses related to the initiator should be considered.

Figure 8.13 shows the reaction rate throughout three batches with a small amount, a medium amount and a large amount of initiator allowed. The small amount is represented by a batch where the maximum amount was 32.5 kg, the medium amount was 45 kg and the large amount was 60 kg.

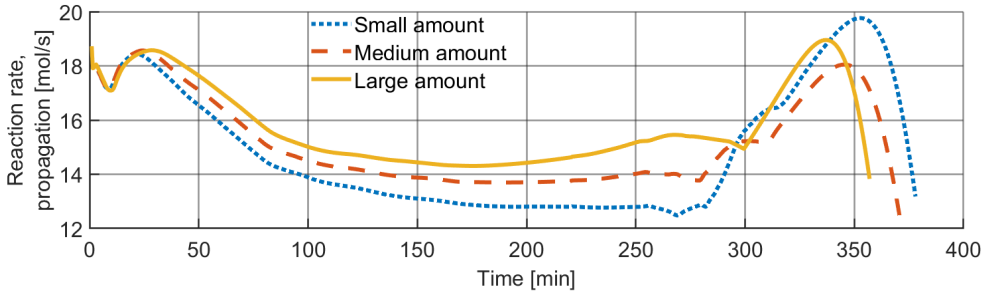

Figure 8.13: Propagation rate throughout a batch with a small amount, medium amount and a large amount of allowed initiator. The medium amount is not discussed in detail and is included mainly for comparison with the small and large amount.

The decreasing trend in figure 8.12 can be explained by the overall larger polymerization rate through the batch for a large amount of initiator allowed. For a large amount of initiator allowed the polymerization rate does not reach the same peak value as for a small amount of initiator, but it is larger for the majority of the batch. This leads to the "accumulated" polymerization rate being larger for a large amount of initiator allowed. The relative increase in the polymerization rate is larger for the small amount than for the large amount.

8.4.1 Example simulations

Simulation results from a simulation with a small amount and a simulation with a large amount of initiator allowed are presented. The two example simulations are first presented and discussed individually, then they are discussed in context of each other.

Case study 2.1 - Small amount of initiator

Figure 8.14 shows the reactor temperature, the reactor pressure, the conversion average temperature and the cooling for a simulation with a small amount of initiator allowed. Both the reactor temperature in figure 8.14a and reactor pressure in figure 8.14b lies well within their constraints and ensures safe operation of the reactor. The conversion average temperature in figure 8.14c obtains larger value than the desired setpoint at the end of the batch which is not desirable. However, the obtained end value is still acceptable considering the small amount of initiator allowed which can affect the behavior of the kinetics. The cooling capacity in figure 8.14d has a steady decrease before it drops down to the cooling demand right before 300 minutes. After this drop it increases and consequently the difference between the capacity and the demand increases before the reflux is shut off.

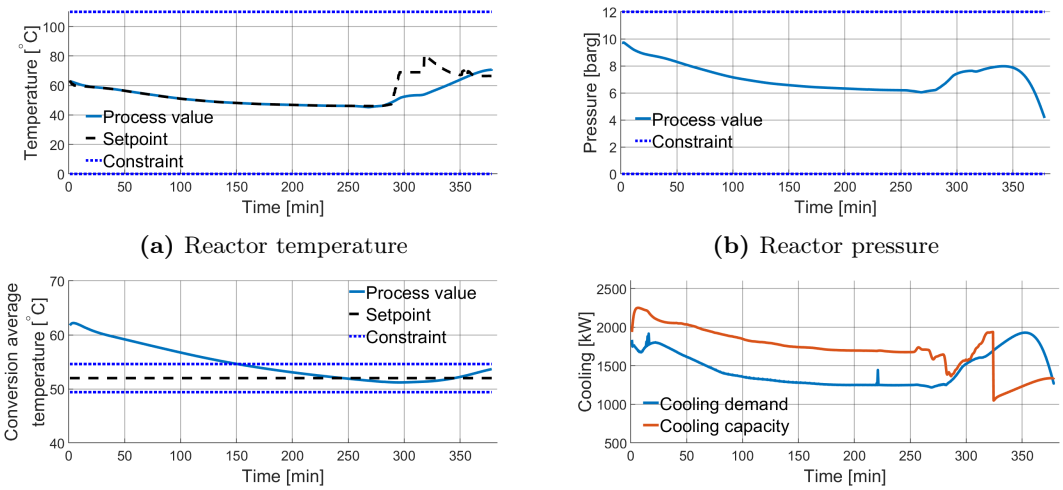

(a) Reactor temperature

(b) Reactor pressure

(c) Conversion average temperature

(d) Cooling

Figure 8.14: Model outputs from simulation with a small amount of initiator allowed.

The rise in the reactor temperature towards the end of the batch might be a result of the controller trying to increase the polymerization rate in order to get the conversion average temperature up to its setpoint, but the resulting reactor temperature increase instead causes an overshoot for the conversion average temperature.

Figure 8.15 shows how the three MV's operate through the batch. The setpoint for the inlet temperature to the jacket in figure 8.15a is saturated a short period at the start of the batch and after the reflux is shut off. Other than these two periods it operates in the range 10-20°C, except between 250 and 300 minutes. The setpoint for the volume flow to the reflux condenser in figure 8.15b quickly obtains a constant value before it varies some and then goes to zero as the reflux is shut off. As the allowed amount of initiator is small, the mass flow of initiator in figure 8.15c is conservative. The mass flow is initially large, but it quickly drops to zero and then operates at lower flow rates until the accumulated mass of initiator reaches its upper constraint.

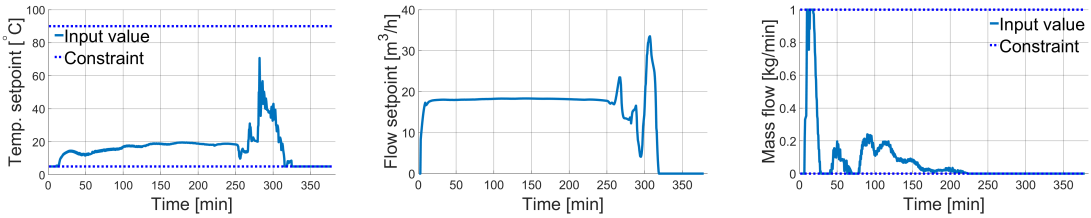

(a) Setpoint, inlet temperature of water to cooling jacket

(b) Setpoint, volume flow of water to reflux condenser

(c) Mass flow of initiator, excluding the initial dose

Figure 8.15: Inputs from simulation with a small amount of initiator allowed.

As mentioned above, the setpoint for the inlet temperature to the jacket varies between 250 and 300 minutes. In this time period it oscillates, and this behavior can be due to the large increase in the polymerization rate caused by the increase in the reactor temperature. The large rise in the polymerization leads to a large increase in the cooling demand and it looks like the controller tries to constantly adjust the setpoint for the inlet temperature to the jacket in order to control the reactor temperature and the conversion

average temperature. This oscillating behavior can also be a consequence of the low weight on the input move for the setpoint for the inlet temperature to the jacket, listed in table 8.4. The low weight makes it easy to move the input in order to control the CV's such as the reactor temperature and conversion average temperature.

The conservative initiator dosing affects the polymerization rate shown in figure 8.13. With a smaller polymerization rate throughout the batch, more monomer is present when the setpoint for the reactor temperature increases at about 300 minutes. Since there is more monomer left in the system at this stage, an increase in the reactor temperature has a larger effect on the polymerization rate. This can explain the large increase in the polymerization rate around 300 minutes which in turn could have caused the oscillating behavior observed in the setpoint for the inlet temperature to the jacket and the overshoot in the conversion average temperature.

Case study 2.2 - Large amount of initiator

Figure 8.16 shows the reactor temperature, the reactor pressure, the conversion average temperature and the cooling for a simulation with a large amount of initiator allowed. Both the reactor temperature in figure 8.16a and the reactor pressure in figure 8.16b lies well within their bounds and ensures safe operation of the reactor. The conversion average temperature in figure 8.16c obtains an end value slightly below the desired setpoint, but it still considered to be an acceptable result. Both the cooling capacity and the cooling demand in figure 8.16d decreases at the start of the batch and the difference is approximately 400 kW for the majority of the batch.

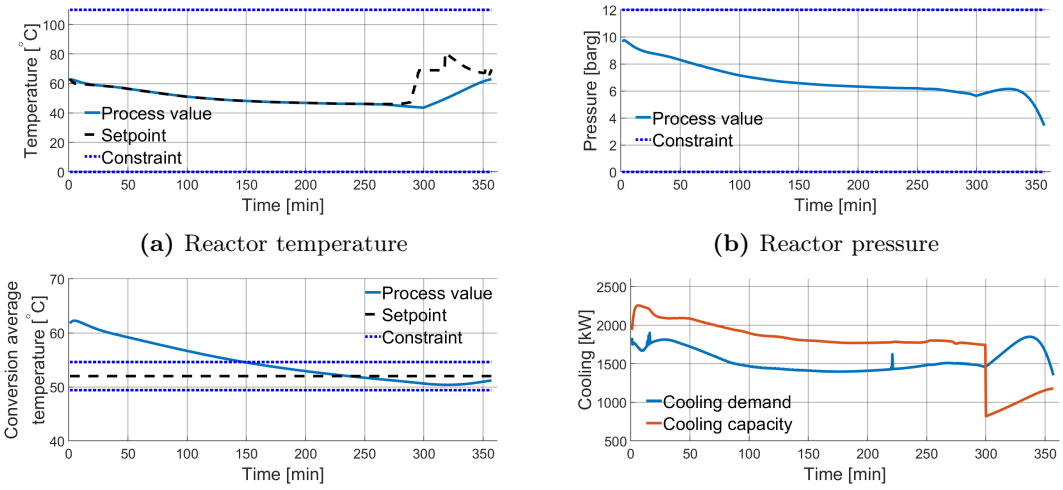

(a) Reactor temperature

(b) Reactor pressure

(c) Conversion average temperature

(d) Cooling

Figure 8.16: Model outputs from simulation with a large amount of initiator allowed.

The reactor temperature starts to increase after the setpoint increases. This delayed increase can be due to the polymerization rate in figure 8.13 being large throughout the batch. Due to the large "accumulated" polymerization rate the amount of monomer is not as large when the setpoint for the reactor temperature increases. Consequently, the increase in the polymerization is not substantial even though the CF-polynomial in equation 8.1 speeds up the polymerization rate towards the end of the batch. The lesser increase in both the polymerization rate and the reactor temperature could also explain the conversion average temperature ending the batch below its desired end setpoint.

Figure 8.17 shows how the three MV's operate through the batch. The setpoint for the inlet temperature to the jacket in figure 8.17a saturates for a short period at the start of the batch and also at about 250 minutes, which is before the reflux is shut off. An increase before the reflux is shut off can be observed for the setpoint for the volume flow to the reflux in figure 8.17b. Before the increase a constant value is maintained. The dosing of initiator in figure 8.17c occurs mainly in two large sequences.

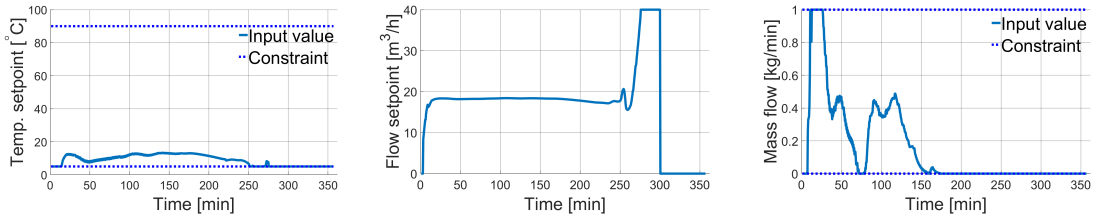

(a) Setpoint, inlet temperature of water to cooling jacket

(b) Setpoint, volume flow of water to reflux condenser

(c) Mass flow of initiator, excluding the initial dose

Figure 8.17: Inputs from simulation with a large amount of initiator allowed.

The reactor temperature in figure 8.16a decreases slightly just before 300 minutes and the main contributor to this decrease is the reflux. This can be seen from the increase in the setpoint for the volume flow to the reflux. The extra cooling from the reflux allows the conversion average temperature to decrease even further as a result of the reactor temperature.

When the initiator dosing in figure 8.17c is active it is generous with the initiator. This is due to the large amount allowed. As a result of the large dosing, more initiator is accumulated and the accumulated initiator is sufficient to keep the polymerization reaction at the high, steady rate observed in figure 8.13. It is worth mentioning that the large amount is almost double of what is being used at the real plant today. A plant replacement is simulated which never will resemble the real process perfectly. This means that having such a large amount could lead to unsafe operation at the real plant. If the controller should be implemented, tests regarding this case study, and initiator usage in general, should be conducted.

Comparison of the simulation results

Comparing the cooling demand in figure 8.14d and figure 8.16d, it is evident that the case with a large amount of initiator requires more cooling than the case with a small amount of initiator. This is a logical result as this case has a larger supply of initiator which implies a larger value of $\bar{n}$.

Both the setpoint for the inlet temperature to the jacket and the setpoint for the volume flow to the reflux for the case with a large amount behaves smoother than for the case with a small amount. This is especially evident around 300 minutes when the setpoint for the reactor temperature increases. The polymerization rate for the case with a small amount is more sensitive to a temperature change due to more monomer present. Consequently, the controller becomes nervous when trying to compensate for the large increase in the polymerization rate in figure 8.13 in order to control the reactor temperature and conversion average temperature. This leads to poorer control performance than for the case with a large amount of initiator.

For both cases, the main portion of the initiator dosing start and end at the same time in the two simulations. However, for the case with a large amount of initiator the dosing is more generous as mentioned above. Comparing the behavior of the mass flow of initiator in figure 8.15c and 8.17c, it is clear that the dosing drops off to a lower value much more quickly in the former.

The total amount of initiator allowed is in this thesis preset in the recipe of the batch and does not change from batch to batch, except for in this case study. Consequently, it can be thought that a retuning of the controller could have been performed when the maximum amount of initiator was changed. This would most likely have lead to better performance for a case where the amount of initiator allowed is abnormal, such as in case of a small amount of initiator. In this thesis retuning of the controller for the cases with different amounts of initiator allowed was not performed as this would have required significant more amounts of work and time.

8.5 Case study 3: Initial dose of initiator

The initial dose of initiator is an important parameter for the operation of the polymerization reactor. It is fed to the reactor as a rapid burst at the start of the batch and kick-starts the polymerization reaction. This case study was performed to study the effect the initial dose had on the batch time. Establishing a relation between the batch time and the initial dose could be helpful for the operators and control engineers when changing the recipe of the batch. Varying the initial dose also tests the controller's ability to handle varying doses. At the real plant, the valve for the dosing of initiator might not work properly or get stuck. This can lead to irregular initial doses. Consequently, how the controller responds to irregular initial doses is an interesting control aspect.

In all simulations presented in this section the total amount of initiator allowed was set to 45 kg, while the initial dose was varied. The CV's and MV's were as described in section 8.2.2 and the controller was tuned according to section 8.2.3.

Figure 8.18 shows how the batch time varies with the size of the initial dose. When an initial dose is utilized the batch time is declining in a linear fashion. The results substantiates the need for an initial dose as discussed in section 7.3. A significant decrease can be observed when comparing the batch time when not utilizing an initial dose and when utilizing an initial dose of 1 kg. Despite the trend declining as the initial dose increases, the effect is the largest when going from no initial dose to just even a small initial dose.

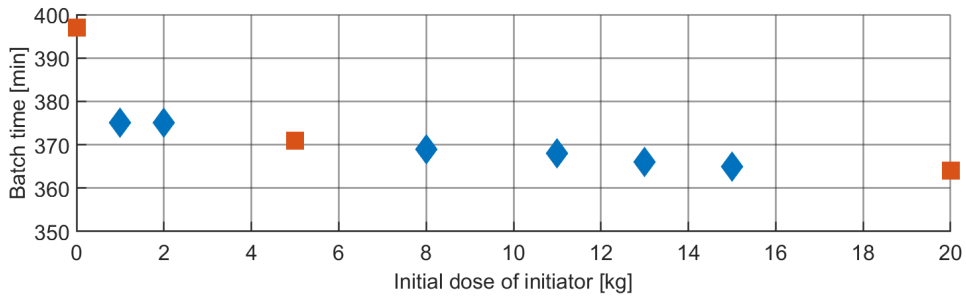

Figure 8.18: Batch time as a function of the initial dose of initiator. The data points displayed with a red square are the data points used to illustrate the polymerization rate in figure 8.19.

The trend in figure 8.18 can be explained by looking at the polymerization rate for different initial doses. Figure 8.19 shows the evolution of the polymerization rate when utilizing no initial dose, a medium initial dose and a large initial dose. After the initial phase of the batch, the three profiles for the polymerization rate resembles each other. This implies that the decrease in batch time is mainly a result of the large polymerization rate at the start of the batch.

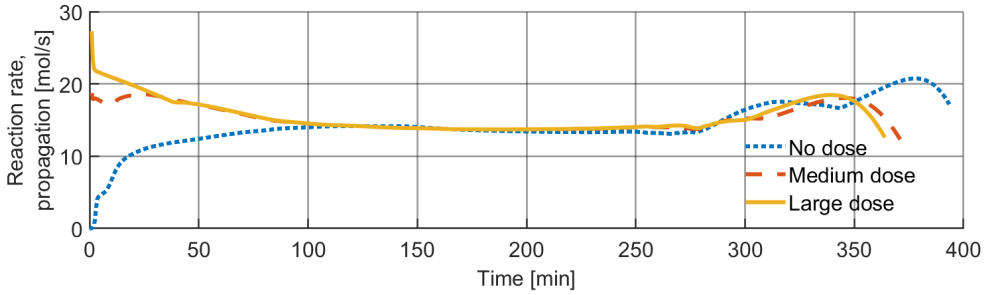

Figure 8.19: Propagation rate throughout a batch with no initial dose, a medium initial dose and a large initial dose of initiator.

Without an initial dose, the polymerization rate starts off slow compared to the ones with an initial dose. It takes some time before it becomes as large as the two utilizing an initial dose. Figure 8.19 also illustrates that increasing the initial dose from a medium amount (5 kg) to a large amount (20 kg) does not make a significant impact on the polymerization rate for the majority of the batch. The largest effect is during the initial phase of the batch.

8.5.1 Example simulations

Simulation results from a simulation without an initial dose and a simulation with a large initial dose of initiator are presented. The two example simulations are first presented and discussed individually, then they are discussed in context of each other.

Case study 3.1 - No initial dose

Figure 8.20 shows the reactor temperature, the reactor pressure, the conversion average temperature and the cooling for a simulation without an initial dose of initiator. Both the reactor temperature in figure 8.20a and the reactor pressure in figure 8.20b lies well within their bounds and ensures safe operation of the reactor. The conversion average temperature in figure 8.20c obtains a satisfactory end value despite the reaction rate being small in the beginning of the batch. Figure 8.20d shows that the cooling capacity is much larger than the cooling demand at the start of the batch due to the low polymerization rate. When the setpoint for the reactor temperature increases at about 270 minutes the capacity drops down to the demand before it becomes larger than the demand again while the reflux is active.

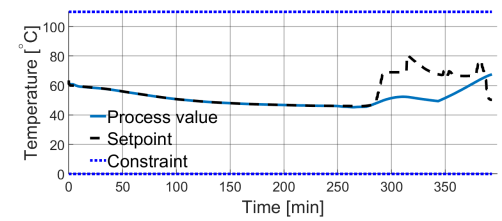

(a) Reactor temperature

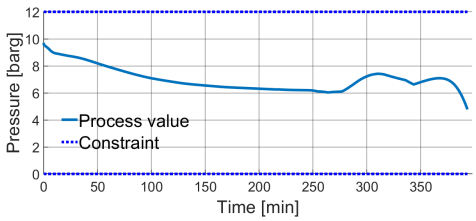

(b) Reactor pressure

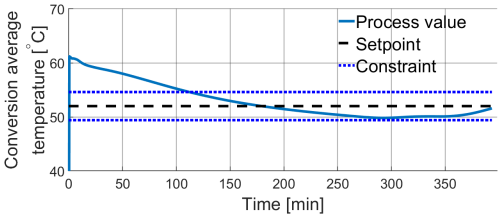

(c) Conversion average temperature

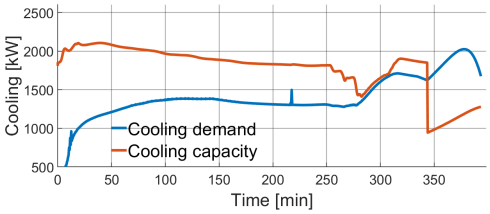

(d) Cooling

Figure 8.20: Model outputs from simulation without an initial dose of initiator.

The reactor temperature has two periods of increase at 260 minutes and 340 minutes. This same behavior can also be seen for the polymerization rate in figure 8.19. The two periods of increase are separated by a decreasing trend. This decrease can be an explanation to why the conversion average temperature undershoot significantly before it rises to its desired end setpoint. The conversion average temperature moves more slowly than the reactor temperature, and especially the polymerization rate which is related to the rapid kinetics. The conversion average temperature does not increase in concert with the reactor temperature and the polymerization rate. Consequently, when the dip in the two process outputs at about 310 minutes occur, the conversion average temperature has not yet increased.

Figure 8.21 shows how the three MV's operate through the batch. The setpoint for the inlet temperature to the jacket in figure 8.21a start the batch at about 40 °C. This is to keep the reactor temperature at its setpoint when the heat of reaction is small. Additionally, the setpoint for the volume flow to the reflux in figure 8.21b does not increase at the start of the batch since the reflux cooling is not needed as a result of the small heat of reaction. The mass flow of initiator in figure 8.21c is conservative at the start of the batch, but increases and obtains a constant value which it maintains until the initiator is fully used.

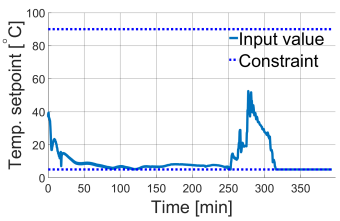

(a) Setpoint, inlet temperature of water to cooling jacket

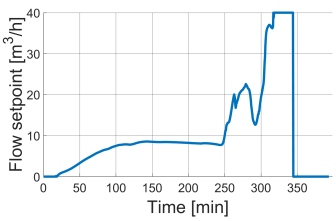

(b) Setpoint, volume flow of water to reflux condenser

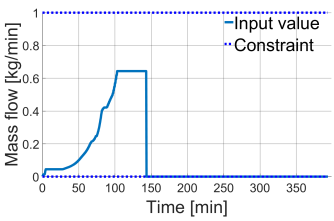

(c) Mass flow of initiator, excluding the initial dose

Figure 8.21: Inputs from simulation without an initial dose of initiator.

The first increase in the reactor temperature at about 260 minutes is most likely due to the increase in the setpoint for the inlet temperature to the jacket, while the following

decrease is a result of the increased setpoint for the volume flow to the reflux. When the polymerization rate in figure 8.19 is constant between 100 and 250 minutes, the setpoint for the volume flow to the reflux is approximately constant. In the same period the setpoint for the inlet temperature to the jacket only has some small fluctuations, and it is most likely used to keep the reactor temperature at its setpoint by making small adjustments.

An explanation for the low initiator dosing at the start could be the interplay between the conversion average temperature and the polymerization rate. Table 8.4 shows that the conversion average temperature is weighted higher than the polymerization rate, which implies that the controller probably prioritizes minimizing the deviation in the conversion average temperature before increasing the polymerization rate by increasing the mass flow of initiator.

Case study 3.2 - Large initial dose

Figure 8.22 shows the reactor temperature, the reactor pressure, the conversion average temperature and the cooling for a simulation with a large initial dose of initiator. Right at the start of the batch, the reactor temperature in figure 8.22a deviates some from its setpoint, but it quickly tracks the setpoint. The pressure in figure 8.22b behaves as expected and together with the reactor temperature it ensures safe operation of the reactor. Figure 8.22c shows that the conversion average temperature only undershoots its setpoint slightly and obtains a satisfactory end value. The initial cooling demand in figure 8.22d is larger than the cooling capacity, but it quickly drops below while the reflux is active.

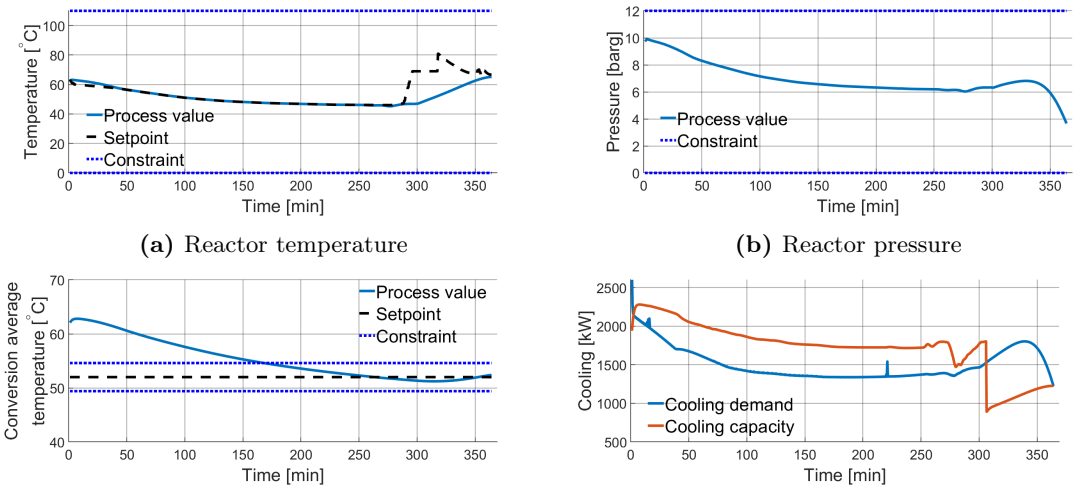

(a) Reactor temperature

(b) Reactor pressure

(c) Conversion average temperature

(d) Cooling

Figure 8.22: Model outputs from simulation with a large initial dose of initiator.

The reason for the initial deviation in the reactor temperature is due to the large initial dose. This results in a large initial polymerization rate, as figure 8.19 illustrates. Consequently, the cooling demand is initially larger than the cooling capacity and the cooling system is in deficit. The large initial dose causes a spike in $\bar{n}$, but this spike quickly drops and consequently decreases the cooling demand below the cooling capacity. Another result of the large initial polymerization rate is the initial increase for the conversion average temperate. This increase is small, but it delays the reduction of the deviation.

Apart from the initial part of the batch, the batch behaves predictable. The controller manages to calm the polymerization reaction down in order to stabilize the process for the rest of the batch.

Figure 8.23 shows how the three MV's operate through the batch. The setpoint for the inlet temperature to the jacket in figure 8.23a is saturated for a while during the initial phase of the batch. This is due to the large polymerization rate discussed above. Additionally, the setpoint for the volume flow to the reflux in figure 8.23b quickly obtains a constant value which it maintains before increasing at the end of the active period for the reflux. The mass flow of initiator in figure 8.23c has two main sequences after an initial wait.

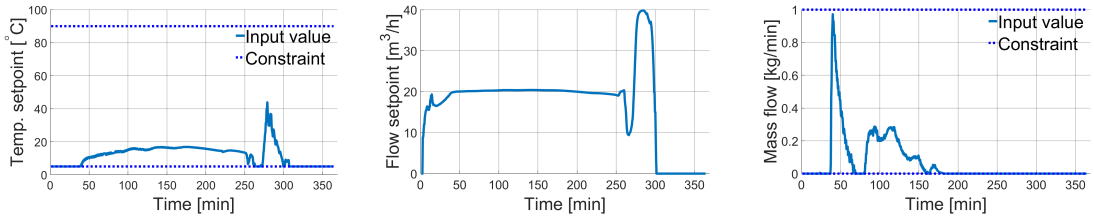

(a) Setpoint, inlet temperature of water to cooling jacket

(b) Setpoint, volume flow of water to reflux condenser

(c) Mass flow of initiator, excluding the initial dose

Figure 8.23: Inputs from simulation with a large initial dose of initiator.

The initial behavior of the MV's can be seen in context of the polymerization rate in figure 8.19. Due to the large initial polymerization rate, the reactor needs cooling. Cooling is provided both directly and indirectly. The direct cooling comes from the setpoint for the inlet temperature to the jacket and the setpoint for the volume flow to the reflux. Indirect cooling is provided by the absence of initiator dosing. By not dosing initiator and providing cooling, the reactor temperature swiftly tracks the setpoint after the initial deviation. When the reactor temperature control is satisfactory, the setpoint for the inlet temperature to the jacket is no longer saturated and the mass flow of initiator is non-zero.

Comparison of the simulation results

Due to the low initial polymerization rate, the conversion average temperature in figure 8.20c drops quicker than the one in figure 8.22c. As a result of the quicker decline it also undershoots its setpoint more. Despite this it obtains a satisfactory end value. Looking at the two example simulations, a type of opposite behavior for obtaining a satisfactory end value for the conversion average temperature can be observed. Since the polymerization rate without an initial dose is small in the beginning, the controller compensates by increasing the reactor temperature more towards the end of the batch. The opposite is observed with a large initial dose where the initial polymerization rate is large. Consequently, the need for an increase in the reactor temperature towards the end of the batch is less. The increase in the reactor temperature is in both cases provided by an increase in the setpoint for the inlet temperature to the jacket. For the case without an initial dose the increase is present for a longer period of time than for the case with a large initial dose. This is again reflected on the reactor temperature rise at about 260 minutes for both cases.

The batch times without an initial dose and with a large initial dose was 397 minutes and 364 minutes, respectively. This is a significant difference. As mentioned on previous occasions, it highlights the importance of the initial dose of initiator. In both cases the

controller is able to ensure safe operation throughout the batch in addition to obtaining the desired end quality specifications. This indicates that the controller is adaptable when it comes to handling varying initiator concentrations at the start of the batch.

8.6 Case study 4: Reduced heat transfer coefficient

A simulation with a decreased heat transfer coefficient between the cooling jacket and the reactor ($U_{J,R}$) was performed. The initial dose of initiator was 5 kg and the total amount of initiator allowed was 45 kg. The CV's and MV's were as described in section 8.2.2 and the controller was tuned according to section 8.2.3.

The results demonstrates the controller's ability to account for the decreased cooling capabilities of the cooling jacket. At the real plant, fouling on the reactor walls does occur and the simulation presented in this section replicates a batch with fouling on the reactor walls. This was done by reducing the heat transfer coefficient in the simulator in RealSim, but not in the controller and estimator.

Figure 8.24 shows the reactor temperature, the reactor pressure, the conversion average temperature and the cooling for the simulation with a 15% decrease in the overall heat transfer coefficient. Both the reactor temperature in figure 8.24a and the reactor pressure in figure 8.24b behaves such that safe operation of the reactor is achieved. The conversion average temperature in figure 8.24c obtains a satisfactory end value, while the cooling capacity in figure 8.24d is sufficient when the reflux is active.

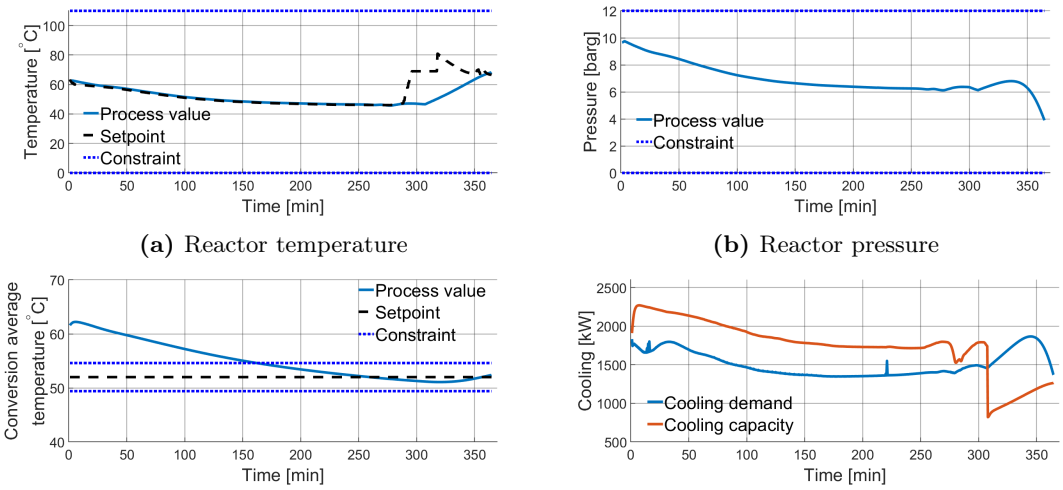

(a) Reactor temperature

(b) Reactor pressure

(c) Conversion average temperature

(d) Cooling

Figure 8.24: Model outputs from simulation with 15% decrease in the overall heat transfer coefficient.

Even though the heat transfer coefficient was reduced, the results show that the cooling capacity is similar to that in figure 8.6d where there is no reduction in the heat transfer coefficient. An explanation for this can be that the cooling capacity is dependent on several model outputs, as equation 6.9 and 6.11 show. The setpoint for the inlet temperature to the jacket in figure 8.25a behaves differently than the one in figure 8.7a. This results in a different behavior of the outlet temperature of the cooling, which affects the capacity of the cooling jacket.

The other process outputs for reduced heat transfer between the jacket and the reactor

look similar to the ones in section 8.3.1 (Case study 1.1). Despite this, the MV's behave differently in order to obtain similar process outputs. Figure 8.25 shows how the three MV's operate through the batch. The setpoint for the inlet temperature to the jacket in figure 8.25a is saturated at the start of the batch and after the reflux is shut off. A steady increase in the setpoint for the volume flow to the reflux in figure 8.25b is observed, while the mass flow of initiator in figure 8.25c occurs in four sequences.

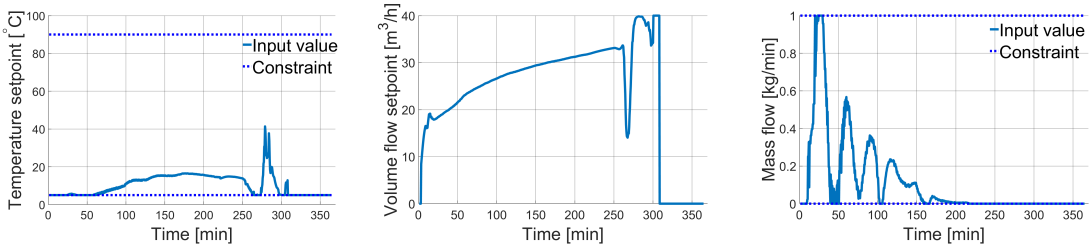

(a) Setpoint, inlet temperature of water to cooling jacket

(b) Setpoint, volume flow of water to reflux condenser

(c) Mass flow of initiator, excluding the initial dose

Figure 8.25: Inputs from simulation with 15% decrease in the overall heat transfer coefficient.

The reason that the setpoint for the inlet temperature to the jacket is saturated for a longer period than in case study 1.1 is the reduced cooling capability of the jacket. This is also the reason for the steady increase in the setpoint for the volume flow to the reflux. As the jacket has less cooling capabilities, the reflux provides more cooling. This was the desired response since the reflux condenser typically does not operate at its capacity, implying that it has more cooling effect to provide if necessary. Compared to the setpoint for the volume flow to the reflux in figure 8.7b, it is a bit more aggressive in this case.

The mass flow of initiator moves more than the mass flow of initiator in figure 8.7c. A reason for the bigger movement can be that the initiator dosing has a more prominent role in finer control of the reactor temperature in this case than in case 1.1.

The simulation results presented in this section shows that the controller is able to adjust for the case where there are a significant amount of fouling on the reactor. Accompanied by the estimator, the controller achieves safe operation and satisfactory end quality. The MV's behave more aggressive than in figure 8.7, but the behavior is still considered to be acceptable.

8.7 Case study 5: Length of horizons

This case study was performed to investigate whether or not changing the length of the prediction- and control horizon would result in better control of the reactor. The initial dose of initiator was 5 kg and the total amount of initiator allowed was 45 kg. The CV's and MV's were as described in section 8.2.2 and the controller was tuned according to section 8.2.3, except for the varying horizon lengths.

Table 8.5 shows the length of the prediction- and control horizons along with their parameterization in each case.

Table 8.5: Length of control- and prediction horizon for the case studies simulated. Numbers in parenthesis represent the parameterization, and the lengths and parameterzations are listed as number of samples.

	Control horizon	Prediction horizon
Case study 5.1	10 (0, 2, 5, 10)	40 (every second sample)
Case study 5.2	10 (0, 2, 5, 10)	100 (every second sample)
Case study 5.3	30 (0, 8, 16, 30)	100 (every second sample)
Case study 5.4	49 (0, 12, 25, 49)	100 (every second sample)

Table 8.5 shows that the longest prediction horizon utilized was 100 samples (50 minutes). It was quickly discovered that increasing the prediction horizon further caused the system to diverge in the prediction horizon. This is most likely because the system is open-loop unstable as a consequence of the kinetics. The kinetic model is stiff, and sensitive to the initiator dosing. This implies that the prediction horizon used in the other case studies in this thesis was almost as long as it could be without running into this problem.

If a prediction horizon as long as the entire batch was possible, this would have been an aspect to look into. A prediction horizon as long as the entire batch could have improved control of the reactor if the real-time requirement was not considered a problem. With a prediction horizon as long as the entire batch the conversion average temperature could have been weighted only at the very end of the batch. Then the controller could have utilized the cooling capacity better at the start of the batch while still ensuring that the conversion average temperature reaches a satisfactory end value. The controller would not have to account for the conversion average temperature before the very end of the batch. This would might give the controller more freedom to increase the polymerization rate and consequently the cooling demand at the start of the batch to better utilize the available cooling capacity.

Simulation results for case study 5.2 - 5.4 showed similar behavior as the results from section 8.3.1 (Case study 1.1) and are consequently not included in this section since they provided no new insight. Case study 5.1 on the other hand gave quite different simulation results and it is included in this section.

8.7.1 Example simulation

The results from the simulation with both a short prediction- and control horizon are presented. As case study 5.2 with a short control horizon and a long prediction horizon showed very similar results as case study 1.1 in section 8.3.1, it was considered that the length of the prediction horizon was the principal contributor to the deviating behavior in case study 5.1.

Case study 5.1: Short prediction- and control horizon

Figure 8.26 shows the reactor temperature, the reactor pressure, the conversion average temperature and the cooling for the simulation with a short prediction- and control horizon. The reactor temperature in figure 8.26a and the reactor pressure in figure 8.26b still ensures safe operation of the reactor. The reactor temperature overshoots its setpoint towards the end of the batch. This is most likely the cause of the large end value for the conversion average temperature in figure 8.26c. The cooling capacity in figure 8.26d drops

significantly around 270 minutes as a result of the large increase in the setpoint for the inlet temperature to the jacket in figure 8.27a.

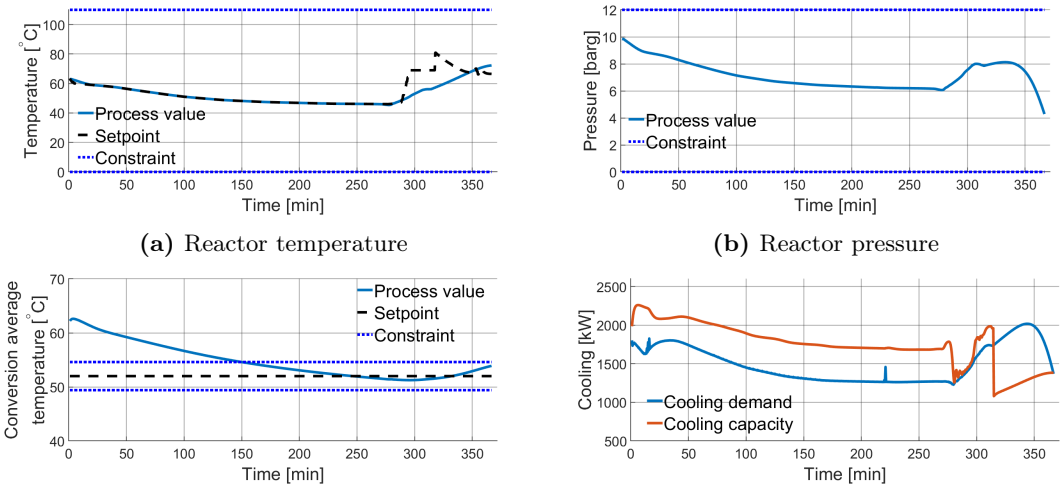

(a) Reactor temperature

(b) Reactor pressure

(c) Conversion average temperature

(d) Cooling

Figure 8.26: Model outputs from simulation with both short control horizon and prediction horizon.

Figure 8.27 shows how the three MV's operate through the batch. More aggressive and nervous behavior can be observed in the setpoint for the inlet temperature to the jacket in figure 8.27a and the setpoint for the volume flow to the reflux in figure 8.27b. The mass flow of initiator in figure 8.27c operates at its upper constraint for a short period before it steadily declines.

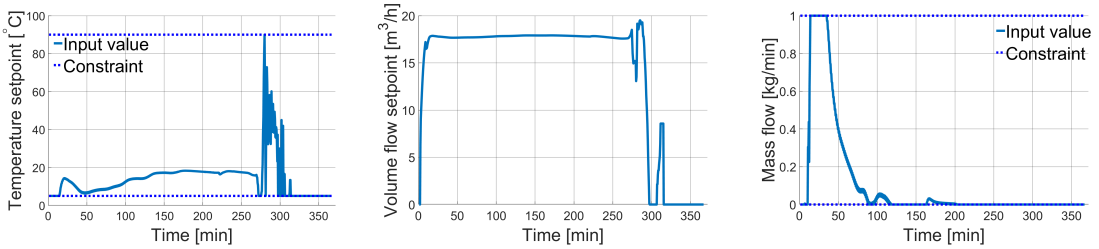

(a) Setpoint, inlet temperature of water to cooling jacket

(b) Setpoint, volume flow of water to reflux condenser

(c) Mass flow of initiator, excluding the initial dose

Figure 8.27: Inputs from simulation with both short control horizon and prediction horizon.

The setpoint for the inlet temperature to the jacket operates satisfactory until about 270 minutes when the reactor temperature setpoint increases. As a consequence of the short prediction horizon, the controller thinks the reactor temperature setpoint increases indefinitely, while in fact it flattens out at about 290 minutes. The controller then tries to increase the reactor temperature by increasing the setpoint for the inlet temperature to the jacket drastically. These drastic control moves are not beneficial for the control. The drastic fluctuations in the setpoint for the inlet temperature to the jacket only cause unnecessary wear and tear on the actuators. The same problem is observed in the behavior of the setpoint for the volume flow to the reflux. The setpoint for the volume flow volume drops to zero at 300 minutes, which is even before the reflux is shut off.

The mass flow of initiator operates at its upper constraint at the start of the batch. This implies that a lot of initiator is used at the start. Consequently, the total amount of initiator is fully used early in the batch, which can be observed by the minuscule initiator mass flow after 120 minutes. This might also be a consequence of the short prediction horizon as the controller does not think about future control in the same manner as with a long prediction horizon. For a longer prediction horizon the controller are aware of the consequences of current control moves longer into the future. Consequently, it can adjust the mass flow of initiator to lower values since it observes that the maximum amount of initiator is achieved quick with larger mass flows. By doing this the polymerization rate can be maintained at a large value for a longer period.

The simulation results in figure 8.26 and 8.27 indicate that a too short prediction horizon worsens the controller performance. Since a single shooting method was utilized to solve the optimization problem in the controller, the length of the prediction horizon does not have a significant affect on the computation time as long as the input blocking remains the same. Additionally, a too long prediction horizon was not obtainable due to the system being open loop unstable. This suggested that a prediction horizon of 80 samples (40 minutes), which was used in all other case studies, was a satisfactory approach.

8.8 Case study 6: Parameterization of the inputs

The case study presented in this section was performed to investigate how the input blocking affected both the computation time and the controller behavior. The initial dose of initiator was 5 kg and the total amount of initiator allowed was 45 kg. The CV's and MV's were as described in section 8.2.2 and the controller was tuned according to section 8.2.3, except for the varying number of input blocks.

In an application implemented at a real plant the computation time for each sample might become an important aspect to consider. Only the input blocking, and not the CV- parameterization, was varied as it was considered to be the most important factor for the computation time. This is because a single shooting method as described in section 3.1.3 was utilized in the NMPC controller. In a single shooting approach the decision variables for the optimization problem in the controller are the MV's. This implies that the computation time should scale along with the number of unknown input variables/input blocks.

Table 8.6 shows the input parameterization for the cases simulated in this section. The mean and max computation time for one sample are also listed.

Table 8.6: Mean and max computation time for one sample performed by the NMPC controller listed for the different input parameterizations. Numbers in parenthesis represent the parameterization, and the control horizon length is listed as number of samples.

	Control horizon	Mean [s]	Max [s]
Case study 6.1	20 (0, 20); 2 input blocks	1.236	3.297
Case study 6.2	30 (0, 10, 30); 3 input blocks	1.628	3.543
Case study 6.3	30 (0, 8, 16, 30); 4 input blocks	1.797	4.105
Case study 6.4	30 (0, 5, 14, 22, 30); 5 input blocks	2.108	4.879
Case study 6.5	30 (0, 4, 8, 15, 22, 30); 6 input blocks	2.306	5.692
Case study 6.6	30 (0, 2, 5, 10, 16, 22, 30); 7 input blocks	3.299	8.441

Table 8.6 shows that both the mean and max computation time grows as the number of input blocks increases. This was an expected trend due to the nature of the single shooting approach. In case study 6.1 the optimization problem solved at each sample had six decision variables (3 MV's $\times$ 2 input blocks), while in case study 6.6 it had 21 (3 MV's $\times$ 7 input blocks). It then becomes evident the extra computational load required to solve the optimization problem.

8.8.1 Example simulations

Simulation results from a simulation with two input blocks and a simulation with seven input blocks are presented. The two example simulations are first presented and discussed individually, then they are discussed in context of each other.

Case study 6.1 - Two input blocks

Figure 8.28 shows the reactor temperature, the reactor pressure, the conversion average temperature and the cooling for the simulation with two input blocks. The behavior of both the reactor temperature in figure 8.28a and the reactor pressure in figure 8.28b ensures safe operation throughout the entire batch. The conversion average temperature in figure 8.28c has a steady decline and undershoots its setpoint before it obtains a satisfactory end value. Both the cooling capacity and cooling demand in figure 8.28d behaves as expected with the capacity being sufficient up until the reflux is shut off.

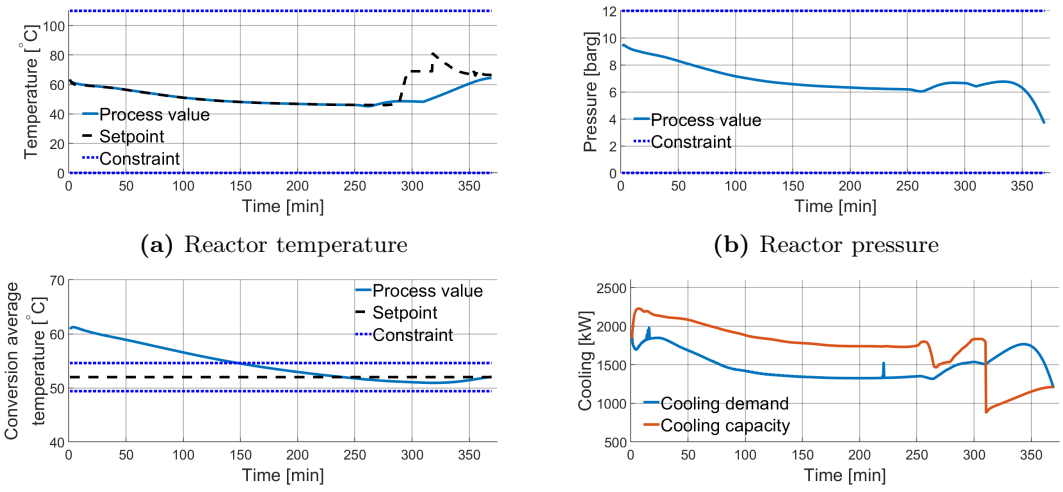

(a) Reactor temperature

(b) Reactor pressure

(c) Conversion average temperature

(d) Cooling

Figure 8.28: Model outputs from simulation with two input blocks.

The hypothesis was that the control performance would not be as good with only two input blocks. This was substantiated by that there are less freedom for the controller in the control horizon as a result of fewer input blocks. However, even with only two input blocks the controller ensures satisfactory control of the reactor in terms of both safety and quality specifications.

Figure 8.29 shows how the three MV's operate through the batch. The setpoint for the inlet temperature to the jacket in figure 8.29a is practically saturated even a short period before the reflux is shut off. The familiar increase in the setpoint for the volume flow to

the reflux in figure 8.29b can be observed at 250 minutes. Three main sequences can be observed for the mass flow of initiator in figure 8.29c.

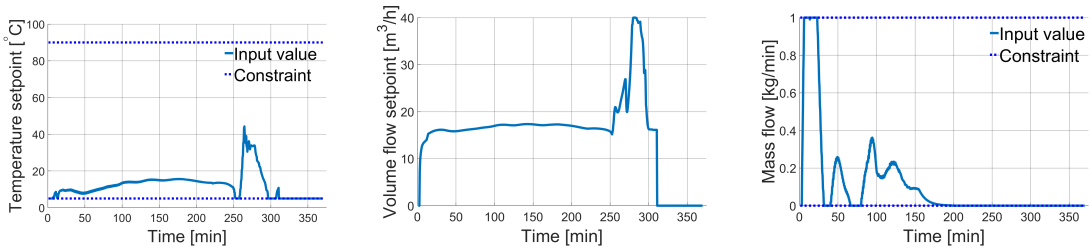

(a) Setpoint, inlet temperature of water to cooling jacket

(b) Setpoint, volume flow of water to reflux condenser

(c) Mass flow of initiator, excluding the initial dose

Figure 8.29: Inputs from simulation with two input blocks.

Case study 6.6 - Seven input blocks

Figure 8.30 shows the reactor temperature, the reactor pressure, the conversion average temperature and the cooling for the simulation with seven input blocks. The reactor temperature in figure 8.30a behaves similar to the reactor temperature in figure 8.28a, but achieves a lower increase towards the end. In addition to the reactor pressure in figure 8.30b, the reactor temperature ensures safe operation of the reactor. The conversion average temperature in figure 8.30c obtains an end value below its desired setpoint, but it is still considered a satisfactory result. Both the cooling capacity and the cooling demand in figure 8.30d behaves similar to the capacity and demand in figure 8.28d.

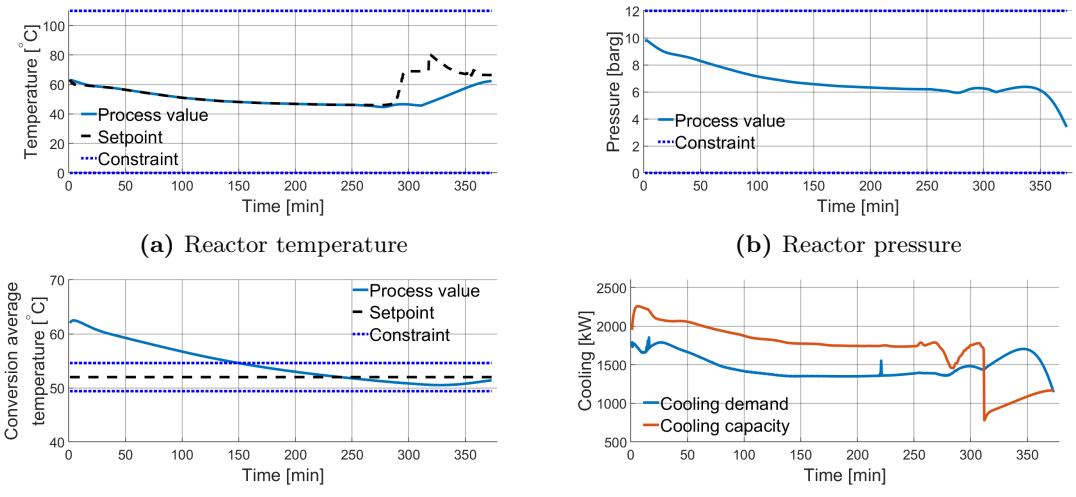

(a) Reactor temperature

(b) Reactor pressure

(c) Conversion average temperature

(d) Cooling

Figure 8.30: Inputs from simulation with seven input blocks.

Figure 8.31 shows how the three MV's operate through the batch. The setpoint for the inlet temperature to the jacket in figure 8.31a shows a narrower period of increase at about 250 minutes compared to the one in figure 8.29a. This can explain the lesser increase in the reactor temperature and consequently the low end value for the conversion average temperature. In addition, the increase in the setpoint for the volume flow to the reflux in figure 8.31b occurs in a wider period of time compared to the one in figure 8.29b. This

results in more cooling to the reactor and prevents the reactor temperature from increasing as much. The mass flow of initiator in figure 8.31c occurs in three sequences with the last one being the largest.

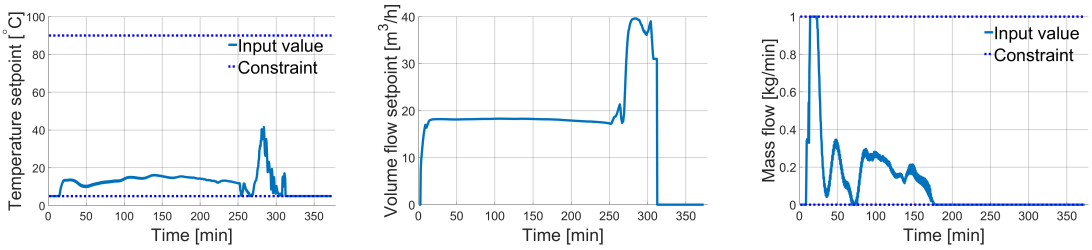

(a) Setpoint, inlet temperature of water to cooling jacket

(b) Setpoint, volume flow of water to reflux condenser

(c) Mass flow of initiator, excluding the initial dose

Figure 8.31: Inputs from simulation with seven input blocks.

Comparison of the simulation results

The process outputs for the two cases look similar. In addition, the batch times for the two cases were approximately the same. For two input blocks the batch time was 370 minutes, while for seven input blocks it was 373 minutes. The slight differences in the reactor temperature and consequently the conversion average temperature is not considered to be significant and the end quality for both cases is satisfactory.

The MV's in the two cases also operated similarly. Only some minor differences that led to the differences in the process outputs can be observed. For the case with seven input blocks, a higher degree of input moves can be observed. This can come from the larger number of input blocks, which allows the controller to move the inputs more in the control horizon and thus find more sensitivity towards the objective function in the controller formulation.

As already mentioned, the results from the two cases showed similar behavior. A significant improvement by increasing the number of input blocks is not observed. This suggests that a fewer number of input blocks can be chosen without sacrificing control performance. Table 8.6 shows that the number of input blocks affects the maximum computation time. For the implementation in this thesis the sample time was 30 seconds, but for a real-life implementation the sample time will most likely be lower and the computation time could prove to become a critical parameter for the NMPC application. If the computation time becomes larger than the sample time, the real-time requirement would not be satisfied. The controller would then lag further and further behind for each sample. An easy approach for reducing the computation time would then be to reduce the number of input blocks. Other approaches for reducing the computation time could be to simplify the model or to optimize the code, but in this case the principal approach would have been to reduce the number of input blocks.

9 Conclusion and recommendations for further work

This chapter aims to summarize the findings of this report. Some conclusions are presented before comments regarding further work are made.

The purpose of this thesis was first to finalize and extend the model established in the preliminary work, and further implement NMPC to the semi-batch reactor for miniemulsion polymerization of VCM. This was performed in Cybernetica's software where the controller was tuned and the application also was tested by performing various case studies.

9.1 Conclusion

This report presented the necessary theoretical foundation for polymerization, which was based on literature research performed during the preliminary project. Further, the theoretical foundation of constrained optimization, NMPC, and state- and parameter estimation was presented. The initial phase of the thesis involved extensions and refinement of the model established in the preliminary project. Extensions made were simulated and validated against measurements provided by INOVYN. With the necessary model extensions implemented and tested, an environment for the control system was established and implemented in Cybernetica's software. This allowed for simulating and evaluating the controller on a plant replacement model. The model used as the plant replacement was chosen to be the same as the model in the NMPC.

In section 8.1 the implemented model extensions were validated against measured data. The conversion average temperature showed a small deviation for the end value, but it was considered to be a satisfactory result regarding further use in the NMPC implementation. Some extensions to the cooling system were performed. This included modelling the dynamics of the inlet temperature to the cooling jacket and the volume flow to the reflux condenser. In the preliminary project these parameters were used as inputs to the model, but for control of the reactor their respective setpoints had to be used instead. The implemented extensions in equation 6.5 and 6.6 showed to be satisfactory representations of the dynamics. The polynomial for CF in equation 8.1, describing the unmodelled aspects of the system, was successfully implemented with an improvement in the ballistic simulations.

Due to the lack of available measurements at the plant, some modifications to the control structure in figure 5.3 were necessary. The existing cascade- and split range structure was replaced by a structure where the inlet temperature to the cooling jacket and the volume flow to the reflux were controlled by PID controllers. The setpoints for their respective PID controllers were provided by the NMPC controller instead of the master controller represented by TIC-1 (reactor temperature) in figure 5.3. The resulting control structure in figure 8.5 was considered to be a satisfactory solution in terms of capturing the dynamics of the system and testing various aspects of the reactor control. Constraints and setpoints for the CV's and MV's in the NMPC controller were based on a combination of operating specifications from INOVYN and process knowledge. A significant portion of the NMPC implementation involved controller tuning and getting the interplay between the variables correct. The obtained values in table 8.4 gave satisfactory results for a broad variety of operating conditions.

Three approaches for the reactor temperature control were tested. All three approaches showed promising results regarding product quality specifications and safe operation throughout the batch. For all approaches the cooling capacity were sufficient until the reflux was

shut off. The dosing of initiator was finished early in the batch for all three approaches. During the initiator dosing, some initiator was accumulated. This accumulated mass was sufficient for the rest of the batch as a result of various phenomena modelled by the CF-polynomial. As the approach with a setpoint profile for the reactor temperature was the most relevant, this approach was chosen for the other case studies performed in this thesis. Even though the setpoint profile was recognized to not be optimal for the plant replacement model, it was considered to be a satisfactory approach in order to test the controller.

Different operations of the initiator were tested. This was done to study both how the initiator affected the batch time, and how the controller handled abnormal operating conditions. The batch time showed a decreasing trend for larger amounts of initiator allowed in case study 2, which was expected. For a low amount of initiator allowed the conversion average temperature obtained a too large end value, but it was considered acceptable. For a large amount of initiator allowed the conversion average temperature obtained a satisfactory end value. The controller behaved poorer and more aggressive for a small amount of initiator allowed. In case study 3 the effect of the initial dose of initiator was studied. Figure 8.18 illustrates the importance of the initial dose of initiator. The batch time was reduced significantly going from no initial dose to utilizing an initial dose. Without an initial dose the controller was still able to obtain satisfactory control of the reactor even though the batch time was longer. For a large initial dose the initial cooling demand was larger than the cooling capacity, but the controller still managed to achieve a satisfactory end value for the conversion average temperature. This demonstrated the controllers ability to handle abnormal initial doses of initiator, which can occur if the valve for the initiator gets stuck.

Case study 4 showed that the controller in conjunction with the estimator handled a reduction in the heat transfer coefficient between the cooling jacket and the reactor satisfactory. As a result of the reduced heat transfer in the jacket, the reflux contributed more which was exactly the desired behavior. This case study was meant to replicate fouling on the reactor walls which is a relevant aspect in the real plant.

The effect of changing the lengths of the prediction- and control horizon, and the number of control blocks were studied in case study 5 and 6, respectively. A prediction horizon longer than 100 samples (50 minutes) was not possible to test due to the stiffness of the system caused by the kinetic model. Short prediction- and control horizon were tested, and this resulted in an aggressive controller and less satisfactory behavior for the process outputs. Increasing the number of input blocks did not yield a significant improvement in the control. This suggested that few control blocks could be chosen to reduce the computation time without losing any significant control performance. In a real-life implementation this could prove helpful as the computation time might become critical if the sample time is reduced.

The model for the miniemulsion polymerization of VCM in a semi-batch reactor, along with the implementation of NMPC on the reactor system were considered to be successful. The results indicated that the controller was able to handle varying operating approaches and anomalies related to the usage of the initiator, especially abnormal initial doses. It obtained safe operation during the batch and it also met quality specifications at the end for most operating conditions and control strategies. Even though the results were promising, they can not be confirmed before the controller is implemented and tested on the real process.

9.2 Recommendations for further work

Further work could focus on increasing the level of complexity for the process model. As seen from table 8.6 the average computation time was below five seconds and the maximum computation time was approximately eight seconds. This implies that some additional complexity can be added to the model while still adhering to the real-time requirement, even if the sample time is reduced. The most immediate extension would be to model the heat exchangers and valves related in the red box in figure 5.3. This would however require the installation of flow- and temperature measurements. Consequently, this is most relevant for a future project where the application is actually implemented to the real plant.

Tuning of the controller is a time extensive exercise, and due to time limitations the controller tuning phase of this thesis had to be stopped to have time for testing the controller. It is recognized that the controller tuning obtained in table 8.4 might not be the optimal. The simulation results in this thesis showed promising results with the obtained tuning, but further work could try different sets of tuning parameters which might lead to better control.

In this thesis a setpoint profile for the reactor temperature provided by INOVYN was utilized. For a real-life application a setpoint profile should ideally be tailored for the specifics of each batch. This can be achieved by implementing a batch optimizer which would work alongside the NMPC, only with a lower sampling frequency. The batch optimizer would have a prediction horizon as long as the batch. This would allow the batch optimizer to find the optimal reactor temperature trajectory with respect to safe operation and quality specifications. The implementation of a batch optimizer would be especially beneficial for the control of the conversion average temperature since only its end value is important. During the work in this thesis, the implementation of a batch optimizer was discussed, but it was not started due to time limitations. Consequently, further work could include the implementation of a batch optimizer.

References

[1] S. Ore and A. Stori. *Polymerer*. https://snl.no/polymerer. Accessed: 13/5-23.

[2] Lars Egil Helseth. *Polyvinylklorid*. http://snl.no/polyvinylklorid. Accessed: 13/5-23.

[3] W. Harmon Ray and Carlos M. Villa. "Nonlinear dynamics found in polymerization processes — a review". In: *Chemical Engineering Science* 55.2 (2000), pp. 275–290. DOI: https://doi.org/10.1016/S0009-2509(99)00323-1.

[4] G Özkan et al. "Nonlinear control of polymerization reactor". In: *Computers & Chemical Engineering* 25.4-6 (2001), pp. 757–763.

[5] José M Asua. "Emulsion polymerization: from fundamental mechanisms to process developments". In: *Journal of Polymer Science Part A: Polymer Chemistry* 42.5 (2004), pp. 1025–1041.

[6] Paula Marie Hidalgo and CB Brosilow. "Nonlinear model predictive control of styrene polymerization at unstable operating points". In: *Computers & chemical engineering* 14.4-5 (1990), pp. 481–494.

[7] C Kiparissides et al. "Dynamic simulation of industrial poly (vinyl chloride) batch suspension polymerization reactors". In: *Industrial & engineering chemistry research* 36.4 (1997), pp. 1253–1267.

[8] John Dimitratos, Guillermo Elicabe, and Christos Georgakis. "Control of emulsion polymerization reactors". In: *AIChE journal* 40.12 (1994), pp. 1993–2021.

[9] Jørgen Troøyen. *Modelling and estimation of a semi-batch reactor for miniemulsion polymerization of vinyl chloride monomer*. https://folk.ntnu.no/jaschke/Masters/ProjectTheses/2022/JorgenTrooyen/. TKP4580 - Chemical engineering, specialization project, Dept.Chem.Eng., NTNU, 2022.

[10] George Odian. *Principles of polymerization*. John Wiley & Sons, 2004. ISBN: 9780471478751. DOI: https://doi.org/10.1002/047147875X.ch1.

[11] Paul C Painter. *Fundamentals of polymer science : an introductory text*. eng. Boca Raton, Fla, 1997.

[12] Lars Egil Helseth. *Homopolymerer*. https://snl.no/homopolymerer. Accessed: 25/3-23.

[13] Lars Egil Helseth. *Kopolymerer*. https://snl.no/kopolymerer. Accessed: 25/3-23.

[14] Paul J Flory. "Fundamental principles of condensation polymerization." In: *Chemical Reviews* 39.1 (1946), pp. 137–197.

[15] Krzysztof Matyjaszewski and Thomas P. Davis. *Handbook of radical polymerization*. eng. New York: Wiley-Interscience, 2002. ISBN: 047139274X.

[16] Jose Asua. *Polymer reaction engineering*. John Wiley & Sons, 2008. ISBN: 9781405144421.

[17] A.S. Sarac. "Redox polymerization". In: *Progress in Polymer Science* 24.8 (1999), pp. 1149–1204. DOI: https://doi.org/10.1016/S0079-6700(99)00026-X.

[18] Peter A. Lovell and F. Joseph Schork. "Fundamentals of Emulsion Polymerization". In: *Biomacromolecules* 21.11 (2020), pp. 4396–4441. DOI: 10.1021/acs.biomac.0c00769.

[19] José M. Asua. "Miniemulsion polymerization". In: *Progress in Polymer Science* 27.7 (2002), pp. 1283–1346. DOI: https://doi.org/10.1016/S0079-6700(02)00010-2.

[20] F Joseph Schork et al. "Miniemulsion polymerization". In: *Polymer particles* (2005), pp. 129–255.

[21] CS Chern. "Emulsion polymerization mechanisms and kinetics". In: *Progress in polymer science* 31.5 (2006), pp. 443–486.

[22] William D Harkins. "A general theory of the reaction loci in emulsion polymerization". In: *The Journal of chemical physics* 13.9 (1945), pp. 381–382.

[23] J Ugelstad, MS El-Aasser, and JW Vanderhoff. "Emulsion polymerization: Initiation of polymerization in monomer droplets". In: *Journal of Polymer Science: Polymer Letters Edition* 11.8 (1973), pp. 503–513.

[24] M. Cioffi, A.C. Hoffmann, and L.P.B.M. Janssen. "Reducing the gel effect in free radical polymerization". In: *Chemical Engineering Science* 56.3 (2001), pp. 911–915. DOI: https://doi.org/10.1016/S0009-2509(00)00305-5.

[25] A.M. van Herk. "Introduction to Radical (Co)Polymerisation". In: *Chemistry and Technology of Emulsion Polymerisation*. John Wiley & Sons, Ltd, 2013. Chap. 2, pp. 23–42. ISBN: 9781118638521. DOI: https://doi.org/10.1002/9781118638521.ch2.

[26] Wendell V Smith and Roswell H Ewart. "Kinetics of emulsion polymerization". In: *The journal of chemical physics* 16.6 (1948), pp. 592–599.

[27] E Peggion, F Testa, and G Talamini. "A kinetic study on the emulsion polymerization of vinyl chloride". In: *Die Makromolekulare Chemie: Macromolecular Chemistry and Physics* 71.1 (1964), pp. 173–183.

[28] Stuart C Thickett and Robert G Gilbert. "Emulsion polymerization: State of the art in kinetics and mechanisms". In: *Polymer* 48.24 (2007), pp. 6965–6991.

[29] Bo-Geng Li and Brian W Brooks. "Prediction of the average number of radicals per particle for emulsion polymerization". In: *Journal of Polymer Science Part A: Polymer Chemistry* 31.9 (1993), pp. 2397–2402.

[30] J Ugelstad et al. "A kinetic investigation of the emulsion polymerization of vinyl chloride". In: *Journal of Polymer Science Part C: Polymer Symposia*. Vol. 27. 1. Wiley Online Library. 1969, pp. 49–68.

[31] Mohamed S El-Aasser, E David Sudol, et al. "Miniemulsions: Overview of Research and applications". In: *JCT Res* 1.1 (2004), pp. 21–31.

[32] Bjarne Foss and Tor Aksel N. Heirung. *Merging Optimization and Control*. Mar. 2016. ISBN: 978-82-7842-201-4.

[33] S. Wright and J. Nocedal. *Numerical Optimization*. eng. 2nd ed. New York, NY: Springer, 2006. ISBN: 0-387-40065-6.

[34] Moritz Diehl and Sébastien Gros. "Numerical optimal control". In: *Optimization in Engineering Center (OPTEC)* (2011).

[35] James Blake Rawlings, David Q Mayne, and Moritz Diehl. *Model predictive control: theory, computation, and design*. Nob Hill Publishing Madison, WI, 2017.

[36] Morten Hovd. "A brief introduction to Model Predictive Control". In: *Engineering Cybernetics Department, NTNU* (2004).

[37] Sigurd Skogestad. "Control structure design for complete chemical plants". In: *Computers & Chemical Engineering* 28.1-2 (2004), pp. 219–234.

[38] Mark L Darby and Michael Nikolaou. "MPC: Current practice and challenges". In: *Control Engineering Practice* 20.4 (2012), pp. 328–342.

[39] Sigurd Skogestad. "Simple analytic rules for model reduction and PID controller tuning". In: *Journal of process control* 13.4 (2003), pp. 291–309.

[40] Dan Simon. *Optimal State Estimation: Kalman, H∞, and Nonlinear Approaches*. 2006. ISBN: 9780470045343.

[41] Tor Steinar Schei. "A finite-difference method for linearization in nonlinear estimation algorithms". In: *Automatica* 33.11 (1997), pp. 2053–2058.

[42] H. Scott Fogler. *Elements of chemical reaction engineering*. eng. 4th ed. Boston: Prentice Hall, 2016. ISBN: 978-0-13-388751-8.

[43] Ahmed H. Abdel-Alim and A. E. Hamielec. "Bulk polymerization of vinyl chloride". In: *Journal of Applied Polymer Science* 16.3 (1972), pp. 783–799. DOI: https://doi.org/10.1002/app.1972.070160321.

[44] Thor Mejdell et al. "Modelling of industrial S-PVC reactor". In: *Chemical engineering science* 54.13-14 (1999), pp. 2459–2466.

[45] Holger Nilsson, Christer Silvegren, and Bertil Törnell. "Swelling of PVC latex particles by VCM". In: *European Polymer Journal* 14.9 (1978), pp. 737–741.

[46] Johannes Brandrup et al. *Polymer handbook*. Vol. 89. Wiley New York, 1999. ISBN: 0471166286.

[47] Kendall E. Atkinson. *Numerical solution of ordinary differential equations*. eng. Hoboken, New Jersey, 2009.

A Model equations and assumptions

A preliminary project was conducted during the fall of 2022 where the model equations and assumptions presented in this section were established. It is emphasized that the model equations listed in this section are based on the preliminary project[9]. They are restated here as they are used in the implementation of the NMPC as well as in the plant replacement model in this thesis.

The underlying assumptions are listed in section A.1, followed by equations related to the kinetics in section A.2 and material balances in section A.3. Phase equilibria calculations are presented in section A.4 and the energy balances are presented last in section A.5.

A.1 Assumptions

In order to establish the model during the preliminary project, some assumptions were made to simplify the modelling of the system. Unless something else is stated, the assumptions listed in this section are valid for both the preliminary project and the master thesis. In addition to the assumption listed below, other assumption are presented in other sections when necessary.

- The initiator is assumed to be described as a thermal initiator due to the complex nature of the redox mechanism, and the initiator is assumed to decompose in the water phase.
- Monomer- and polymer droplets are assumed to be monodisperse.
- The reaction mixture is assumed to be ideal.
- The reactor is assumed to be a lumped system with no spatial variations.
- Coalescence of particles is neglected.
- All droplets formed before VCM is added are assumed to be nucleated.
- The number of particles is assumed to be constant during the entirety of the batch.
- Nucleation occurs through droplet nucleation, and micellar and homogeneous nucleation are neglected. However, due to the pre-prepared mixture that is first charged into the reactor the number of particles is considered to be constant through the whole batch. This implies that the nucleation stage (interval I) is not present and the system can be considered as a seeded system.
- The only reaction contributing to the heat of reaction is the propagation reaction in equation 2.19.
- Additives are approximated as water with respect to physical properties and the material balances.

A.2 Kinetics

The kinetic model for a miniemulsion polymerization process can be made as complex as desired, but a complex model requires higher computational power. A trade-off between precision and computational performance is necessary, and the presented kinetic model is believed to yield accurate results without introducing unnecessary complexity.

A.2.1 Initiator system

The initiator used in this process is a redox initiator system, as already mentioned in section 5.1. As this is a highly complex and intertwined system the initiator system is assumed to be a thermal initiator which is a simpler mechanism to model. The model requires both the decomposition rate of the initiator and the rate of chain initiation which are shown in equation A.1 and A.2, respectively.

$$R_d = k_d[I]^w \tag{A.1}$$

$$R_I = 2k_d f[I]^w \tag{A.2}$$

Here k_d is the rate constant for the decomposition, $[I]^w$ is the concentration of initiator in the water phase and f is the initiator efficiency.

A.2.2 Polymerization rate

As mentioned in section 2.4.7 the polymerization rate is set equal to the propagation rate, and this results in the polymerization rate expression in equation 2.19. For completeness the expression is restated in equation A.3.

$$R_p = k_p[M]^p \bar{n} N_T \tag{A.3}$$

An underlying assumption when using this expression is that the propagation of polymer chains in the water phase is neglected[30].

A.2.3 Termination and chain transfer

The termination reaction in the polymer phase affect the number of radicals per particle and the concentration of radicals in the water phase. Termination in the polymer phase can occur through two mechanisms, as mentioned in section 2.3.3. The parameter ϵ was introduced to describe the relation between the two mechanisms. In a polymerization of VCM, termination by disproportionation is the most dominant mode, resulting in $\epsilon = 1$[43]. This gives the termination rate constants shown in equation A.4.

$$\begin{aligned} k_{td} &= k_t^p \\ k_{tc} &= 0 \end{aligned} \tag{A.4}$$

where k_{td} is the rate constant for termination by disproportionation, k_{tc} is the rate constant for termination by combination and k_t^p is the total termination rate constant in the polymer phase. Along with the termination in the polymer phase (k_t^p), termination in the water phase (k_t^w), desorption (k_{des}) and absorption (k_{abs}) of radicals also affect the number of radicals per particle and the concentration of radicals in the water phase. This is presented in further detail in section A.2.4 along with the radical distribution.

Chain transfer is used to alter the properties of the produced polymer by altering the chain length. It can also be utilized to add functionality to the chain ends[15]. Even though chain transfer do occur, it is not considered in the model in this project.

A.2.4 Radical Distribution

The average number of radicals per particle is modelled using an approximation proposed by Li & Brooks[29]. The differential equation describing $\bar{n}$ is shown in equation A.5.

$$\frac{d\bar{n}}{dt} = \sigma - k_{des}\bar{n} - \Phi C\bar{n}^2 \tag{A.5}$$

Here σ is the average rate at which radicals enter the particles, k_{des} is the rate constant for radical desorption from the particles, C is the relative rate coefficient for radical termination in the polymer phase and Φ is a coefficient ranging between 0 and 2[29]. Expressions for σ, Φ and C are shown in equations A.6, A.7 and A.8, respectively.

$$\sigma = \frac{k_{ads}n_R^w}{V^w} \tag{A.6}$$

$$\Phi = \frac{2(2\sigma + k_{des})}{2\sigma + k_{des} + C} \tag{A.7}$$

$$C = \frac{k_t^p N_T}{V^p} \tag{A.8}$$

In the above equations k_{abs} is the rate constant for absorption on the particles and n_R^w is the amount of radicals in the water phase. The amount of radicals in the water phase will evolve during the batch and the differential equation describing this evolution is shown in equation A.9.

$$\frac{dn_R^w}{dt} = R_I V^w + k_{des}\bar{n}N_T - k_t^w\frac{n_R^{w2}}{V^w} - \frac{k_{abs}n_R^w}{V^w}N_T, \tag{A.9}$$

Here k_t^w is the termination rate constant in the water phase[16].

A.2.5 Correction factor for kinetic parameters

Numeric values for the kinetic parameters were mainly unknown or taken from models of other VCM polymerization processes. Thus, a correction factor for the kinetic model was introduced such that the entire kinetic model could be altered by only adjusting one parameter. The implementation of the correction factor (CF) is shown in equation A.10.

$$\begin{aligned} k_d &= CF \cdot k_d' \\ k_p &= CF \cdot k_p' \\ k_t^p &= CF \cdot k_t^{p'} \\ k_t^w &= CF \cdot k_t^{w'} \\ k_{des} &= CF \cdot k_{des}' \\ k_{abs} &= CF \cdot k_{abs}' \end{aligned} \tag{A.10}$$

Here the dashed rate constants represent the numerical values before the multiplication with the correction factor, while the non-dashed parameters represent the values which are used for calculations in the model.

A.2.6 Number of Particles

Predicting the number of particles in a miniemulsion polymerization is a difficult exercise, and Smith & Ewart's theory presented in equation 2.14 falls short in describing the system in this work. Consequently, an approach which assumes a constant number of particles is utilized. The number of particles is calculated based on measurements from a previous batch. This leads to the expression of the amount of particles shown in equation A.11.

$$N_T = \frac{m_p^{tot}}{m_p^{particle} N_A} = \frac{m_M^{tot} X_M^{final}}{v^p \rho_P N_A} \tag{A.11}$$

Here N_T is the total amount of particles in moles, m_M^{tot} is the total mass of monomer fed to the reactor from a previous batch, X_M^{final} is the final conversion from a previous batch, ρ_P is the density of the polymer particle, N_A is Avogadro's number and v^p is the volume of a polymer particle. The volume of a spherical polymer particle can be written as

$$v^p = \frac{\pi}{6} d_p^3 \,, \tag{A.12}$$

where d_p is the diameter of the polymer particle and is found from analysis of the produced polymer from a previous batch. This approach leads to a constant amount of particles independent of disturbances. Some inaccuracies are expected, but according to INOCYN the pre-made mixture in section 5.1.1 is repeatable. Consequently, the amount of particles will also be quite repeatable and stable from batch to batch.

A.3 Material Balances

The material balances for all species except polymer is written on a molar basis. The generic material balance for a semi-batch reactor can be written as

$$\frac{dn_i}{dt} = \hat{n}_i + R_i, \qquad n_i(0) = n_{i,0}, \tag{A.13}$$

where the left side represents the molar rate of change of specie i, $\hat{n}_i$ represents the molar inflow of specie i, R_i is the generation/consumption of specie i and $n_{i,0}$ is the initial amount of specie i[42]. Using equation A.13 as a basis, the total material balances for monomer, water, surfactant and initiator can be written as in equation A.14 - A.17.

$$\frac{dn_M}{dt} = \hat{n}_M - R_p, \qquad n_M(0) = n_{M,0} \tag{A.14}$$

$$\frac{dn_I}{dt} = \hat{n}_I - R_d V^w, \qquad n_I(0) = n_{I,0} \tag{A.15}$$

$$\frac{dn_W}{dt} = \hat{n}_W, \qquad n_W(0) = n_{W,0} \tag{A.16}$$

$$\frac{dn_S}{dt} = \hat{n}_S, \qquad n_S(0) = n_{S,0} \tag{A.17}$$

The material balance for polymer is expressed on a mass basis due to the varying molecular weight of the polymer chains. Equation A.18 expresses the material balance for the polymer.

$$m_P(t) = X_M(t) M_M \int_0^t \hat{n}_M \, dt \tag{A.18}$$

Here M_M is the molar mass of monomer and $X_M(t)$ is the time dependent monomer conversion, which can be expressed by equation A.19[42].

$$X_M(t) = \frac{\int_0^t \hat{n}_M \, dt - n_M(t)}{\int_0^t \hat{n}_M \, dt} \tag{A.19}$$

A.4 Monomer Distribution and Phase Equilibria Calculations

The calculations in this section are adapted from models of S-PVC reactors developed by Kiparissides et al.[7] and Mejdell et al.[44]. A sufficient description of the system can be obtained from the equations presented. Some additional assumptions to the ones in section A.1 were made when developing the model for the phase equilibria calculations, and these are listed below.

- During the polymerization the model assumes equilibrium at all times between all phases.
- The solubility of monomer in the polymer phase follows Flory-Huggins equation.
- The solubility of monomer in water phase follows Henry's law.
- The vapour phase follows the ideal gas law.
- The polymer is insoluble in the monomer.
- The gas phase is assumed to only contain monomer- and water vapor. Some residual air might be present in the gas, but the amount is assumed to be negligible.
- Volume additivity is assumed to be valid.

The assumption of equilibrium between all phases leads to an equal fugacity of the monomer in all four phases. This relation is expressed in equation A.20.

$$\hat{f}_M^m = \hat{f}_M^p = \hat{f}_M^w = \hat{f}_M^g \tag{A.20}$$

Here $\hat{f}_M^i$ represents the fugacity of the monomer in phase i.

The Flory-huggins equation is used differently depending on which interval the reaction find itself in. This will become clear when considering the different intervals. Equation A.21 shows the general form of the Flory-huggins equation which is used in all three intervals[7].

$$\ln(\alpha_M) = \ln(1 - \varphi) + \varphi + \chi\varphi^2 \tag{A.21}$$

Here α_M is the monomer activity, φ is the volume fraction of polymer in the polymer phase and χ is the temperature dependent Flory-Huggins interaction parameter. The monomer activity is defined as

$$\alpha_M = \frac{\hat{f}_M^p}{\hat{f}_M^0} \, , \tag{A.22}$$

where $\hat{f}_M^0$ is the fugacity of pure monomer at reactor temperature and saturation pressure[7].

Interval I and II

Interval I and II are merged together due to the assumption of modelling the system as a seeded system. Consequently, interval I is not considered when modelling the system.

When the free monomer phase is present the monomer activity is set equal to one, which results in equation A.23[7].

$$\ln(1) = 0 = \ln(1-\varphi) + \varphi + \chi\varphi^2 \tag{A.23}$$

Flory-Huggins equation are in interval I and II used to calculate the volume fraction of polymer in the polymer phase. The volume fraction of polymer in the polymer phase is calculated by equation A.23. This is done iteratively since an analytical solution cannot be obtained. The code used for solving equation A.23 is shown in appendix E.2 and E.5, and it includes the expression for the interaction parameter χ. The code which performs the rest of the calculations for interval I and II is listed in appendix E.1.

Using φ obtained from equation A.23 the mass of monomer in the polymer phase can be calculated from equation A.24.

$$m_M^p = K_s \left(\frac{\rho_M^l m_p}{\rho_P}\right)\left(\frac{1-\varphi}{\varphi}\right) \tag{A.24}$$

Here m_M^p is the mass of monomer in the polymer phase, ρ_P and ρ_M^l are the density of polymer and liquid monomer, respectively. K_s is a correction factor for the solubility of the monomer in the polymer phase and it is purely a modelling parameter. For the derivation of equation A.24, the reader is advised to the preliminary project[9].

The mass of monomer in the gas phase, m_M^g, can be obtained through equation A.25

$$m_M^g = (V_R - V_{fluid,s})\frac{\rho_M^l \rho_M^g}{\rho_M^l - \rho_M^g} \tag{A.25}$$

Here V_R is the reactor volume, ρ_M^g is the gas density of the monomer and $V_{fluid,s}$ is defined as

$$V_{fluid,s} = \frac{m_W}{\rho_W^l} + \frac{m_M}{\rho_M^l} + \frac{m_P}{\rho_P} \tag{A.26}$$

It represents the volume of the liquid and solids in the system if neither monomer or water were present in the gas phase. m_W and m_M are the total mass of water and monomer in the system. The derivation of equation A.25 was performed in the preliminary project[9].

The mass of monomer dissolved in the water phase is obtained from equation A.27 and is based on Henry's law.

$$m_M^w = K_H \alpha_M m_W \tag{A.27}$$

The constant K_H is the VCM-in-water solubility constant and its value is equal to 0.0088 $\frac{\text{kgVCM}}{\text{kgH}_2\text{O}}$ [45]. Conservation of mass is used to calculate the mass of monomer in the free monomer phase.

$$m_M^f = m_M - m_M^p - m_M^g - m_M^w \tag{A.28}$$

The distribution of monomer in all four phases during interval I and II is fully described by equation A.24, A.25, A.27 and A.28

The total reactor pressure is the sum of the partial pressures of gaseous monomer and water. In interval I and II the partial pressures will be equal to their respective saturation pressures evaluated at the reactor temperature. Equation A.29 shows the expression for the reactor pressure, while A.30 and A.31 shows the molar gas fractions of monomer and water, respectively[7].

$$p_R = p_M + p_W = p_M^{sat} + p_W^{sat} \tag{A.29}$$

$$y_M = 1 - y_W \tag{A.30}$$

$$y_W = \frac{p_W^{sat}}{p_R} \tag{A.31}$$

Here p_M and p_W are the partial pressures of monomer and water, while p_M^{sat} and p_W^{sat} are their respective saturation pressures. The temperature dependent expressions for the saturation pressures are listed in appendix C. For interval I and II the gas temperature will be the same as the temperature of the liquid. The temperature of the liquid is obtained from an energy balance over the reactor.

The model also requires the volumes of the four phases to describe the system. Expressions for the volume of the gas phase, the polymer phase, the free phase, the water phase and the liquid phase are listed in equation A.32 - A.36.

$$V^g = \frac{m_M^g}{y_m \rho_M^g} \tag{A.32}$$

$$V^p = \frac{m_P}{\rho_P} + \frac{m_M^p}{\rho_M^l} \tag{A.33}$$

$$V^f = \frac{m_M^f}{\rho_M^l} \tag{A.34}$$

$$V^w = V^l - V^p - V^f \tag{A.35}$$

$$V^l = V_R - V^g \tag{A.36}$$

The concentration of monomer in the polymer phase can be obtained through equation A.37.

$$[M]^p = \frac{m_M^p}{M_M V^p} \tag{A.37}$$

Finally, the mass of water in the gas phase can be described by equation A.38.

$$m_W^g = \frac{y_W p_R V^g M_W}{R T^g} \tag{A.38}$$

Here R is the gas constant and M_W is the molar mass of water.

When the excess monomer is fully consumed ($m_M^f = 0$) and the system enters interval III, some adjustments in the description are necessary.

Interval III

For interval III the activity of the monomer is no longer equal to one, thus the Flory-Huggins equation cannot be used to calculate φ since it also contains α_M as an unknown. The volume fraction of polymer in the polymer phase is instead obtained by solving equation A.24 with respect to φ, while α_M is calculated by inversely solving equation A.21. An iterative calculation procedure is necessary to obtain both these values. The iterative procedure is based on an initial guess that assumes all monomer is in the polymer phase. The iterative procedure for interval III is summarized in algorithm 2, while the necessary code is shown in appendix E.3 and E.4.

Another result of the monomer activity not longer being equal to one is that the partial pressure of monomer is no longer equal to the saturation pressure. The expression for the partial pressure of monomer now has to consider the activity, as shown in equation A.39. This results in the expression for the total reactor pressure shown in equation A.40, which still is the sum of the partial pressures of monomer and water.

$$p_M = \alpha_M p_M^{sat} \tag{A.39}$$

$$p_R = \alpha_M p_M^{sat} + p_W^{sat} \tag{A.40}$$

In interval III the gas temperature is now set equal to the saturation temperature of the monomer at the given partial pressure obtained in equation A.39. The code which perform this calculation is listed in appendix E.6. Apart from the above-mentioned differences, all other calculations for interval III are the same as the ones in interval I and II, with $m_M^f = 0$.

Algorithm 2: Iterative calculation procedure for interval III

Set initial guess of monomer in the polymer phase equal to the total amount of monomer in the system

for $i = 0, 1, 2, 3$ **do**

- Compute φ from eq. A.24
- Compute α_M from eq. A.21
- Compute reactor pressure from eq. A.40
- Compute gas temperature from partial pressure of monomer given in eq. A.39
- Compute mass of monomer in gas phase and water phase as in interval I and II
- Compute mass of monomer in polymer phase from conservation of mass from eq. A.28 with $m_M^f = 0$
- Update initial guess as the weighted sum of previous value and the new calculated value of monomer in the polymer phase

end

Proceed with the same calculations as in interval I and II.

A.5 Energy Balances

The presented energy balances are adapted from the general energy balance given by Fogler[42] and were derived in the preliminary project[9].

A.5.1 Reactor Temperature

A sufficiently accurate model of the reactor temperature is necessary for tight control of the reactor temperature. The energy balance for the reactor temperature is shown in equation A.41.

$$\frac{dT_R}{dt} = \frac{Q_{R,amb} + Q_{J,R} + Q_{feed} + Q_{rx} + Q_{reflux}}{\sum m_i C_{p,i} + m_{steel} C_{p,steel}} \,, \tag{A.41}$$

where $\frac{dT_R}{dt}$ is the rate of change in the reactor temperature, $Q_{R,amb}$ heat lost to the surroundings, $Q_{J,R}$ is the heat exchange with the cooling jacket, Q_{feed} is the energy change due to post-dosing of species, Q_{rx} is the reaction heat, Q_{reflux} is the heat exchange with the reflux condenser, $\sum m_i C_{p,i}$ is the heat capacity of the reaction mixture and $m_{steel} C_{p,steel}$ is the heat capacity of the reactor steel. The terms in the numerator in equation A.41 are defined as follows:

$$Q_{R,amb} = U_{R,amb} A_{R,amb} (T_{amb} - T_R) \tag{A.42}$$

$$Q_{J,R} = U_{J,R} A_{J,R} (T_J - T_R) \tag{A.43}$$

$$Q_{feed} = \sum \hat{m}_i^{feed} C_{p,i}^{feed} (T_i^{feed} - T_R) \tag{A.44}$$

$$Q_{rx} = (-\Delta H_{rx}) R_p \tag{A.45}$$

$$Q_{reflux} = \begin{cases} \hat{V}_{cw}^{reflux} \rho_W^l C_{p,CW}^{reflux} (T_{reflux}^{in} - T_{reflux}^{out}), & \text{when } \textit{Condition 1} \\ 0, & \text{when } \textit{Condition 2} \end{cases} \tag{A.46}$$

In the above equations T_{amb} is the ambient temperature, $A_{i,j}$ are the heat transfer area, $U_{i,j}$ are the overall heat transfer coefficient, $C_{p,i}^{feed}$ is the heat capacity of inlet specie i, $\hat{m}_i^{feed}$ is the inflow of specie i, T_i^{feed} is the temperature of inlet specie i, ΔH_{rx} is the heat of reaction, $C_{p,CW}^{reflux}$ is the heat capacity of the cooling water, $\hat{V}_{cw}^{reflux}$ is the volume flow of cooling water to the reflux condenser, ρ_W^l is the density of water, while T_{reflux}^{in} and T_{reflux}^{out} are the inlet- and outlet temperature of the cooling water for the condenser. The cooling jacket temperature T_J is defined as

$$T_J = \frac{T_J^{in} + T_J^{out}}{2} \tag{A.47}$$

It is the average of the inlet- and outlet temperature of the water to the cooling jacket.

Condition 1 and *Condition 2* in equation A.46 determines when the reflux condenser is operational or not. The reflux is shut off using the valves depicted in figure 5.2 when *Condition 2* is met. The exact details of these conditions are confidential, but in this thesis the definition of *Condition 1* and *Condition 2* is

$$\begin{aligned} &\textit{Condition 1: } X_M \leq 78\% \\ &\textit{Condition 2: } X_M > 78\% \end{aligned} \tag{A.48}$$

A.5.2 Cooling Jacket Outlet Temperature

The change in the outlet temperature of the cooling jacket can be written as

$$\frac{dT_J^{out}}{dt} = \frac{Q_{J,amb} - Q_{J,R} + Q_{flow}}{m_J C_{p,J}} \,, \tag{A.49}$$

where $Q_{J,amb}$ is the heat lost to the surrounding, $Q_{J,R}$ is as defined in equation A.43, Q_{flow} is the energy change from the flow of cooling water and $m_J C_{p,J}$ is the heat capacity of the water inside the cooling jacket. Q_J^{amb} and Q_{flow} are defined as

$$Q_{J,amb} = U_{J,amb} A_{J,amb} (T_{amb} - T_J) \tag{A.50}$$

$$Q_{flow} = \hat{m}_J C_{p,J} (T_J^{in} - T_J^{out}) \,, \tag{A.51}$$

where $\hat{m}_J$ is the water flow to the cooling jacket and T_J^{in} is the temperature of the inlet water.

A.5.3 Reflux Condenser Outlet Temperature

The change in temperature of the cooling water out of the reflux condenser is shown in equation A.52.

$$\frac{dT_{reflux}^{out}}{dt} = \frac{Q_{reflux} + Q_{ex}}{m_{reflux} C_{p,reflux}} \tag{A.52}$$

Here $m_{reflux} C_{p,reflux}$ is the heat capacity of the water inside the reflux condenser, Q_{reflux} is as defined in equation A.46 and Q_{ex} is defined as follows:

$$Q_{ex} = U_{reflux} A_{reflux} (T^g - T_{reflux}) \tag{A.53}$$

In equation A.53 T^g is the gas temperature in the reactor and T_{reflux} is defined as the average between the inlet- and outlet temperature of the cooling water as shown in equation A.54.

$$T_{reflux} = \frac{T_{reflux}^{in} + T_{reflux}^{out}}{2} \tag{A.54}$$

B Results from the preliminary project and parameter adjustments

The main results from the preliminary project are presented first before the results from the parameter adjustment are presented. In the initial phase of this master thesis adjustments to some model parameters were performed to make the model more fit to be used in the NMPC implementation. The main results are compared to make it clear that the considerations made in the preliminary project are still highly relevant for the work done in this thesis.

B.1 Preliminary project

Some of the main results from the preliminary project are presented. This is done to give a brief introduction to how the system behaves, but the reader is strongly encouraged to the preliminary project report for further details and discussions[9].

The kinetic parameters obtained in the preliminary project are listed table B.1. Rate constant values related to the propagation and termination reactions were obtained from literature[7], while the other process parameters where obtained from offline parameter estimation in ModelFit or by trial-and-error. The values for f and ϵ were set in accordance with the theory presented in section 2.3.

Table B.1: Parameter values used in the preliminary project. Values for the propagation rate constant, termination rate constant and the intermediate calculation parameter, K_c, was obtained from literature[7]. Kinetic parameters for the initiator, parameters related to the number of particles and the reactor design are not listed due to confidentiality.

Parameter	Value	Unit
k_p	$5 \cdot 10^5 \exp(-3320/T_R)$	$m^3/mol/s$
K_c	$1.01 \cdot 10^{-7} \exp(-5740(1/T_R - 1/333.15))$	$m^3/mol/s$
k_t^p	$2k_p^2/K_c$	$m^3/mol/s$
k_{ads}	0.2	$m^3/mol/s$
k_{des}	10^{-5}	$1/s$
k_t^w	0.9	$m^3/mol/s$
$U_{J,R}$	320	$W/m^2/K$
U_{reflux}	330	$W/m^2/K$
f	0.7	-
ϵ	1	-
K_s	1.2	-
CF	3.6	-

The ballistic simulations gave tolerable results, but some deviations from the measurements were observed. Especially the deviation in the reactor temperature in figure B.1a motivated the implementation of online state- and parameter estimation. Due to the exothermic nature of the polymerization reaction, accurate predictions of the reactor temperature is critical for the control and safe operation of the reactor. Figure B.1b shows the reactor temperature from the simulation with online state- and parameter estimation. The predicted reactor temperature now follows the measured reactor temperature closely, with only some minor deviations towards the end of batch. This substantiates the estimators

ability to track the measurements.

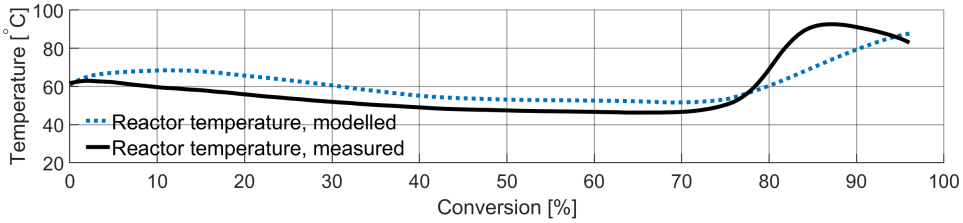

(a) Modelled and measured reactor temperature. The simulation was run ballistic.

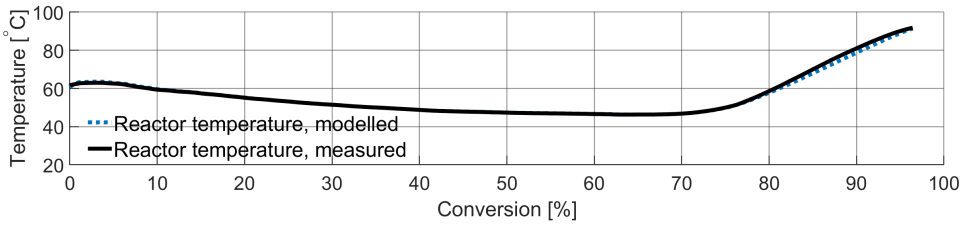

(b) Modelled and measured reactor temperature. The simulation was run with recursive filtering.

Figure B.1: Reactor temperature as a function of conversion from both a ballistic simulation and a simulation with recursive filtering.

The online state- and parameter estimation was implemented by tuning a Kalman filter. For the filtering, the correction factor for the kinetic model (CF), the heat transfer coefficient between the reactor and cooling jacket ($U_{J,R}$) and the heat transfer coefficient for the reflux condenser (U_{reflux}) were the parameters chosen to be estimated. The reactor temperature (T_R), the outlet temperature of the cooling jacket (T_J^{out}) and the outlet temperature of the reflux condenser (T_{reflux}^{out}) were chosen as the active measurements.

An additional three batches were simulated to validate the model. Figure B.2 shows the parameter profiles for the three estimated parameters. Figure B.2a shows that CF has a systematic trend for all four batches, which substantiated the performance of the model. During the initial phase of the master thesis a polynomial was fitted to the average trend for CF and implemented to the model. This is further presented in section 8.1.3.

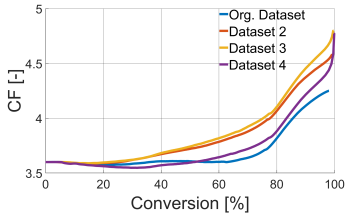

(a) Parameter profiles, CF.

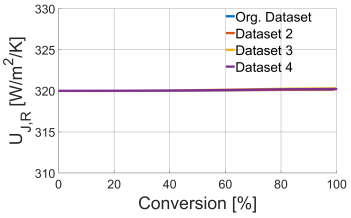

(b) Parameter profiles, $U_{J,R}$.

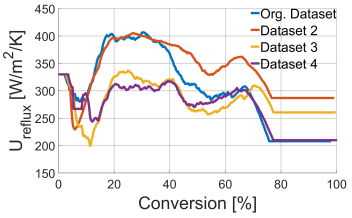

(c) Parameter profiles U_{reflux}

Figure B.2: Parameter profiles for the three estimated parameters. The parameter profiles were obtained from simulations of the four batches with online state- and parameter estimation during the preliminary project.

It is emphasized that some parameter adjustments were performed during the initial phase of the master thesis. These adjustments changed the quantitative behavior of the results slightly, but the qualitative behavior of the results are the same. This is further discussed in section B.2, but is also mentioned here to avoid confusion.

B.2 Parameter adjustments

In order to make the model more fit to use in NMPC, adjustments to some model parameters were performed during the initial phase of the thesis. It is emphasized that the parameter adjustments added no significant aspects to the discussion or conclusion in the preliminary project due to similar behavior for the majority of the model outputs.

The obtained values after the parameter adjustments are listed in table B.2.

Table B.2: Parameter values after the parameter adjustment. The values listed in bold text are different from the ones used in the preliminary project.

Parameter	Value	Unit
k_p	$5 \cdot 10^5 \exp(-3320/T_R)$	$m^3/mol/s$
K_c	$1.01 \cdot 10^{-7} \exp(-5740(1/T_R - 1/333.15))$	$m^3/mol/s$
k_t^p	$2k_p^2/K_c$	$m^3/mol/s$
k_{ads}	**0.032**	$m^3/mol/s$
k_{des}	**0.00092**	$1/s$
k_t^w	**0.3**	$m^3/mol/s$
$U_{J,R}$	**400**	$W/m^2/K$
U_{reflux}	330	$W/m^2/K$
f	0.7	-
K_s	1.2	-
CF	**4.8**	-

The main motivation for the parameter adjustments were to make $\bar{n}$ more sensitive to post-dosage of initiator as the dosing of initiator is an important MV for the control of the reactor. Figure B.3 shows that the profile for $\bar{n}$ after the parameter adjustments obtains a slightly lower value and decreases through the batch. It also shows that $\bar{n}$ has some small oscillations, which is due to the post-dosing of initiator. This is not seen for the results obtained from the preliminary project where $\bar{n}$ lies flat through the batch and there is no sensitivity towards the initiator dosing. As a result, the dosing of initiator will have a larger influence on the polymerization rate and consequently the reactor temperature.

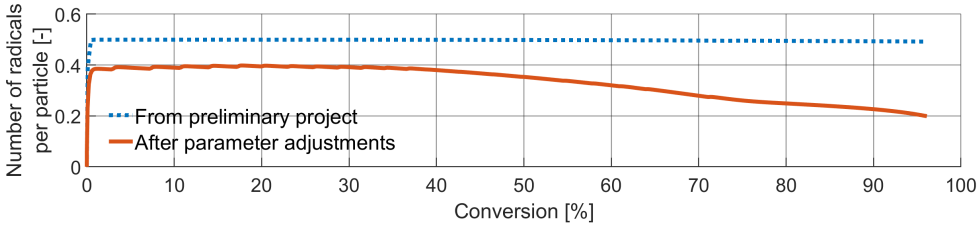

Figure B.3: Comparison of the average number of radicals per particle ($\bar{n}$) from the preliminary project and after the parameter adjustments. The unit on the x-axis is conversion since the two simulations have different duration.

Apart from the changed profile in $\bar{n}$, the results with the altered parameter values are very alike the results obtained in the preliminary project. The ballistic simulations after the parameter adjustments shows the same trends as the ballistic simulations from the preliminary project. This is exemplified by the reactor temperature in figure B.4a. The same deviations can be observed at the same locations as the ballistic simulations in

figure B.1a. A slightly larger deviation to the measurements can be seen, but this is not considered to be significant regarding the discussion and conclusion of the results and it has no influence on the work performed in this master thesis.

Figure B.4b shows that the modelled reactor temperature from the simulation with online state- and parameter estimation tracks the measured reactor temperature well with only minor deviations towards the end of the batch. This is in accordance with the corresponding simulation in figure B.1b from the preliminary project.

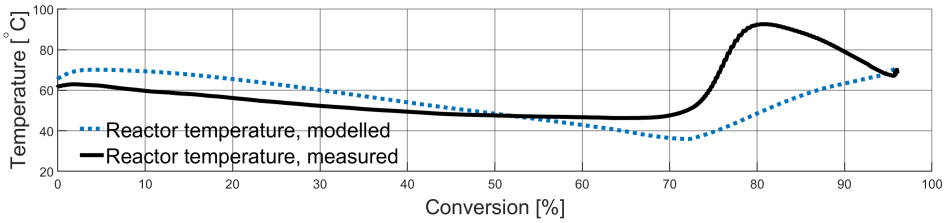

(a) Modelled and measured reactor temperature. The simulation was run ballistic.

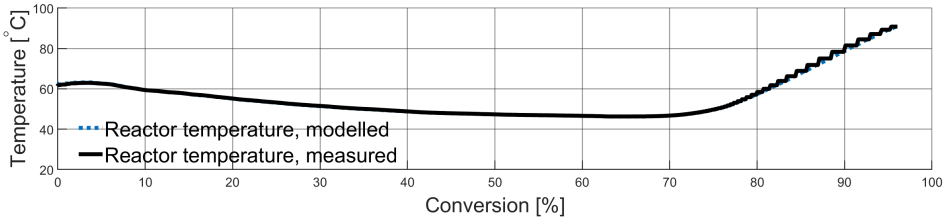

(b) Modelled and measured reactor temperature. The simulation was run with recursive filtering.

Figure B.4: Reactor temperature as a function of conversion from both a ballistic simulation and a simulation with recursive filtering.

Figure B.4b also illustrates the estimators ability to track the measured reactor temperature. Consequently, the results for the parameter adjustments were as satisfactory as the results from the preliminary project and the discussion and conclusion the same.

Figure B.5 shows the parameter profiles for CF, $U_{J,R}$ and U_{reflux}. All three parameters show the same trends as the ones in figure B.2 with only the numeric values shifted; CF shows the same increase towards the end of the batch, $U_{J,R}$ stays approximately constant through the batch and the trends for U_{reflux} are similar, but each batch are shifted vertically to each other.

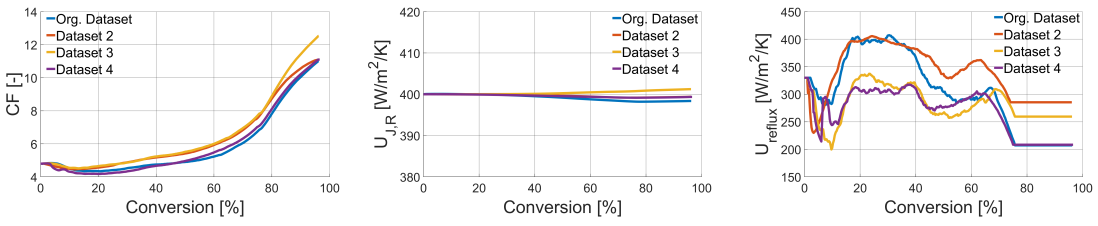

(a) Parameter profiles, CF. **(b)** Parameter profiles, $U_{J,R}$. **(c)** Parameter profiles, U_{reflux}

Figure B.5: Parameter profiles obtained for four batches.

As a result of the smaller value of $\bar{n}$ in figure B.3, CF obtains a bigger value than in the preliminary project. Despite this, the systematic trend in all four batches can be observed

with the new parameter values as well. This systematic trend in CF can be utilized by fitting a polynomial to the average trend and implementing the polynomial to the model to account for unmodelled aspects. This is presented and discussed in further detail in section 8.1.3.

The main results are presented and compared to the results from the preliminary project. This is done to demonstrate that the model behaves similar with the adjusted parameter values, compared to the preliminary project. The discussions and conclusion from the preliminary are still highly relevant for the work in this thesis and the reader is again strongly encouraged to the preliminary project for more detailed results and discussions[9].

C Physical properties

Expressions and values for the physical properties used in the model equations are listed below. The parameter ϑ is defined as $\vartheta = T - 273.15$ and is the temperature in °C. Physical properties for the components are taken from Kiparissides et al.[7], while the value for the heat of reaction are taken from Brandrup et al.[46].

$$M_W = 18 \cdot 10^{-3} \quad [\text{kg/mol}] \tag{C.1}$$

$$\rho_W^l = 1011.0 - 0.4484\vartheta \quad [\text{kg/m}^3] \tag{C.2}$$

$$C_{p,W} = 4.02 \cdot 10^3 \exp\left(1.99 \cdot 10^{-4} T\right) \quad [\text{J/kg/K}] \tag{C.3}$$

$$p_W^{sat} = \exp\left(72.55 - 7206.7/T - 7.1382 \ln(T) + 4.046 \cdot 10^{-6} T^2\right) \quad [\text{Pa}] \tag{C.4}$$

(C.5)

$$M_M = 62.5 \cdot 10^{-3} \quad [\text{kg/mol}] \tag{C.6}$$

$$\rho_M^l = 947.1 - 1746\vartheta - 3.24 \cdot 10^{-3}\vartheta^2 \quad [\text{kg/m}^3] \tag{C.7}$$

$$C_{p,M} = 66.848(18.67 + 0.0758\vartheta) \quad [\text{J/kg/K}] \tag{C.8}$$

$$p_M^{sat} = \exp\left(126.85 - 5760.1/T - 17.914 \ln(T) + 2.4917 \cdot 10^{-6} T^2\right) \quad [\text{Pa}] \tag{C.9}$$

$$\Delta H_{VCM}^{vap} = 1.1093 \frac{R T_b (\ln(p_c) - 1)}{M_M \left(0.93 - \frac{T_b}{T_c}\right)} \exp\left(0.38 \ln\left(\frac{T_c - T}{T_c - T_b}\right)\right) \quad [\text{J/kg}] \tag{C.10}$$

$$\rho_P = 10^3 \exp\left(0.4296 - 3.274 \cdot 10^{-4} T\right) \quad [\text{kg/m}^3] \tag{C.11}$$

$$C_{p,P} = 0.934 \quad [\text{J/kg/K}] \tag{C.12}$$

(C.13)

$$\Delta H_{rx} = -97.6 \quad [\text{kJ/mol}] \tag{C.14}$$

(C.15)

$$C_{p,steel} = 502.416 \quad [\text{J/kg/K}] \tag{C.16}$$

(C.17)

$$R = 8.314 \quad [\text{J/K/mol}] \tag{C.18}$$

Table C.1: Values for VCM: critical pressure and temperature, in addition to the boiling point at atmospheric pressure.

T_b	259.1 K
T_c	425 K
p_b	51.5 bar

In addition to the expressions listed above, the density of gaseous monomer, ρ_M^g, is required for the model. The density of the gaseous monomer is calculated from the virial equation of state. The necessary code is shown below with permission from Peter Singstad, Cybernetica.

```
double rho_vcm_g(   // Out: Dens. for water, kg/m3
  double T,    // In: temperature, K
  double p     // In: Pressure, Pa
)
{
  double rho, Bm, Bw, Bmw;

  fugpar(&Bm, &Bw, &Bmw, T);
  rho = MWm * p / (R_un_gas * T + Bm * p);

  return rho;
}

void fugpar(
  double* Bm,      /* Out: [m3/kmol]    */
  double* Bw,      /* Out: [m3/kmol]    */
  double* Bmw,       /* Out: [m3/kmol]    */
  double T         /* In:  [K]        */
)
{
  double Tc_m = 432.0;       /* [K]             */
  double Tc_w = 647.5;       /* [K]             */
  double Tc_mw = 528.9;      /* [K]             */
  double Pc_m = 56.e5;       /* [Pa]            */
  double Pc_w = 220.5e5;       /* [Pa]            */
  double Pc_mw = 107.e5;       /* [Pa]            */
  double acfm = 0.1048;      /* [-]             */
  double acfw = 0.3342;      /* [-]             */
  double acfmw = 0.2195;       /* [-]             */
  double Trm, Trw, Trmw;

  Trm = T / Tc_m;
  Trw = T / Tc_w;
  Trmw = T / Tc_mw;

  *Bm = R_un_gas * Tc_m / Pc_m * ((0.083 - 0.422 / pow(Trm, 1.6))
    - acfm * (0.139 - 0.172 / pow(Trm, 4.2)));
  *Bw = R_un_gas * Tc_w / Pc_w * ((0.083 - 0.422 / pow(Trw, 1.6))
    - acfw * (0.139 - 0.172 / pow(Trw, 4.2)));
  *Bmw = R_un_gas * Tc_mw / Pc_mw * ((0.083 - 0.422 / pow(Trmw, 1.6))
    - acfmw * (0.139 - 0.172 / pow(Trmw, 4.2)));
}
```

D Euler's method

The numerical integration method used in this thesis is Euler's method, which is the simplest numerical method[47]. Consider the system

$$\frac{dx}{dt} = f(t, x(t)) \,, \tag{D.1}$$

where x is the system state, t is the time and $f(\cdot)$ is the model equation. Then the evolution of the system states can be obtained by numerically integrating the system utilizing Euler's method which can be written as

$$x_{k+1} = x_k + hf(t_k, x_k) \tag{D.2}$$

Here x_{k+1} is the system state at the next time step, x_k is the state at the current time step, h is the integration step length and $f(\cdot)$ is evaluated at the current time step.

In this thesis the integration step length was set to 0.1 seconds, which proved to be sufficient even for the stiff kinetic model. Since Euler's method was sufficient, more accurate and computationally demanding numerical methods was not necessary

E Relevant code

The following code is presented with permission from Peter Singstad at Cybernetica. The rest of the model code along with the code for the implementation of the NMPC and estimator is not presented as it is confidential.

E.1 Monomer distribution and phase equilibria for interval I and II

The following code performs the phase equilibria calculations for interval I and II. The function inputs and outputs are briefly described at the start of the function. Some comments are added to briefly describe the calculations performed. The calculations performed are presented in section A.4.

```
int phase_distribution_free(  // Out: Value is 1 if no free phase is found
  double* p,           // Out: Pressure, Pa
  double* Tg,          // Out: Gas temperature, K
  double* mm_p,          // Out: Mass of monomer solved in polymer, kg
  double* mm_w,          // Out: Mass of monomer solved in water, kg
  double* mm_g,          // Out: Mass of monomer in gas phase, kg
  double* mm_f,          // Out: Mass of monomer in free phase, kg
  double* V_l,         // Out: Volume of liquid and solids, m3
  double* cm_p,        // Out: Concentration of monomer in polymer phase, mol/
      m3
  double* mw_g,        // Out: Mass of water in gas phase, kg
  double* V_p,         // Out: Volume of polymer phase, m3
  double* V_f,         // Out: Volume of free phase, m3
  double* V_g,         // Out: Volume of gas phase, m3
  double* V_w,         // Out: Volume of water phase, m3

  double T,            // In:  Temperature, K
  double mm,           // In:  Monomer mass, kg
  double mw,           // In:  Water mass, kg
  double mp,           // In:  Polymer mass, kg
  double Vr,           // In:  Reactor volume, m3
  double Ks,           // In:  Correction factor for VCM solvability in PVC
  double mm_dos,         // In:  Amount of added monomer, kg
  double Xm          // In:  Conversion of monomer
)
{
  double rhoW, rhoP, rhoM, rhoG, vf, am, pM, pW, V_fluid_s, z, yM, yW;

  psat(&pM, &pW, T);       // Get saturation pressures at given reactor
      temperature
  *p = pM + pW;
  *Tg = T;
  am = 1.0;

  // Calculate densities at given reactor temperature
  rhoW = rho_w(T);
  rhoP = rho_pvc(T);
  rhoM = rho_vcm(T);
  rhoG = rho_vcm_g(*Tg, pM);

  FloryPVC(&vf, am, T);    // Calculation of the volume fraction

  // Molar fractions in gas phase
  yW = pW / *p;
  yM = 1 - yW;
```

```
    // Monomer distribution
    V_fluid_s = mw / rhoW + mp / rhoP + mm / rhoM;
  *mm_g = (Vr - V_fluid_s) * rhoM * rhoG / (rhoM - rhoG);
  *mm_p = (rhoM * Ks * mp * (1 - vf)) / (rhoP * vf);
  *mm_w = 0.0088 * am * mw;
  *mm_f = mm - *mm_g - *mm_w - *mm_p;

  // Volume of phases and total liquid volume (volume in reactor which is not
      gas)
  *V_g = * mm_g / (yM * rhoG);
  *V_l = Vr - *V_g;
  *V_p = (Xm * MWm * mm_dos) / rhoP + *mm_p / rhoM;
  *V_f = *mm_f / rhoM;
  *V_w = *V_l - *V_p - *V_f;

  // Concentration of monomer in polymer phase
  *cm_p = *mm_p / (MWm * *V_p);

  //Mass of water in gas phase
  *mw_g = (MWw * yW * *V_g * *p) / (R_un_gas * *Tg);

  if (*mm_f < 0) {
    *mm_f = 0.0;  // There is no free VCM
    return 1;
  }
  return 0;
}
```

E.2 Calculation of volume fraction of polymer in the polymer phase for interval I and II

The following code computes the volume fraction of polymer in the polymer phase for interval I and II. The calculation appears in the code in appendix E.1. This calculation also includes the calculation of the interaction parameter.

```
void FloryPVC(
  double* vf,    // Out: volume fraction of solid material
  double am,     // In: activity coefficient
  double T       // In: temperature [K]
)
{
  double x, r, dr, c0, c1, c2, c3, c4;
  long i;

  // Check for singularity - in case of no monomer present
  if (am < 1.0e-15) {
    *vf = 1.0;
    return;
  }
  else if (am > 1.0) {
    am = 1.0;
  }

  // Parameters for Flory-Huggin's relation adapted for PVC
  CoeffFlory(&c4, &c3, &c2, &c1, &c0, T, am);

  // Initial guess
```

```
  x = 1.0 - 0.25 * am * am * am * (1.0 + (T - 323.15) / 500);

  // Newton-Raphson iteration to find volume fraction
  for (i = 0; i < 3; i++) {
    r = log(1 - x) + (((c4 * x + c3) * x + c2) * x + c1) * x + c0;
    dr = 1 / (x - 1) + ((4 * c4 * x + 3 * c3) * x + 2 * c2) * x + c1;

    x = x - r / dr;
  }
  *vf = x;
}
```

E.3 Monomer distribution and phase equilibria for interval III

The following code performs the phase equilibria calculations for interval III. The function inputs and outputs are briefly described at the start of the function. Some comments are added to briefly describe the calculations performed. The calculations performed are presented in section A.4.

```
void phase_distribution_unfree(
  double* p,         // Out: Pressure, Pa
  double* Tg,        // Out: Gas temperature, K
  double* mm_p,        // Out: Mass of monomer solved in polymer, kg
  double* mm_w,        // Out: Mass of monomer solved in water, kg
  double* mm_g,        // Out: Mass of monomer in gas phase, kg
  double* mw_g,      // Out: Mass of water in gas phase, kg
  double* cm_p,      // Out: Concentration of monomer in polymer phase, mol/m3
  double* V_l,       // Out: Volume of liquid and solids, m3
  double* V_g,       // Out: Volume of gas phase, m3
  double* V_p,       // Out: Volume of polymer phase, m3
  double* V_w,       // Out: Volume of water phase, m3

  double T,          // In:  Temperature, K
  double mm,         // In:  Monomer mass, kg
  double mw,         // In:  Water mass, kg
  double mp,         // In:  Polymer mass, kg
  double Vr,         // In:  Reactor volume, m3
  double Ks,         // In:  Correction factor for VCM solvability in PVC
  double mm_dos,       // In:  Amount of added monomer
  double Xm       // In:  Conversion of monomer
)
{
  // This function assumes no free VCM present in the system
  double rhoW, rhoP, rhoM, rhoG, mm_p_iter, vf, am, pM, pW, V_fluid_s, yM, yW,
       z;
  int i;

  // Parameters in the numerical solution
  double zeta = 0.5;
  int N = 3;

    // Calculation of densities at give nreactor temperature
  rhoW = rho_w(T);
  rhoP = rho_pvc(T);
  rhoM = rho_vcm(T);

  mm_p_iter = mm; // First assume that all VCM is in the polymer phase. ''
      Initial guess''
```

```
  for (i = 1; i <= N; i++) {
    vf = (rhoM * Ks * mp) / (rhoM * Ks * mp + rhoP * mm_p_iter);   //
        Calculation of volume fraction
    InvFloryPVC(&am, T, vf);  // Activity from inversely solving Flory-Huggins
         eq
    psat(&pM, &pW, T);  // Saturation pressures at given reactor temperature

    if (am > 1) {
      am = 1.0;
    }
    *p = pM * am + pW;
    *Tg = Tsat_vcm(pM * am); // Gas temperature at given partial pressure of
        VCM
    rhoG = rho_vcm_g(*Tg, pM * am);
    // Monomer distribution
    V_fluid_s = mw / rhoW + mp / rhoP + mm / rhoM;
    *mm_g = (Vr - V_fluid_s) * rhoM * rhoG / (rhoM - rhoG);
    *mm_w = 0.0088 * am * mw;
    *mm_p = mm - *mm_g - *mm_w;
     // Update value of mass of monomer in polymer phase
    mm_p_iter = zeta * *mm_p + (1 - zeta) * mm_p_iter;
  }

  // Molar fraction in gas
  yM = 1 - pW / (*p);
  yW = pW / (*p);

  // Volume of phases and total liquid volume (volume in reactor which is not
      gas)
  *V_g = * mm_g / (yM * rhoG);
  *V_p = *mm_p / rhoM + (mm_dos * Xm * MWm) / rhoP;
  *V_l = Vr - *V_g;
  *V_w = *V_l - *V_p;

  // Concentration of monomer in polymer phase
  *cm_p = * mm_p / (MWm * *V_p);

  // Mass of water in gas phase
  *mw_g = (yW * *p * *V_g * MWw) / (R_un_gas * *Tg);
}
```

E.4 Calculation of monomer activity for interval III

The following code computes the activity of the monomer in interval III. The calculation is a part of the calculation routine outlined in algorithm 2 and also appears in the code in appendix E.3. This calculation also includes the calculation of the interaction parameter.

```
void InvFloryPVC(
  double* am,       // Out: activity coefficient
  double T,     // In: temperature [K]
  double vf     // In: volume fraction of solid material
)
{
  double c0, c1, c2, c3, c4;

  // Parameters for Flory-Huggin's relation adapted for PVC
  CoeffFlory(&c4, &c3, &c2, &c1, &c0, T, 1.0);

  if (vf >= 1.0) {
```

```
    *am = 0.0;
    return;
  }
  else if (vf <= 0.0) {
    *am = 1.0;
    return;
  }

  // Inverse solution of the Flory-Huggins equation. The c-coefficients are
      part of the calculation of the interaction parameter
  c0 = log(1 - vf) + (((c4 * vf + c3) * vf + c2) * vf + c1) * vf;
  *am = exp(c0);
}
```

E.5 Flory-Huggins coefficients

The following code calculates the parameters used in the Flory-Huggins equation. The parameters are used in the calculation of the Flory-Huggins interaction parameter.

```
void CoeffFlory(
  double* c4,    // Out: Parameter
  double* c3,    // Out: Parameter
  double* c2,    // Out: Parameter
  double* c1,    // Out: Parameter
  double* c0,    // Out: Parameter
  double T,      // In: temperature [K]
  double am      // In: activity coefficient
)
{
  double FH_Xs  = 0.26;          // [ - ]
  double FH_a = 0.15524;         // [ - ]
  double FH_b = 0.35311;         // [ - ]
  double FH_c = -0.50527;        // [ - ]
  double FH_d = 11.3605;         // [K]
  double FH_e = 199.96;        // [K]
  double FH_f = 6244.49;         // [K]

  double cT;

  cT = FH_f / T;

    // Parameters for the Flory-Huggins equation adapted to PVC
  *c4 = cT * FH_b;
  *c3 = cT * FH_c;
  *c2 = (FH_e + FH_f * FH_a + cT * FH_d) / T + FH_Xs;
  *c1 = 1.0;
  *c0 = -log(am);
}
```

E.6 Gas temperature in interval III

The following code calculates the gas temperature in interval III. The gas temperature is calculated from the partial pressure of the monomer.

```
double Tsat_vcm(
  double p      /* In: Pressure [Pa]  */
)
{
```

```
  double T, pvcm, pw;

  double a = 5e5 / 20;
  int i;
  T = (p - 1e6) / a + 60 + 273.15;
  for (i = 0; i < 5; i++) {
    psat(&pvcm, &pw, T);
    T = (p - pvcm) / a + T;
  }
  return T;
}
```

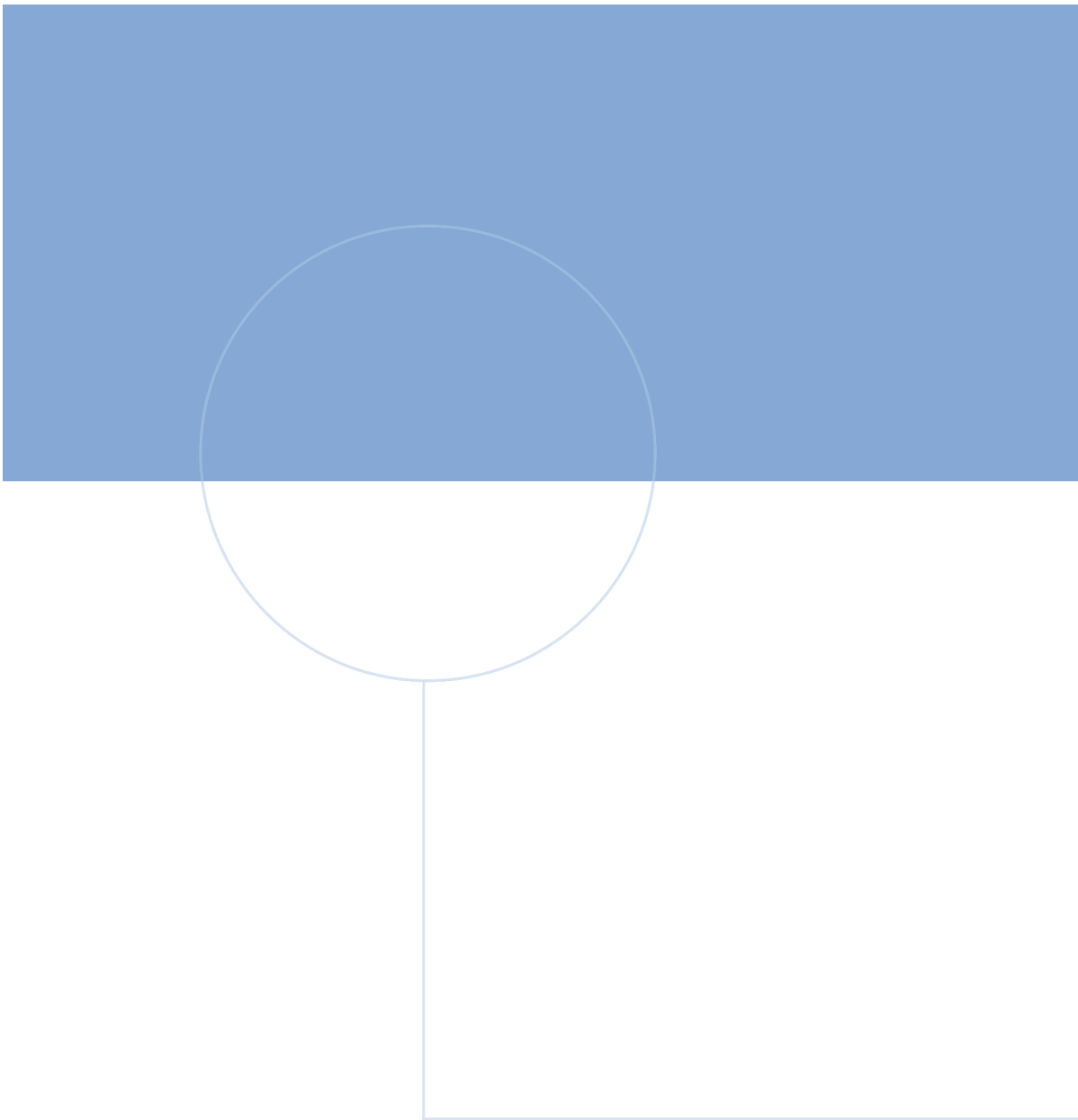

NTNU

Norwegian University of
Science and Technology